PREPARATION, CHARACTERIZATION AND ELECTROANALYTICAL APPLICATIONS OF CARBON NANO-ONION MODIFIED SURFACES.

Joanne Piñera Bartolome

Dipòsit Legal: T 1461-2015

Joanne Piñera Bartolome

PREPARATION, CHARACTERIZATION AND ELECTROANALYTICAL APPLICATIONS OF CARBON NANO-ONION MODIFIED SURFACES

DOCTORAL THESIS

Departament d'Enginyeria Química

UNIVERSITAT ROVIRA I VIRGILI

Joanne Piñera Bartolome

PREPARATION, CHARACTERIZATION AND ELECTROANALYTICAL APPLICATIONS OF CARBON NANO-ONION MODIFIED SURFACES

DOCTORAL THESIS

Supervised by Dr. Alex Fragoso

Departament d'Enginyeria Química

UNIVERSITAT ROVIRA I VIRGILI

Tarragona

2015

UNIVERSITAT ROVIRA I VIRGILI

Departament d'Enginyeria Quimica
Universitat Rovira i Virgili
Campus Sescelades,
Avda. Països Catalans, 26
43007 Tarragona
Tel: 977 55 85 79
Fax: 977 55 96 67

Dr. Alex Fragoso

CERTIFIES:

That the present study, entitled "PREPARATION, CHARACTERIZATION AND ELECTROANALYTICAL APPLICATIONS OF CARBON NANO-ONION MODIFIED SURFACES" presented by Joanne Piñera Bartolome for the award of the degree of Doctor, has been carried out under my supervision at the Department of Chemical Engineering of Universitat Rovira i Virgili,

Tarragona, July 11th 2015.

Dr. Alex Fragoso

ACKNOWLEDGEMENTS

"Everything is theoretically impossible, until it is done."
-Robert A. Heinlein

I am thankful and indebted to Dr. Alex Fragoso, my supervisor, for sharing expertise, continuous advice, valuable guidance and encouragement extended to me during the entire studies beginning in the Master until now.

I am expressing my sincere gratitude to all the NBG and BBG group members, especially to the group leaders, Dr. Ciara O'Sullivan and Dr. Ioanis Katakis, for the unique help and support. To Dr. Mayreli Ortiz, Mª Carmen Bermudo, Joseph Lluis Acero and Mary Luz Botero, for guidance and help throughout my work. Also to the former members of the group, especially to Dr. Samuel Dulay for unending encouragement and help throughout my stay here in Spain. Special thanks to Dr. Pascal Blondeau, of the Department of Analytical and Organic Chemistry, for sharing ideas and helping in some of my experimental work and to Dr. Enrique Parra, for his help and experimental assistance in the realization of one chapter of this work.

I am grateful to my loving parents, Tatay Anton and Nanay Berna, who have raised me for what I am now. For their unending love and support that kept me stronger throughout. To my siblings, my sisters Jorelyn and Emely and my brother Jover for their moral support. To my kulit nephew Mico for his innocent humor.

I also thank the Department of Chemical Engineering for a pre-doctoral scholarship. Financial support from Ministerio de Economía y Competitividad (grant BIO2012-30936) is also gratefully acknowledged.

Above all to God, the Creator, for the gift of wisdom.

JOANNE

ABBREVIATIONS

AA: Ascorbic acid
AFM: atomic force microscopy
ALP: alkaline phosphatase
CEA: Carcinoembryonic antigen
CMC-NH2- aminated- carboxymethyl cellulose
CNO: Carbon nano-onion
DMF: Dimethyl formamide
EDC: 1-ethyl-3-(3-dimethyl-aminopropyl) carbodiimide
ESEM: Environmental scanning microscopy
Fc: Ferrocene
FT-IR: Fourier transform infrared spectroscopy
GCE- glassy carbon electrode
HQ: Hydroquinone
HQDP: Hydroquinone diphosphate
HRP: Horseradish peroxidase
HRTEM: High-resolution transmission microscopy
IgG: Immunoglobulin G
ND: Nanodiamond
NHS: N-hydroxysuccinimide
oAP: ortho-aminophenol
PAA: Phenylacetic acid
PBS: Phosphate buffered saline
PM: Phenylmaleimide
RFP: Radio frequency plasma
SAM: Self-assembly monolayer
SEM: Scanning electron microscopy
HRTEM: High-Resolution Transmission electron microscopy
TGA: Thermogravimetric analysis
TMB: 3,3',5,5'-tetramethylbenzidine
XPS: Xray photoemission spectroscopy
XRD: Xray Diffraction

Table of contents

Summary

The focus of the present thesis is to explore strategies for the preparation and modification of novel nanoarchitectures based on carbon nano-onions to expand their current applications in the construction of novel detection systems with improved performances.

Chapter 1 is a general introduction and literature review, which covers the general information on carbon allotropes with emphasis in carbon nano-onions, their preparation and functionalization methods, and their current applications in electronic devices, catalysis and biology.

Chapter 2 illustrates the synthesis and characterization of carbon nano-onions by annealing of commercially available nanodiamonds. Heat treatment of nanodiamonds at 1200ºC for 6 hours under argon atmosphere afforded small round nano-onion particles of 3-4 nm diameter and 5-6 graphitic shells. The prepared CNOs were visualized by HRTEM and showed the characteristic XRD and Raman features. The results have been compared with a sample prepared by annealing at 1600ºC. An annealed sample was treated with radiofrequency plasma in a controlled Ar/O_2 atmosphere and analyzed by XPS, revealing the presence of oxygenated functionalities.

Chapter 3 explores the possibility to use crown ether/ammonium interactions for the dispersion of CNOs in water using biocompatible polymers. For this, CNOs were functionalized by reaction of diazotized 4-aminobenzo-18-crown-6. In the presence of biocompatible polymers containing pendant amino groups, such as aminated carboxymethyl cellulose ($CMC\text{-}NH_2$) and poly-L-lysine, the modified CNOs

formed dispersions in water at acidic pH. Precipitation of the CNO-18C6 under basic conditions and in the presence of excess K^+ cation indicates that the ammonium/crown ether interactions are the major driving force in the formation of the CNO dispersions.

Chapter 4 is dedicated to the modification of glassy carbon electrodes with CNOs followed either by covalent functionalization of ortho-aminophenol through in-situ electrochemical grafting of diazonium salt or by physical adsorption of thionine. These electrodes were used for the detection of nitrite and ascorbic acid at different potentials, simultaneously. DC amperometry measurements were used to probe the electrocatalytic capability of the modified surface of GCE/CNO/oAP and GCE/CNO/thionine for the detection of nitrite and ascorbic acid. Nitrite was detected at potential 750mV higher than the potential of ascorbic acid at 200mV. Both results showed excellent enhancement in the current response and lower limit of detection as compared to GCE/oAP and GCE/thionine controls.

In **Chapter 5**, CNO-containing glassy carbon electrodes were modified with diazonium salts bearing terminal carboxylic acid and maleimide groups. The modified electrodes were used for the amperometric detection of a model DNA target sequence associated with the human papillomavirus in both synthetic sequences and clinical samples. The analytical parameters of the developed biosensors were compared with glassy carbon electrodes without CNOs. In both cases, the incorporation of CNOs resulted in an enhancement in sensitivity and a decrease in detection limits ascribed to a combination of large surface areas and enhanced electron transfer properties of the CNO-modified electrodes. These results offer promise for the construction of other CNO-based biomolecule detection platforms with enhanced sensitivities.

Finally, **Chapter 6** describes the construction of an immunosensor platform based on CNO-modified electrodes employing a sandwich assay. Electrodeposited diazonium chemistry served to immobilize whole antibodies on the surface of CNOs. As model targets immunoglobilin G (IgG) and carcinoembryonic antigen (CEA) were selected and we also explore different labels such as HRP and ALP-modified antibodies. The presence of CNOs enhanced the sensitivity of the assay by a factor of 2 and the substitution of HRP for ALP as label of the secondary antibody decreased the LOD by a factor of 6. Therefore, the incorporation of CNO had a positive effect in the biosensor performance and are thus promising materials in immunosensor development.

Overall, the presented thesis has contributed to the understanding of the chemistry and properties of carbon nano-onions and the development of novel applications of these materials in the field of surface modification and biosensing. These nanomaterials were prepared in a controlled manner by nanodiamond annealing and were deposited on electrode surfaces by simple casting methods. They were successfully dispersed in aqueous solution using a supramolecular strategy and implemented in detection systems for small molecules, proteins and DNA with enhanced sensitivity and improved analytical properties. Although some of the biosensor platforms developed in this work were not fully optimized, it is clear that the use of carbon nano-onions in biosensing has many promising advantages over other nanomaterials. Our results also open up new possibilities for many other applications such as photovoltaics or molecular electronics in which the interfacial and electronic properties of carbon nano-onions can play an important role in the fabrication and performance of these devices.

Chapter 1

Introduction

1.1 Carbon nanomaterials

The fascinating world of carbon nanomaterials, with their significant roles in the developing world of sensor technology, is being widely investigated and becoming one the hottest topics in materials research nowadays. Their diversity and ubiquity in nature makes them attractive candidates for the constructions of novel devices with improved analytical performances. Since their reactivity is limited by a poor solubility, they may be difficult to incorporate in devices or show poor compatibility with biomolecules. To overcome these problems, several functionalization and modification strategies have been investigated. Some of these well-known carbon nanomaterials will be described in the following sections.

Fullerenes were the first synthesized carbon nanomaterials using vaporization of graphite by a focused pulse laser [1]. This zero-dimensional (0D) carbon form with distinctive clusters of *n* carbon atoms (C_n) in a cage structure such as the famous C_{60}, gathered intense research interest after its discovery. Nowadays, it is the most investigated molecule due to their properties, reactivity and applications as reviewed by Delgado et. al [2]. The electrochemical properties of fullerene and their derivatives are extensively discussed in the review of Sherigara et. al [3], probing that the future of modified sensing electrodes with fullerenes would be a great advance in research especially as electrocatalysts and sensors for various chemical and biochemical reactions. For example in 2000, Gavalas and Chaniotakis [4] described the first C_{60}-mediated amperometric biosensor for glucose. The C_{60} was adsorbed on a porous

carbon electrode and operated as an efficient mediator for electron transfer by lowering the optimum operating potentials. In addition, higher loads of C_{60} in the surface exhibited faster response time, improved sensitivity and dynamic range. Recently, Lanzelotto et al. [5] prepared a novel nanostructured enzymatic biosensor made of gold nanoparticles, fullerenols and laccase assembled layer-by-layer in a gold electrode. The biocatalytic biosensor was preliminarily used for the detection of polyphenols such as gallic acid, which showed a rapid amperometric response and high stability of the surface.

In the two decades after their discovery, carbon nanotubes (CNTs) were also widely exploited and subsequently produced in large scale using arc-discharge evaporation techniques [6]. CNTs are one-dimensional (1D) materials that can be classified into single-walled CNTs (SWCNTs), the simplest form, and multi-walled CNTs (MWCNTs), ranging from 2 to *n*-th rolls of graphitic layers wrapped around together to form a cylindrical tube. The perfectly aligned lattice of sp^2 hybridized carbon atoms in a cylindrical shape give CNTs a high conductivity, excellent strength and stiffness [7]. The progress and latest developments in the bulk synthesis and applications of CNTs and their influence in the future of nanomaterial industry and engineering were recently described by Huang et al. [8]. Other examples of CNT and fullerene applications in biological and environmental technology, electronics, optoelectronics and chemical sensors can be found in the literature [9-12].

With the advent of graphene, none thought that a two-dimensional (2D) sp^2 carbon layer prepared from graphite would produce a fascinating material that is as durable as diamond, single atom thick, more conductive than copper, and the most promising nanomaterial nowadays. Graphene was first described and isolated by Geim's group [13] in 2004 by an exfoliation method using a simple adhesive tape. Consequently, the

rapid evolution of powerful equipment in nanotechnology paved the way for the characterization of graphene and other methods to produce it led to the understanding of its unusual properties such as electrochemical, electronic and optical properties [10, 13-16].

Although diamonds have been used and known for a long time dating back to pre-history, its "new" form, nanometric in size, called nanodiamonds also meant a significant breakthrough as material for nanotechnology due to their atypical properties when compared to the bulk material. They can be naturally found, even in the space [17-19] but became of wider interest when first produced in the laboratory by detonation [20, 21]. The structural properties and applications of nanodiamonds are described in this recently published review article [22].

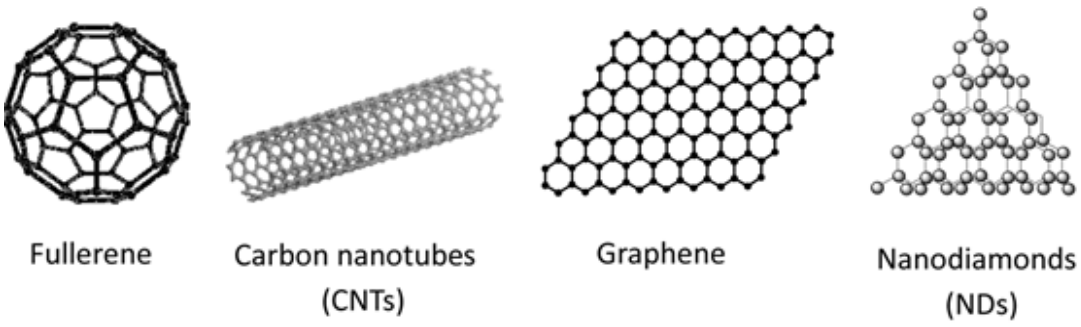

Figure 1.1 Graphic representation of the most common carbon nanomaterials [23].

1.2 Carbon Nano-onions

Carbon nano-onions (CNOs) also known as multilayered fullerenes, were discovered in the same period as CNTs but remain away from the limelight of other popularly investigated nanocarbons. Not as trendy as other carbon nanomaterials cited previously, CNOs also show very attractive properties and are expected to impact the nanotechnology world in the future.

1.2.1 Preparation, Synthesis and Characterization

In 1992, Ugarte [24] exposed an electron beam on amorphous carbon, which began to graphitize and with the time curled up until to form a closed circle. He called it onion-like graphitic particles, now known as carbon nano-onions or onion-like carbon. This is also the first time that CNOs were made from amorphous carbon as starting material by exposing it to irradiation. Several attempts on the production of CNOs using this technique were tried with some modifications like incorporating Al nanoparticles [25]. Furthermore, many other methods of synthesis have been tried such as arc discharge, chemical vapor deposition (CVD), radio frequency (RF) and microwave plasma, carbon ion implantation, thermolysis and template synthesis. In subsequent paragraphs each of these methods will be briefly described.

Basically, arc-discharge is an old technique for producing nanomaterials that uses two high-purity graphite electrodes as the anode and cathode, usually submerged in a special media. Direct current is passed through the two separated electrodes under inert gas atmosphere until the graphite vaporizes. Sano et al. [26] were the first that made use of this simple method for producing a large quantity of spherical CNOs collected from the water surface at a production rate of 15.9 mg/min of CNOs with approximate size averages of 4-36 nm in diameter, as viewed in high resolution transmission electron microscopy (HRTEM). The same group proposed a formation mechanism of CNOs by this technique [27] while Xu and his group [28] made several attempts to use the arc-discharge to synthesize CNOs in different media such as liquid benzene or under aqueous solution with addition of catalyst and the combination of chemical vapor deposition and arc discharge. CNOs produced from metal catalysts usually form M@CNOs clusters, in which metal atoms from the catalyst are encapsulated on CNO frameworks. However, neither of these methods produced size homogenous and pure

CNOs, since the same method was also used for the synthesis of CNTs and therefore other carbonaceous impurities can be found. Recently, a new optimized under-water arc-discharge method designed to produce CNOs with high purity and narrow polydispersity has been investigated by Borgohain et al. [29]. In their report, they were able to control the growth of CNOs to a size about 20-50nm under optimized conditions of the equipments and developed an efficient purification method to screen-out CNOs only. The electrochemical properties of the synthesized product were also studied by cyclic voltammetry based on the redox peak separations and heterogenous electron transfer rate of some electroactive species. The results showed higher and faster electrochemical performance as compared to bare glassy carbon electrode.

Chemical vapor deposition involves three stages for the synthesis of thin solid films, typically substrate heating/conditioning, growth with precursor gases and substrate cooling. Usually CNOs produced in this method are metal-containing materials since the process requires catalysts such as Fe, Co, Ni and/or their combinations. Some of the precursor gases that act as carbon sources are methane, acetylene and cyclohexane vapor [30, 31]. Lately, efficient methods were reported by Zhang et al. [32] to synthesize hollow CNOs at controllable size. Initially, they used CVD technique with Fe-Ni alloy as catalyst and the growth started under CH_4/N_2. The product obtained after cooling was CNOs-encapsulated with Fe-Ni alloy, which was further subjected to high temperature annealing leading to the escape of the metal located in the center of the particle producing a hollow CNO in which the mean size was approximately 20 nm.

Liu and co-workers [33-35] suggested that radio frequency and microwave plasma, a technique used in synthesizing other carbon nanomaterials, can be also utilized in producing CNOs from coal by changing some parameters in the process. Coal as starting material was exposed to an electromagnetic field of radio frequency or

microwave at low pressure of inert gas acting like a plasma. The plasma in the chamber is enough to break any bonds structure in coal but not all, especially for aromatic structures, and most of the time they form pentagonal rings favorable for fullerene formation. However, there are some impurities in coal such as Si, Al and Fe acting as catalyst believed to help the formation and growth of CNOs.

Carbon ion implantation was first introduced by Cabioc'h group in 1995 [36] and the method has been continuously optimized until today [37-39]. The implantation procedure for synthesizing CNOs is based on the introduction of carbon ions in thin films of silver or copper onto different substrates at high temperatures. By varying the synthesis conditions, the particle diameter can be tuned from 3 up to 30 nm. Thermolysis is also a heating technique that was developed by Bystzejewski et al. [40] for the synthesis of CNOs without using catalysts. Sodium azide (NaN_3) and hexachlorobenzene (C_6Cl_6) were mixed homogenously in a mechanical shaker, and then loaded in a quartz crucible in a calorimetric bomb. The compounds were decomposed by heat inside the chamber producing CNOs of large diameter (30-100 nm) along with other impurities that were removed in a purification step. Another way to synthesize CNOs was thermal reduction of a mixture of glycerin and magnesium at 650˚C inside a stainless steel autoclaveto yield CNOs of a diameter of 60-90 nm [41]. Interestingly, a simple and easy gram-scale synthesis of CNOs by continuous explosion of naphthalene vapor onto a glass or ceramic substrate was probed. The carbon material collected in the substrate was then purified by heating under vacuum. The process yields 20% carbon recovery with the size of the CNOs to have an average of 50 nm with 50 shells [42].

The methods mentioned previously produce big CNOs until Kuznetsov's group [43] tried the precise production of homogenous and small onions approximately consisting of 5-8 carbon shells by annealing ultra-dispersed nanodiamonds in vacuum at high

temperatures. The progress of transformation begins at the outer surface and moves to the inward of the bulk nanodiamond crystal (Figure 1.2-1). The final diameter sizes of CNOs will depend on the initial size of the nanodiamond. So far, this is the only technique that has the potential for industrial application due to the yield close to 100%. A detailed evaluation of the early stage transformation of nanodiamond to graphitic CNOs using thermal annealing (Figure 1.2-2) under inert atmosphere were investigated recently by Cebik et al. [44].

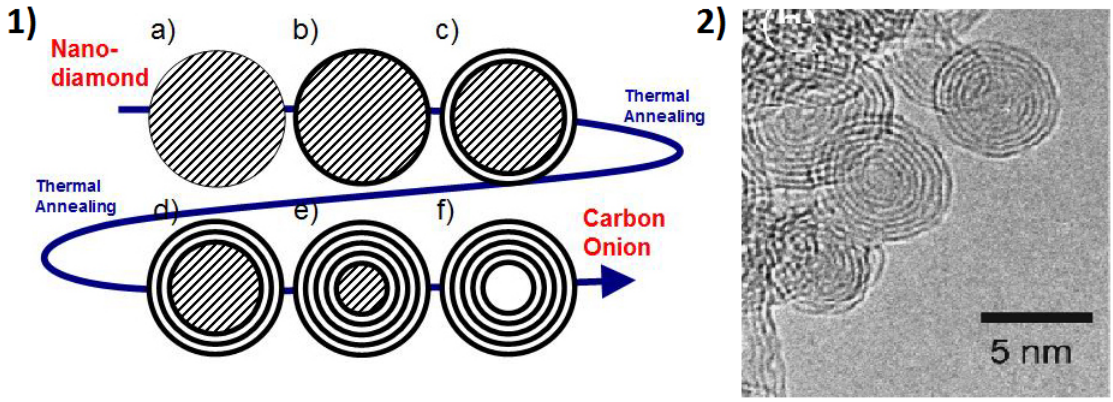

Figure 1.2: 1) the structural changes of nanodiamond during thermal annealing [44] 2) a typical HRTEM image of synthesize CNO in this process [45].

To improve the graphitic layer of CNOs produced by high temperature annealing of ultradispersed nanodiamonds, a post-modification by annealing at low temperature around 450˚C in the presence of carbohydrates such as glucose or starch as carbon precursors has been employed [46]. The synthesized product exhibited an increased surface area due to added graphitization of the surface of CNO as evidenced by Brunauer-Emmett-Teller (BET) static nitrogen adsorption technique. Besides, there was an improved electrochemical property of the CNO films when post-modified as revealed in voltammetric measurements.

1.2.2 Characterization of synthesized CNOs

Several techniques have been employed to characterize the synthesized CNOs such as High-Resolution Transmission Electron Microscopy (HRTEM), which is useful to visualize the structural properties and formation of CNOs. In this section we briefly review other important techniques focusing mainly in the transformation of nanodiamonds to CNOs.

Raman spectroscopy is also very useful in such a way that it will distinguish the graphitic structure of CNOs. There are two distinct Raman bands related to the structural features of carbon materials: a) the presence of the D-band at around 1350 cm^{-1} indicates the structural disorder present in the surface of the particle due to the presence of sp^3 carbons and this band increases when CNOs undergoes functionalization whilst b) the presence of the G-band at around 1580 cm^{-1} corresponds to the graphitic layer of the surface or sp^2-hybridized carbon networks. The G-band is very helpful to differentiate nanodiamonds from CNOs due to the change in hybridization from sp^3 to sp^2, respectively [45, 47].

Another valuable technique to characterize CNOs is X-ray diffraction (XRD). Nanodiamonds exhibit a main characteristic narrow peak at ~43˚ which come from the (111) planes of cubic diamond (sp^3). On the onset that nanodiamonds are transformed to CNOs, this peak decreases or broadens and a new peak appears around 25˚ due to the formation of (002) planes of graphitic (sp^2) carbon, which is also associated with that of crystalline graphite [45, 48].

On the other hand, the conductivity behavior of CNOs has been analyzed in the works of Hou et al. [49]. Using ultrahigh vacuum AFM and scanning tunneling microscopy (UHV AFM/STM) they showed that the electrical properties of CNOs were between graphite and single-shell fullerenes. In contrast, the electronic structure of

CNOs was analyzed using core-level and valence-band photoemission spectroscopy by intercalation of CNOs with potassium. This technique revealed a non-rigid shift of valence-band states which means that CNOs behave as small graphite crystals and display bulk-like behavior rather than molecule-like as large fullerenes do [50]. The optical properties of CNOs have also been described extensively using several techniques [51-54].

1.2.3 Functionalization of CNOs

Like any other carbon nanomaterials, CNOs are highly hydrophobic and tend to aggregate due to strong intermolecular interactions such as van der Waals forces [26]. To overcome this problem, surface modification is the method of principal choice to improve dispersibility and other properties (Figure 1.3).

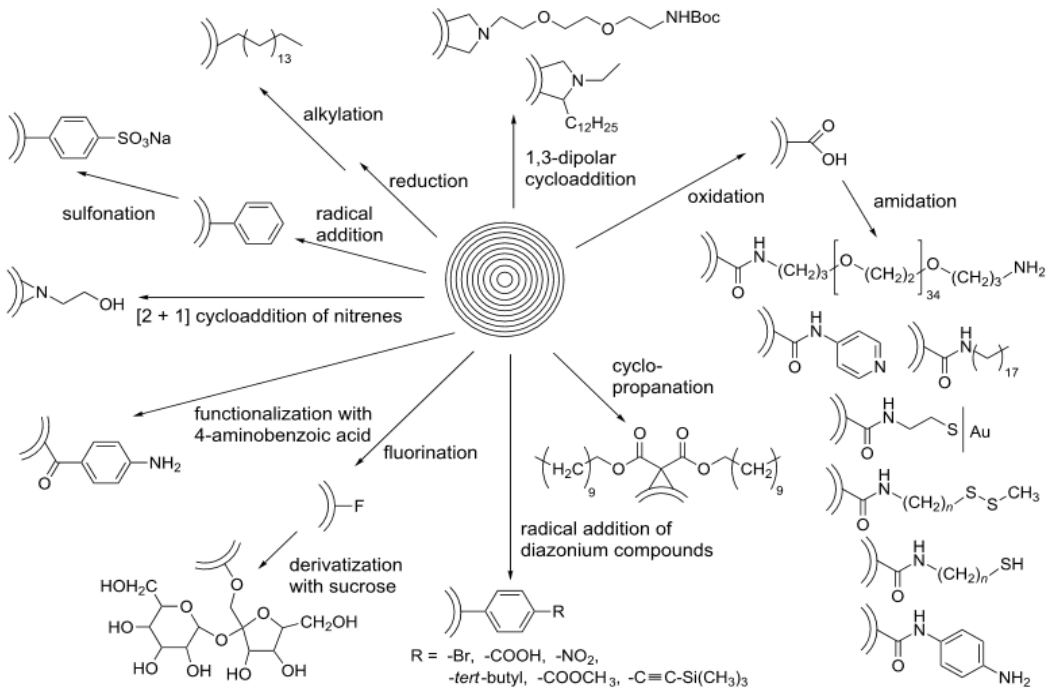

Figure 1.3: Functionalization of CNOs [55].

Many years after their discovery, the covalent functionalization of CNOs was reported in 2003. Pratos' group [56] used CNOs from the raw soot produced by arc-

discharge for organic functionalization. This raw soot was suspended in a mixture of an aminoacid and paraformaldehyde using toluene as solvent and refluxed for several days. The successful functionalization of CNOs was analyzed using ^{1}H NMR spectroscopy, MALDI mass spectroscopy and UV-vis- NIR spectroscopy. The HRTEM studies revealed their sizes ranged between 60-300nm, typically large CNOs, also the presence of amorphous carbon in not dissolve part of the solution was determined. The modified CNOs in this process were used to characterize the optical properties of CNOs for possible use as broad-band optical limiters.

Echegoyen and co-workers have made a significant contribution in the functionalization of CNOs and many of the works in this area are associated with his group. In an early report, his group not only made an attempt to functionalize arc-discharge prepared CNOs but also made a significant advance in the purification of the raw soot derived from the process [57]. Three different functionalization reactions were used to modify the surface of purified CNOs. The CNO-containing-soot powder derived from the water arc-discharge was subjected to a successive process of purification by thermal annealing, microwave heating, acid and supercritical water washing to remove the unwanted impurities from the starting material. Thermogravimetric (TGA) and TEM experiments were used to follow the purification showing a high yield of CNOs in the sample. Due to the acid treatment during the purification the surface of the CNO were modified with carboxylic acid groups, which facilitate further derivatization. The PEGylation of CNOs using diamine-terminated oligomeric poly (ethylene glycol) produced the first water-soluble CNOs. In the amidation of CNOs, they employed two reaction process, the solid state reaction and microwave reaction for rapid amidation, both yielding good results despite the small differences on the TGA results.

The vast majority research in functionalization of CNOs for the years after Pratos' report were carried out using large size of CNOs produced from arc-discharge which have several drawbacks, especially on the difficulty of chemical reactivity on the surface of CNOs. In an effort to have an in-depth study on the properties of CNOs produced by different methods, Palkar et al. [58] compared the methods of nanodiamond annealing and arc-discharge based on the reactivity of the resulting CNOs. Three different kinds of chemical functionalization were tested. The cycloaddition reaction using [2+1] Bingel-Hirsch cyclopropanation was only successful in CNOs prepared by annealing. Second was a free radical addition in which CNOs were refluxed with benzoyl peroxide as radical source in toluene, which also worked out only for annealed CNOs. The last method was the oxidation of surface defects with introduction of carboxylic acid groups in refluxing nitric/sulfuric acid. TEM and TGA measurements reveal that CNOs derived from annealing can be easily oxidized compared to the harsher treatment needed for the oxidation of arc-discharge CNOs..

The first radical addition of a conjugated polymer to purified CNOs via reaction with bis-*o*-diynyl arene (BODA) has been recently reported [59]. CNOs and BODA were ultrasonicated and heated in N-methyl-2-pyrrolidone (NMP) under pressure to yield CNO-BODA copolymers. The products were analyzed by different characterization techniques like gel permeation chromatography (GPC), TEM, TGA, Raman spectroscopy and X-ray photoelectron spectroscopy (XPS). On the other hand, supramolecular complexes of CNOs modified with pyridyl units have also been described [60]. CNOs were oxidized in an acid mixture to generate reactive carboxylic group followed by amidation using 4-aminopyridine. The pyridyl/CNO was soluble in water and was characterized by TEM, NMR, UV-vis, Raman spectroscopy and TGA showed modification of samples as compared to starting material. This modified

pyridyl/CNO was used to construct a self-assembled nanoporous network by complexation with the central zinc atom in a Zn porphirin and the interaction has been confirmed by electrochemistry and NMR spectroscopy.

Zhou et al. [61] introduced a facile and direct organic functionalization of multilayer fullerenes using [2+1] cycloaddition of different nitrene derivatives followed by in-situ grafting strategies of polymerization. This chemistry was used to introduce hydroxyl groups on CNOs using azidoethanol or bromide using azidoethyl 2-bromo-2-methyl propanoate modified surface. The modified CNOs exhibited increased solubility in organic solvents and aqueous solution. Interestingly, CNO-OH showed fluorescence emission characteristics in aqueous solution. Furthermore, the modified CNOs were utilized as microinitiators to conduct surface–initiated ring-opening polymerization (ROP) or atom transfer radical polymerization (ATRP) of in-situ polymerizations of ε-caprolactone or polystyrene. The modifications after the polymerization were characterized by ^{1}H-NMR, SEM, TEM and AFM.

A unique and versatile strategy of functionalization on CNOs was performed by Flavin et al. [62]. Initially, in-situ generated diazonium compounds were reacted onto the surface of CNOs producing different kinds of functional groups such as bromides, benzoic acids, tert-butyl groups, nitro groups, methyl esters and trimethylsilyl (TMS) acetylenes in modified CNOs. Pristine CNOs were suspended in DMF by sonication and the aniline derivative of different functionalities and isoamyl nitrite were subsequently added into the mixture in a stirring condition in an inert atmosphere. The product was collected by centrifugation, dried, then characterized using TGA and Raman spectroscopy. The repeated uses of these reactions further increase the degree of functionalization thus leading to an increased dispersability of CNOs. They further proposed the use of “click” chemistry in which the CNO-TMS acetylide sample was

first deprotected then coupled with zinc triphenyl azidophenyl porphyrin. The diazotization chemistry described above on CNOs was used to incorporate fluoresceinamide-based fluorophores [63] or NIR-emitting aza-boron-dipyrromethenes [64] through amidation onto the surface of benzoic acid modified CNOs and a meso-phenol-substituted borondipyrromethene (BODIPY) fluorophore by esterification [65]. All of the previously mentioned products were applied in cell imaging. Additionally, there was another report on the use of modified benzoic acid/CNO as a template for in-situ chemical oxidative polymerization of polyaniline (PANI) thus creating a coated PANI-CNO [66]. The product has been used to study the vibrational spectroscopic property of the material using infrared absorption and Raman spectroscopy.

Another interesting modification of CNOs under reactive conditions were done by Liu et al. [67]. CNOs were produced by inductive heating of carbon black to give particles of 50-100 nm in diameter and high purity. Fluorination was carried out in a custom-built reactor, CNOs sample loaded into a Monel-foil boat, placed inside the reactor, sealed and purged by continuous flow of inert gas at room temperature then heated at different temperatures. After 2-3 hours, samples of fluorine and hydrogen were introduced separately in the reactor to initiate the reaction. The process was kept for 6 h, thereafter the reaction has been stopped and the products were collected. Various characterization techniques have been employed such as FTIR, SEM/EDX, XRD, XPS, TGA, TEM, Raman and UV-Vis spectroscopy to follow the successful fluorination of the modified-CNOs. Moreover, the authors made outstanding claim that treating the fluorinated-CNOs with hydrazine would defluorinate and “heal” the broken graphene layers in the structure.

The need for “green” technology in functionalizing CNOs, especially for oxidation, has been an urgent call for researchers in which no hazardous chemicals are

involved for improving solubility and dispersion of CNOs in aqueous solution. Ozonolysis is the suggested way to oxidize CNO in a mild but effective way to introduce the oxygen-containing functional groups on the surface of CNO. This process does not damage the structure of CNOs thus improving its properties like increase in hydrophilicity, wettability and conductivity for enhanced performance of aqueous type EDLC [68].

A single molecule CNO structure covalently functionalized via amidation reaction using 2-amino-1-ethane methyl sulfide or 3-amino-propane methyl disulfide to yield CNO-(CONH-$(CH_2)_n$-SH)$_m$ was used to study the conductivity properties of CNO. Their methodology was to entrap the sulfide-terminated CNO between a gold surface and a scanning tunneling microscopy (STM) tip also made of gold and then measure the conductance using the STM-based molecular junction approach, in which the current-distance curves of the scanned surface have been monitored. Unexpectedly, the electrical conductance of CNOs were the same order of magnitude when compared to C_{60} due to the chemical linker attached to the CNOs not directly in-contact between the electrodes [69].

Alkylation of CNOs by a reductive method using Na-K alloy has been investigated by Molina-Ontoria et al. [70]. The incorporation of hexadecyl chains on the surface of CNOs were carried out in two steps. Firstly, CNOs were reduced with a solution of Na-K alloy in 1,2-dimethoxyethane (DME) followed by alkylation with the addition of 1-bromohexadecane. The synthesized CNO-C_{16} showed high solubility in organic solvents enabling ^{1}H-NMR analysis. Additionally, the covalent attachment of hexadecyl groups was further analyzed with FTIR, HRTEM and Raman spectroscopy. The alkylation reaction could be reversed by heating CNO-C_{16} at 415˚C.

Non-covalent incorporation of CNOs in composites is also becoming popular especially for exploring the inherent properties of CNOs and their possible applications, for examples, in supercapacitors, sensors and nanomedicine. Kuzhir et al. [71] reported the electromagnetic absorbing properties of a novel composite material made from CNO and binding matrices such as polymethylmetacrylate (PMMA) and polydimethylsiloxane (PDMS) in microwave frequency range. Other composites based on CNOs and poly(diallyldimethylammonium chloride) (PDDA) or chitosan have been prepared. The PDDA/CNO or chitosan/CNO composites were deposited as films on glassy carbon electrodes and showed a typical capacitive behavior as well as excellent mechanical and electrochemical stability [72]. The electrochemical properties of poly-aniline and (poly(3,4-ethylenedioxythiophene):poly(styrenesulfonate) composites were also studied [73] [74].

Recently, the non-covalent functionalization of CNOs with poly(4-vinylpyridine-co-styrene) (PVPS) and poly(ethylene glycol)/polysorbate 20 (PEG/P20) have been utilized for further incorporation of other moieties [75]. Pristine CNOs mixed with PVS polymers were used as template to integrate thiol-containing compounds like 3-mercaptopropionic (MPA) or 2-mercapto-4-methyl-5-thiazoleacetic (MMTA) acids to generate a carboxyl terminated group onto the surface of CNOs. In the case of modified CNO with PEG/P20, CNOs were oxidized prior to the dispersion in a DMF/EtOH mixture followed by the addition of PEG/P20 to form layers of polymers onto the surface of CNOs that were used to interact with quercetin, a flavonoid compound. In other group, CNOs have been oxidized prior to the impreganation with $RuO_2.xH_2O$ for the development of composites for supercapacitor electrodes [76].

Finally, our group recently prepared highly solubilized cyclodextrin-modified CNOs by supramolecular interactions in aqueous solutions [77]. Oxidized CNOs were

further functionalized with aminated β-cyclodextrin (β-CDs) units by amidation. The supramolecular assembly occurs when a ferrocene-appended dextran (Fc-Dex) polymer was added into the βCD/CNOs suspension in which βCD act as hosts and the ferrocene group of the polymer as guest. The prepared supramolecular structure of βCD/CNO showed a good solubility in aqueous solution.

1.2.4 Applications

The modification and incorporation of moieties on the surface of CNOs enable the possibility of their wide application on many areas of research. Below we describe some limited examples of the exploitation of CNOs in different fields.

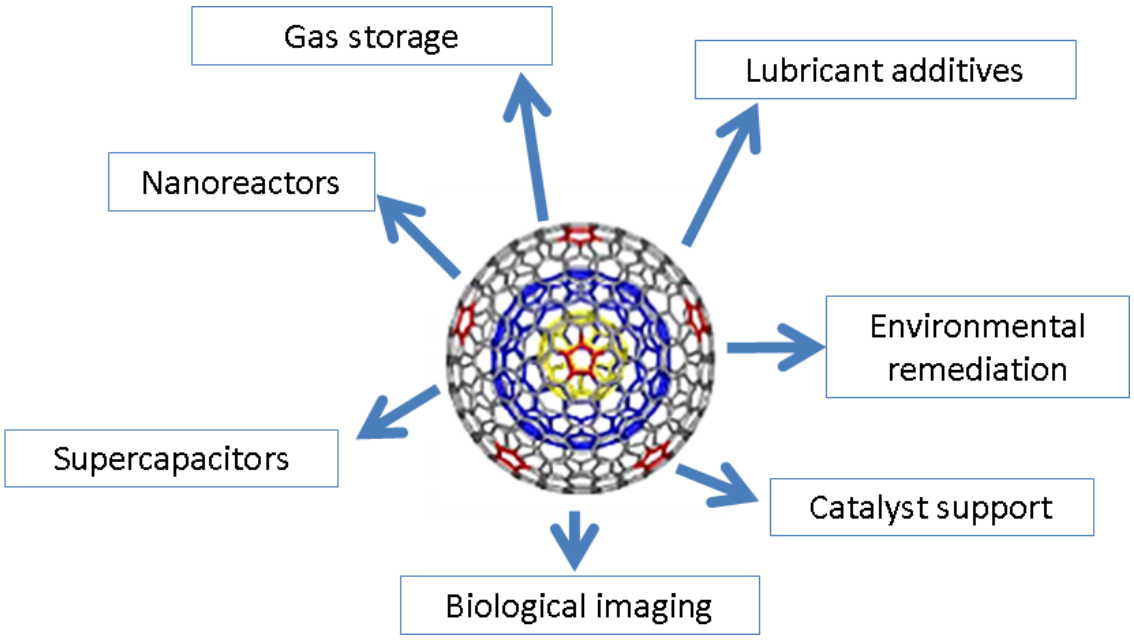

Figure 1.4: Current applications of CNOs.

Electronics/Electrochemical applications

Electrical double layer capacitors (EDLC) are storage devices with the capacity to store charges at the interface between an electrode and tan electrolyte [78, 79]. Carbon materials, such as activated carbons, have been incorporated in electrodes for supercapacitor applications due to their high specific surface area, porosity, high electrochemical conductivity and stability.

In 2007, Portet et al.[80] investigated for the first time the use of CNOs in EDLC along with nanodiamonds, carbon black and multi-walled carbon nanotubes. The results indicate excellent capacitance retention and high discharge rate of the CNO-modified devices due to increase in conductivity. Therefore, small resistance and the modification steps that cause defects in the surface of CNOs improved the ion transport in open-surface systems. Afterwards, Bushueva et al. [81] investigated the EDCL performance of CNOs with water electrolytes. The working electrodes used were made up of composites of CNOs powder synthesized by vacuum annealing at 1800-1900 K of detonation nanodiamonds and polytetrafluoroethylene (PTFE) and displayed specific capacitances of 70-100 Fg^{-1} in acidic electrolytes (1M H_2SO_4), better than in an alkaline electrolytes. Likewise, they also claimed that there is a correlation between specific capacitance, conductivity, specific surface and annealing temperatures of nanodiamonds. Pech et al. [82], on the other hand, prepared microsupercapacitors made up thick layer (7 μm) of nanostructured CNOs deposited onto interdigital gold electrodes utilizing an electrophoretic deposition technique (EPD). The capacitance performance of the CNO-based microsupercapacitors was four orders of magnitude higher than that of electrocatalytic capacitors and the discharged rates exhibited three orders of magnitude higher than conventional supercapacitors. Additionally, the CNO

particles have high surface-to-volume ratio and, used directly in electrodes without binders and polymer separators, enhanced the performance of the microsupercapacitors.

In an effort to study the factors influencing supercapacitor performance such as structure, physical and electrical properties of CNOs and nature of electrolytes, McDonough and co-workers [83] extensively and systematically investigated these parameters. Interestingly, their experimental results on CNO-electrolyte interfaces were supplemented by molecular dynamics (MD) simulations for better understanding of the interactions and migration of ions in the surface of CNOs. The results showed that CNOs capacitive performance exceeds other carbon materials at high charge/discharge rates and CNOs produced at annealing 1800˚C had the highest conductivity and capacitive performance at high rates.

Gao's group has studied the enhancement of the porosity of the surface of CNOs by chemical activation using KOH to efficiently improve the specific area for ion-accessible outer shells [84]. CNOs were prepared by combustion using laser resonant excitation in open air of ethylene molecules followed by KOH activation and the Brunauer-Emmett-Teller surface area and pore volume were measured by N_2 adsorption. Based on their findings, the activation of CNOs with KOH improved the porosity and hydrophilicity of the CNOs thus having a high charge/discharge rates as compared to non-activated CNOs. In another study, Borgohain et al. [76] oxidized CNOs followed by addition and precipitation of RuO_2 to form composites can increase the capacitance of the electrodes to 334 Fg^{-1} as compared to pure CNO materials. Moreover, using other kinds of composites based on CNOs can be also useful for the applications in rechargeable lithium batteries as anodes with improved capacitance performance materials [85-88].

Catalysis

The need for increased global energy consumption and high yield efficiency productions of important materials in industries calls for new catalytic materials to address these problems. Nanoparticles are ideal candidates for this kind of applications due to their high surface area, which means that more catalytic reactions can occur at the same time resulting in an increased catalytic activity.

CNOs obtained by annealing nanodiamonds yield small particles which have potential use for this area. Keller et al. [89] presented for the first time the potential application of CNOs in catalysis, particularly in the oxidative dehydrogenation (ODH) of ethylbenzene to styrene. The results revealed a 92% conversion level after an activation period of 2 h and 62% stability of the styrene product yield, which was better than K-Fe catalysts or other carbon materials. Furthermore, a follow up study of this group about the catalytic behavior of CNOs compared to ultradispersed nanodiamonds with special attention to the sp^3 and sp^2 structures of these materials for ODH catalysis was carried out [90]. It was found that CNOs selectively transformed ethylbenzene to styrene due to the sp^2-rich surface aside from the presence of carbon-oxygen bonds formed as a result of the annealing and oxygen pretreatment giving a higher number active of surface site for styrene formation.

On the other hand, Xu et al. [91] synthesized a Pt/OLFs catalyst by impregnation-reduction method for electro-oxidation of methanol in direct methanol fuel cells (DMFCs). The Pt/OLFs showed higher catalytic activity as compared with Pt/Vulcan Xc-72 by about 20% as measured by cyclic voltammetry for methanol electro-oxidation.

Later, Santiago et al. [92] tested a new method to impregnate Pt into the surface of CNOs with higher loading and smaller Pt particles. Rotating disk-slurry electrode (RoDSE) technique allowed the preparation of a Pt/CNO catalyst as a "greener" way to electrodeposit Pt into the surface of CNO. The highly dispersed catalyst nanomaterial prepared by this method showed significant thermal stability in TGA analysis, lower onset potential for the electrooxidation of methanol as compared to Pt/Vulcan.

Biological Applications

The concern of using new nanomaterials for biological applications must be evaluated in terms of biocompatibility and toxic effect. CNOs, as a relatively new material, are not exempted of these concerns considering the results obtained from the cytotoxic levels of other allotropes of carbon nanomaterials such as CNTs and fullerenes [93, 94].

The first report on the toxic effects of CNOs on human skin fibroblast were reported by Ding et al. [95]. Based on their findings, large CNOs with diameters of 30 nm produced from arc-discharged showed less adverse effects, particularly on the induced stress of the material on cells as compared with MWCNTs. Recently, CNOs prepared by the same method and with similar size were tested for potential adverse effect on the cardiovascular system [96]. After taking all considerations and experimental results, they concluded that unmodified CNOs can induce DNA damage and apoptosis in human umbilical vein endothelial cells (HUVECs) due to the generation of reactive oxygen species (ROS).

Small CNOs (5-6 nm), synthesized by annealing of nanodiamonds, were used for the first time by Luszczyn et al. [97] to covalently bind biomolecules. Initially, the biocompatibility test of oxidized CNOs and PEGylated CNOs were exposed to

fibrolasts for 4 hours. They found that there was no cytotoxic effect and these particles were thus viable for biological applications. In another report by Giordani et al. [63], small CNOs functionalized with fluorescein showed weak inflammatory response and low cytotoxicity in vitro and in vivo compared to CNTs. Moreover, this group made several attempts to use other type of cells like MCF-7 cells [64] and HeLa Kyoto [65] for biological imaging and did not notice any significant cytotoxic effect.

Biological imaging using CNOs has also been an interesting topic for researchers since, intrinsically, CNOs have inherent optical properties as mentioned earlier. Ghosh et al. [98] synthesized CNOs by carbonizing wood wool by pyrolysis followed by surface oxidation to form non-toxic water soluble CNOs (30 nm diameter) that were used for imaging *Drosophila melanogaster*. These water-soluble CNOs exhibited fluorescent properties and, when fed to *D. melanogaster*, it was possible to image the life cycle of the organism from egg to adulthood using fluorescence spectroscopy. Additionally, the organism excretes the fluorescent CNOs without adverse effects. Subsequently, after the success of their work, they were able to apply this in *in vivo* studies of *Escherichia coli* and the small nematode *Caenorhabditis elegans* [99].

Detection systems

Oxidized CNOs have been covalently attached onto a self-assembled layer of cysteamine on gold by amidation, followed by the immobilization of biotin, also via amidation, to form a complete layer of Au/thiol/ox-CNOs/biotin [97]. Subsequently, the layer was utilized to monitor the interaction of biotin and immobilized avidin in the surface using surface plasmon resonance (SPR) spectroscopy. The same group has evaluated CNO composites formed with poly(diallyldimethylammonium chloride

(PDDA) for the electrochemical determination of dopamine in the presence of ascorbic acid and uric acid in solution [100]. The film of PDDA/CNO composite was coated on glassy carbon electrode and then examined for the ability of the modified surface to detect dopamine in a simultaneous assay. The results showed a good selectivity and sensitivity for dopamine in the range between 5×10^{-5} to 4×10^{-3} M. To the best of our knowledge, these are the only studies devoted to the development of detecting systems using CNOs up-to-date.

Other applications

CNOs tribological properties, such as an anti-wear and friction reducing material, make them interesting additives for lubricants [101-104]. CNOs have also been used in environmental remediation by Li and coworkers [105], who found a high sorption capacity for heavy metal ions like Pb^{2+}, Cu^{2+}, Cd^{2+}, Ni^{2+} and Zn^{2+} and a 10-fold higher capacity than that of fullerene C_{60}. Other applications include support for nanoparticle growth [106], gas storage [32] and nanoreactors [107].

1.3 Thesis Objectives

The interest of the researches nowadays for the continuously growing demand and search for novel materials in nanoscience and nanotechnology has make them explore new horizons in materials chemistry. As described in the preceding sections, CNOs are attractive materials with defined structures and remarkable properties. Although up to date they are not commercially available products, it becomes apparent that they can be prepared in large amounts and the possibility to chemically modify their surface to fine tune their properties gives them widespread potential applications.

The overall objective of this thesis is thus to explore strategies for the preparation and modification of novel nanoarchitectures based on CNOs.

To achieve this general objective, we have focused on the following aspects:

1. The preparation and characterization of CNOs by nanodiamond annealing, their characterization and functionalization using RF plasma
2. The obtention of CNO dispersions in water based on supramolecular interactions between crown ether appended CNOs and ammonium containing polymers
3. The immobilization of CNOs on electrode surfaces, their post-functionalization by electrografting of diazonium salts and their electrochemical characterization
4. The application of the CNO modified electrodes bearing reactive functional groups in sensors and biosensors, in particular in the detection of small molecules (ascorbic acid, nitrite), proteins and DNA.

This thesis is thus a contribution to the rapidly growing development of new classes of carbon nano-onion based nanomaterials that aims at expanding their current applications to construct novel detection systems with improved performances.

REFERENCES

1. H.W. Kroto, J. R. Heath, S. C. O'brien, R. F. Curl, R. E. Smalley, *C_{60}: Buckminsterfullerene.* Nature, 1985. **318**: p. 162-163.
2. J.L. Delgado, M. A. Herranz, N. Martin, *The nanoforms of carbon.* Journal of Materials Chemistry, 2008. **18**: p. 1417-1426.
3. B.S. Sherigara, W. Kutner, F. D'Souza, *Electrocatalytic Properties and Sensor Applications of Fullerenes and Carbon Nanotubes.* Electroanalysis, 2003. **15**(9): p. 753-770.
4. V.G. Gavalas, N. A. Chaniotakis, *[60]Fullerene-mediated amperometric biosensors.* Analytica Chimica Acta, 2000. **409**(1-2): p. 131-135.
5. C. Lanzellotto, G. Favero, M.L. Antonelli, C. Tortolini, S. Cannistraro, E. Coppari, F. Mazzei, *Nanostructured enzymatic biosensor based on fullerene and gold nanoparticles: Preparation, characterization and analytical applications.* Biosensors and Bioelectronics, 2014. **55**: p. 430-437.
6. S. Iijima, *Helical microtubules of graphitic carbon.* Nature, 1991. **354**: p. 56-58.
7. P.M. Ajayan, *Nanotubes from carbon.* Chemical Reviews, 1999. **99**(7): p. 1787-1799.
8. Q. Zhang, J. Huang, W. Qian, Y. Zhang, F. Wei, *The road for nanomaterials industry: A review of carbon nanotube production, post treatment and bulk*

applications for composites and energy storage. Small, 2013. **9**(8): p. 1237-1265.

9. S. Liu, X. Guo, *Carbon nanomaterials field-effect-transistors-based biosensors.* NPG Asia Materials, 2012. **4**: p. 1-10.
10. W. Yang, K.R. Ratinac, S.P. Ringer, P. Thordarson, J. Justin Gooding, F. Braet, *Carbon nanomaterials in biosensors: Should you use nanotubes or graphene?* Angewandte Chemie Int. Ed., 2010. **49**: p. 2114-2138.
11. R. Chen, Y. Li, K. Huo, P.K. Chu, *Microelectrode arrays based on carbon nanomaterials: emerging electrochemical sensors for biological and environmental applications.* RSC Advances, 2013. **3**: p. 18698-18715.
12. D. Jariwala, V. K. Sangwan, L.J. Lauhon, T.J. Marks, M.C. Hersam, *Carbon nanomaterials for electronics, optoelectronics, photovoltaics, and sensing.* Chemical Society Review, 2013. **42**: p. 2824-2860.
13. K.S. Novoselov, A.K. Geim, S.V. Morozov, D. Jiang, Y. Zhang, S.V. Dubonos, I.V. Grigorieva, A.A. Firsov, *Electric field effect in atomically thin carbon films.* Science, 2004. **306**: p. 666-669.
14. A.H. Castro Neto, F. Guinea, N.M.R. Peres, K.S. Novoselov, A.K. Geim, *The electronic properties of graphene* Review of Modern Physics, 2009. **81**(1): p. 109-162.
15. A.K. Geim, K.S. Novoselov, *The rise of graphene.* Nature Materials, 2007. **6**: p. 183-191.
16. A.K. Geim, *Graphene, status and prospects.* Science, 2009. **324**: p. 1530-1534.
17. R.S. Lewis, T. Ming, J.F. Wacker, E. Anders, E. Steel, *Interstellar diamonds in meteorites.* Nature, 1987. **326**: p. 160-162.
18. U. Ott, *Interstellar grains in meteorites.* Nature, 1993. **364**: p. 25-33.
19. C. Koeberl, *Diamond everywhere.* Nature, 1995. **378**: p. 17-18.
20. V.V. Danilenko, *On the history of the discovery of nanodiamond synthesis.* Physics Solid State, 2004. **46**: p. 595-599.
21. W.R. Greiner, D.S. Phlips,J.D. Johnson, F. Volk, *Diamonds in detonation soot.* Nature, 1981. **333**: p. 440-442.
22. V.N. Mochalin, O. Shenderova, D. Ho, Y. Gogotsi, *The properties and applications of nanodiamonds.* Nature Nanotechnology, 2012. **7**: p. 11-23.
23. Z. Liu, X. Liang, *Nano-carbons as theranostics.* Theranostics, 2012. **2**(3): p. 235-237.
24. D. Ugarte, *Curling and closure of graphitic networks under electron beam radiation.* Nature, 1992. **359**(6397): p. 707-709.
25. B. Xu, S.Tanaka, *Formation of giant onion-like fullerenes under Al nanoparticles by electron irradiation.* Acta Mater, 1998. **46**(15): p. 5249-5257.
26. N. Sano, H. Wang, M. Chhowalla, I. Alexandrou, G. A. J. Amaratunga, *Nanotechnology: synthesis of carbon "onions" in water.* Nature, 2001. **414**: p. 506-507.
27. N. Sano, H. Wang, I. Alexandrou, M. Chhowalla, K.B.K. Teo, G.A.J. Amaratunga, *Properties of carbon onions produced by an arc discharge in water.* Journal of Applied Physics, 2002. **92**(5): p. 2783-2788.
28. B. Xu, *Prospects and research progress in nano onion-like fullerenes.* New Carbon Materials, 2008. **23**(4): p. 289-301.
29. R. Borgohain, J. Yang, J.P. Selegue, D.Y. Kim, *Controlled synthesis, efficient purification, and electrochemical characterization of arc-discharge carbon nano-onions.* Carbon, 2014. **66**: p. 272-284.

30. X. Wang, B. Xu, X. Liu, J. Guo, H. Ichinose, *Synthesis of Fe-included onion-like Fullerenes by chemical vapor deposition.* Diamond and Related Materials 2006. **15**: p. 147-150.
31. Y. Yang, X. Liu, Y. Han, W. Ren, B. Xu, *Ferromagnetic property and synthesis of onion-like fullerenes by chemical vapor deposition using Fe and Co catalysts supported on NaCl.* Journal of Nanomaterials, 2010. **2011**: p. 6 pages.
32. C. Zhang, J. Li, E. Liu, C. He, C. Shi, X. Du, R.H. Hauge, N. Zhao, *Synthesis of hollow carbon nano-onions and their use for electrochemical hydrogen storage.* Carbon, 2012. **50**: p. 3513-3521.
33. A. Du, X. Liu, B. Xu, *Synthesis and structure characterization of coal-based nanostructured onion-like fullerenes.* Journal of Inorganic Materials, 2005. **20**(4): p. 779-784.
34. A. Du, X. Liu, D. Fu, P. Han, B. Xu, *Onion-like fullerenes synthesis from coal.* Fuel, 2007. **86**(1-2): p. 294-298.
35. D. Fu, X. Liu, A. Du, P. Han, H. Jia, B. Xu, *Synthesis of nanostructured onion-like fullerenes by MW plasma.* Journal of Inorganic Materials, 2006. **21**(3): p. 576-582.
36. T. Cabioc'h, J.P. Riviere, J. Delafond, *A new technique for fullerene onion formation* Journal of Material Science, 1995. **30**(19): p. 4787-4792.
37. T. Cabioc'h, E. Thune, M. Jaouen, *Carbon-onion thin film synthesis onto silica substrates.* Chemical Physics Letters, 2000. **320**(1-2): p. 202-205.
38. T. Cabioc'h, E. Thune, J.P. Riviere, S. Camelio, J.C. Girard, P. Guerin, M. Jaouen, *Structure and properties of carbon onion layers deposited ono various substrates.* Journal of Applied Physics, 2002. **91**(3): p. 1560-1567.
39. T. Cabioc'h, M. Jaouen, M.F. Denanot, P. Bechet, *Influence of the implantation parameters on the microstructure of carbon onions produced by carbon ion implantation.* Applied Physics Letters, 1998. **73**(21): p. 3096-3098.
40. M. Bystrzejewski, M.H. Rummeli, T. Gemming, H. Lange, A. Huczko, *Catalyst-free synthesis of onion-like carbon nanoparticles.* New Carbon Materials, 2010. **25**(1): p. 8 pages.
41. J. Du, Z. Liu, Z. Li, B. han, Z. Sun, Y. Huang, *Carbon onions synthesized via thermal reduction of glycerin with magnesium.* Materials Chemistry and Physics, 2005. **93**: p. 178-180.
42. M. Choucair, J.A. Stride, *The gram-scale synthesis of carbon onions.* Carbon, 2012. **50**: p. 1109-1115.
43. V.L. Kuznetsov, A. L. Chuvilin, Y. V. Butenko, I. Y. Mal'kov, V. M. Titov, *Onion-like carbon from ultra-disperse diamond.* Chemical Physics Letters, 1994. **222**(4): p. 343-348.
44. J. Cebik, J.K. McDonough, F. Peerally, R. Medrano, I. Neitzel, Y. Gogotsi, S. Osswald, *Raman spectroscopy study of the nanodiamond-to-carbon onion transformation.* Nanotechnology, 2013. **24**(20): p. 205703.
45. S. Tomita, T. Sakurai, H. Ohta, M. Fujii, S. Hayashi, *Structure and electronic properties of carbon nano-onions.* Journal of Chemical Physics, 2001. **114**(17): p. 7477-7482.
46. M.E. Plonska-Brzezinska, A. Molina-Ontoria, L. Echegoyen, *Post-modification by low temperature annealing of carbon nano-onions in the presence of carbohydrates.* Carbon, 2014. **67**: p. 304-317.
47. D. Roy, M. Chhowalla, H. Wang, N. Sano, I. Alexandrou, T.W. Clyne, G.A.J. Amaratunga, *Characterisation of carbon nano-onions using Raman spectroscopy.* Chemical Physics Letters, 2003. **373**: p. 52-56.

48. S. Tomita, A. Burian, J.C. Dore, D. LeBolloch, M. Fujii, S. Hayashi, *Diamond nanoparticles to carbon onions transformation: X-ray diffraction studies.* Carbon, 2002. **40**: p. 1469-1474.
49. S.M. Hou, C.G. Tao, G.M. Zhang, X.Y. Zhao, Z.Q. Xue, Z.J. Shi, Z.N. Gu, *Ultrahigh vacuum scanning probe microscopy studies of carbon onions.* Physica E, 2001. **9**: p. 300-304.
50. M. Montalti, S. Krishnamurthy, Y. Chao, Yu. V. Butenko, V.L. Kuznetsov, V.R. Dhanak, M.R.C. Hunt, L. Siller, *Photoemission spectroscopy of clean and potassium-intercalated carbon onions.* Physica Review B, 2003. **67**: p. 113401.
51. A. Ruiz, J. Breton, J.M. Gomez LLorente, *A theoretical model of the photoabsorption spectra of carbon buckyonions.* Journal of Chemical Physics, 2004. **120**(13): p. 6163-6172.
52. S. Tomita, *Optical extinction properties of carbon onions prepared from diamond nanoparticles.* Physical Review B, 2002. **66**: p. 225424.
53. E. Koudoumas, O. Kokkinaki, M. Konstantaki, S. Couris, S. Korovin, P. Detkov, V. Kuznetsov, S. Pimenov, V. Pustovoi, *Onion-like carbon and diamond nanoparticles for optical limiting.* Chemical Physics Letters, 2002. **357**: p. 336-340.
54. S. Tomita, S. Hayashi, Y. Tsukuda, M. Fujii, , *Ultraviolet-Visible absorption spectroscopy of carbon onions* Physics Solid State, 2002. **44**(3): p. 450-453.
55. J. Bartelmess, S. Giodani *Carbon nano-onions (multi-layer fullerenes): chemistry and applications* Beilstein Journal of Nanotechnology, 2014. **5**: p. 1980-1998.
56. V. Georgakilas, D.M. Guldi, R. Signorini, R. Bozio, M. Prato, *Organic functionalization and optical properties of carbn nano-onions.* Journal of American Chemical Society, 2003. **125**: p. 14268-14269.
57. A.S. Rettenbacher, B. Elliot, J.S. Hudson. A. Amirkhanian, L. Echegoyen, *Preparation and functionalization of multilayer fullerenes (carbon nano-onions).* Chemistry a European Journal, 2006. **12**: p. 376-387.
58. A. Palkar, F. Melin, C.M. Cardona, B. Elliot, A.K. Naskar, D.D. Edie, A. Kumbhar, L. Echegoyen, *Reactivity differences between carbon nano onions (CNOs) prepared by different methods.* Chemistry an Asian Journal, 2007. **2**: p. 625-633.
59. A.S. Rettenbacher, M.W.Perpall, L. Echegoyen, J.S. Hudson, D.W. Smith Jr., *Radical addition of a conjugated polymer to multilayer fullerenes (carbon nano-onions).* Chemistry of Materials, 2007. **19**: p. 1411-1417.
60. A. Palkar, A. Kumbhar, A.J. Athans, L. Echegoyen, *Pyridyl-functionalized and water-soluble carbon nano onions: Firts supramolecular complexes of carbon nano onions.* Chemistry of Materials, 2008. **20**: p. 1685-1687.
61. L. Zhou, C. Gao, D. Zhu, W. Xu, F. F. Chen, A. Palkar, L. Echegoyen, E. S. Kong, *Facile functionalization of multilayer fullerenes (carbon nano-onions) by nitrene chemistry and "grafting from" strategy.* Chemistry European Journal, 2009. **15**: p. 1389-1396.
62. K. Flavin, M.N. Chaur, L. Echegoyen, S. Giordani, *Functionalization of multilayer fullerenes (carbon nano-onions) using diazonium compounds and "Click" chemistry.* Organic Letters, 2010. **12**(4): p. 840-843.
63. M. Yang, K. Flavin, I. Kopf, G. Radics, C.H.A. Hearden, G.J. McManus, B. Moran, A. Villalta-Cerdas, L. Echegoyen, S. Giodani, E.C. Lavelle, *Functionalization of Carbon Nanoparticles Modulates Inflammatory Cell*

Recruitment and NLRP3 Inflammasome Activation. Small, 2013. **9**(24): p. 4194-4206.

64. S. Giordani, J. Bartelmess, M. Frasconi, I. Biondi, S. Cheung, M. Grossi, D. Wu, L. Echegoyen, D.F. O'Shea, *NIR fluorescence labelled carbon nano-onions: synthesis, analysis and cellular imaging.* Journal of Materials Chemistry B, 2014. **2**: p. 7459-7463.
65. J. Bartelmess, E. De Luca, A. Signorelli, M. Baldrighi, M. Becce, R. Brescia, V. Nardone, E. Parisini, L. Echegoyen, P.P. Pompa, S. Giordani, *Boron dipyrromethene (BODIPY) functionalized carbon nano-onions for high resolution cellular imaging.* Nanoscale, 2014. **6**: p. 13761-13769.
66. A. Lapinski, A.T. Dubis, M.E. PLonska-Brzezinska, J. Mazurczyk, J. Breczko, L. Echegoyen, *Vibrational spectroscopic study of carbon nano-onions coated with polyaniline.* Physica Status Solidi C, 2012. **9**(5): p. 1210-1212.
67. Y. Liu, R.L. Vander Wal, V.N. Khabashesku, *Functionalization of carbon nano-onions by direct fluorination.* Chemistry of Materials, 2007. **19**: p. 778-786.
68. M.E. Plonska-Brzezinska, A Lapinski, A.Z. Wilczewska, A.T. Dubis, A. Villalta-Cerdas, K. Winkler, L. Echegoyen, *The synthesis and characterization of carbon nano-onions produced by solution ozonolysis.* Carbon, 2011. **49**: p. 5079-5089.
69. S. Sek, J. Breczko, M.E. Plonska-Brzezinska, A.Z. Wilczewska, L. Echegoyen, *STM-based molecular junction of carbo nano-onion.* CHEMPHYSCHEM Communications, 2013. **14**: p. 96-100.
70. A. Molina-Ontoria, M. N. Chaur, M.E. Plonska-Brzezinska, L. Echegoyen, *Preparation and characterization of soluble carbon nano-onions by covalent functionalization, employing a Na-K alloy.* Chemistry Communication, 2013. **49**: p. 2406-2408.
71. P.P. Kuzhir, D.S. Bychamnok, S.A. Maksimenko, A.V. Gusinski, O.V. Ruhavets, V. L. Kuznetsov, S.I. Moseenkov, C. Jones, O. Shenderova, Ph. Lambin, *Onion-like carbon based polymer composite films in microwaves.* Solid State Sciences, 2009. **11**: p. 1762-1767.
72. J. Breczko, K. Winkler, M.E. Plonska-Brzezinska, A. Villalta-Cerdas, L. Echegoyen, *Electrochemical properties of composites containing small carbon nano-onions and solid polyelectrolytes.* Journal of Materials Chemistry, 2010. **20**: p. 7761-7768.
73. M.E. Plonska-Brzezinska, J. Mazurczyk, B. Palys, J. Breczko, A Lapinski, A.T. Dubis, L. Echegoyen, *Preparation and characterization of composites that contain small carbon nano-onions and conducting polyaniline.* Chemistry a European Journal, 2012. **18**: p. 2600-2608.
74. M.E. Plonska-Brzezinska, M. Lewandowski, M. Blaszyk, A. Molina-Ontoria, T. Lucinski, L. Echegoyen, *Preparation and characterization of carbon nano-onion/PEDOT:PSS composites.* CHEMPHYSCHEM 2012. **13**: p. 4134-4141.
75. M.E. Plonska-Brzezinska, D.M. Brus, J. Breczko, L. Echegoyen, *Carbon nano-onions and biocompatible polymers for flavonoid incorporation.* Chemistry a European Journal, 2013. **19**: p. 5019-5024.
76. R. Borgohain, J. Li, J.P. Selegue, Y.T. Cheng, *Electrochemical study of functionalized carbon nano-onions for high-performance supercapacitor* Journal of Physical Chemistry, 2012. **116**: p. 15068-15075.
77. E. Wajs, A. Molina-Ontoria, T.T. Nielsen, L. Echegoyen, A. Fragoso, *Supramolecular Solubilization of cyclodextrin-modified carbon nano-onions by host-guest interactions.* Langmuir, 2015. **31**: p. 535-541.

78. A. Burke, *Ultracapacitors: why, how, and where is the technology?* Journal of Power Sources, 2000. **91**(1): p. 37-50.
79. R. Kotz, M. Carlen, *Principles and applications of electrochemical capacitors.* Electrochimica Acta, 2000. **45**(15-16): p. 2483-2498.
80. C. Portet, G. Yushin, Y. Gogotsi, *Electrochemical performance of carbon onions, nanodiamonds, carbon black and multiwalled nanotubes in electrical double layer capacitors.* Carbon, 2007. **45**: p. 2511-2518.
81. E.G. Bushueva, P.S. Galkin, A.V. Okotrub, L.G. Bulusheva, N.N. Gavrilov, V.L. Kuznetsov, S.I. Moiseekov, *Double layer supercapacitor properties of onion-like carbon materials.* Physica Status Solidi B, 2008. **245**(10): p. 2296-229.
82. D. Pech, M. Brunet, H. Durou, P. Huang, V. Mochalin, Y. Gogotsi, P-L. Taberna, P. Simon, *Ultrahigh-power micrometer-sized supercapacitors based on onion-like carbon.* Nature Nanotechnology, 2010. **5**: p. 651-654.
83. J.K. McDonough, A.I. Frolov, V. Presser, J. Niu, C.H. Miller, T. Ubieto, M.V. Fedorov, Y. Gogotsi, *Influence of the structure of carbon onions on their electrochemical performance in supecapacitor electrodes.* Carbon, 2012. **50**: p. 3298-3309.
84. Y. Gao, Y.S. Zhou, M. Qian, X. N. He, J. Redepenning, P. Goodman, H.M. Li, L. Jiang, Y. F. Lu, *Chemical activation of carbon nano-onions for high-rate supercapacitor electrodes.* Carbon, 2013. **51**(0): p. 52-58.
85. F.D. Han, B. Yao, Y-J. Bai, *Preparation of carbon nano-onions nd their application as anode materials for rechargeable lithium-ion batteries.* Journal of Physical Chemistry, 2011. **115**: p. 8923-8927.
86. Y. Wang, F. Yan, S. W. Liu, A. Y.S. Tan, H. Song, X. W. Sun, H. Y. Yang, *Onion-like carbon matrix supported Co_3O_4 nanocomposites: a highly reversible anode material for lithium ion batteries with excellent cycling stability.* Journal of Materials Chemistry A, 2013. **1**: p. 5212-5216.
87. Y. Wang, S.F. Yu, C.Y. Sun, T. J. Zhu, H. Y. Yang, *MnO_2/onion-like carbon nanocomposites for pseudocapacitors.* Journal of Materials Chemistry, 2012. **22**: p. 17584-17588.
88. Y. Wang, Z.J. Han, S.F. Yu, R.R. Song, H.H. Song, K.K. Ostrikov, H. Y. Yang, *Core-leaf onion-like carbon/MnO_2 hybrid nano-urchins for rechargeable lithium-ion batteries.* Carbon, 2013. **64**: p. 230-236.
89. N. Keller, N.I. Maksimova, V.V. Roddatis, M. Schur, G. Mestl, Y.V. Butenko, V.L. Kuznetsov, R. Schlogl, *The catalytic use of onion-like carbon materials for styrene synthesis by oxidative dehydrogenation of ethylbenzene.* Angewandte Chemie Int. Ed., 2002. **41**(11): p. 1885-1888.
90. D. Su, N.I. Maksimova, G. Mestl, V.L. Kuznetsov,V. Keller, R. Schlogl, N. Keller, *Oxidative dehydrogenation of ethylbenzene to styrene over ultra-dispersed diamond and onion-like carbon.* Carbon, 2007. **45**: p. 2145-2151.
91. B. Xu, X. Yang, X. Wang, J. Guo, X. Liu, *A novel catalyst support for DMFC: Onion-like fullerenes.* Journal of Power Sources, 2006. **162**: p. 160-164.
92. D. Santiago, G.G. Rodriguez-Calero, A. Palkar, D. Barraza-Jimenez, D. H. Galvan, G. Casillas, A. Mayoral, M. Jose-Yacaman, L. Echegoyen, C.R. Cabrera, *Platinum electrodeposition on unsupported carbon nano-onions.* Langmuir, 2012. **28**: p. 17202-17210.
93. C.M. Sayes, J.D. Fortner, W. Guo, D. Lyon, A.M. Boyd, K.D. Ausman, Y.J. Tao, B. Sitharam, L.J. Wilson, J.B. Hughes, J.L. West, V.L. Colvin, *The*

differential cytotoxicity of water soluble fullerene. Nano Letters, 2004. **4**(10): p. 1881-1887.

94. G. Jia, H. Wang, L. Yan, X. Wang, R. Pei, T. Yan, Y. Zhao, X. Guo, *Cytotoxicity of Carbon Nanomaterials: Single-Wall Nanotube, Multi-Wall Nanotube, and Fullerene.* Environmental Science and Technology, 2005. **39**(5): p. 1378-1383.
95. L. Ding, J. Stilwell, T. Zhang, O. Elboudwarej, H. Jiang, J.P. Selegue, P.A. Cooke, J.W. Gray, F.F. Chen, *Molecular characterization of the cytotoxic mechanism of multiwall carbon nanotubes and nano-onions on human skin fibroblast.* Nano Letters, 2005. **5**(12): p. 2448-2464.
96. Y. Xu, S. Wang, J. Yang, X. Gu, J. Zhang, Y. Zheng, J. Yang, L. Xu, X. Zhu, *Multiwall carbon nano-onions induce DNA damage and apoptosis in human umbilical vein endothelial cells.* Environmental Toxicology, 2013. **28**(8): p. 442-450.
97. J. Luszczyn, M.E. Ploska-Brzezinska, A. Palkar, A.T. Dubis, A. Simionescu, D.T. Simionescu, B. Kalska-Szostko, K. Winkler, L. Echegoyen, *Small noncytotoxic carbon nano-onions: first covalent functionalization with biomolecules.* Chemistry a European Journal, 2010. **16**: p. 4870-4880.
98. M. Ghosh, S.K. Sonkar, M. Saxena, S. Sarkar, *Carbon nano-onions for imaging the life cycle of drosophila melanogaster.* Small, 2011. **7**(22): p. 3170-3177.
99. S.K. Sonkar, M. Ghosh, M. Roy, A. Begum, S. Sarkar, *Carbon nano-onions as nontoxic and high-fluorescence bioimgaing agent in food chain- An in vivo study from unicelluar E. coli to multicellular C. elegans.* Materials Express, 2012. **2**(2): p. 105-114.
100. J. Breczko, M.E. Plonska-Brzezinska, L. Echegoyen, *Electrochemical oxidation and determination of dopamine in the presence of uric and ascorbic acids using a carbon nano-onion and poly(diallyldimethylammonium chloride) composite.* Electrochimica Acta, 2012. **72**: p. 61-67.
101. L. Joly-Pottuz, B. Vacher, N. Ohmae, J.M. Martin, T. Epicier, *Anti-wear and friction reducing mechanisms of carbon nano-onions as lubricant additives.* Tribology Letters, 2008. **30**: p. 69-80.
102. L. Joly-Pottuz, E. W. Bulcholz, N. Matsumoto, S.R. Phillpot, S.B. Sinnott, N. Ohmae, J.M. Martin, *Friction properties of carbon nano-onions from experiment and computer simulations.* Tribology Letters, 2010. **37**: p. 75-81.
103. N. Matsumoto, L. Joly-Pottuz, H. Kinoshita, N. Ohmae, *Application of onion-like carbon to micro and nanotribology.* Diamond and Related Materials, 2007. **16**: p. 1227-1230.
104. E.W. Bucholz, S.R. Phillpot, S.B. Sinnott, *Molecular dynamics investigation of the lubrication mechanism of carbon nano-onions.* Computational Materials Science, 2012. **54**: p. 91-96.
105. M.B. Seymour, C. Su, Y. Gao, Y. Lu, Y. Li, *Characterization of carbon nano-onions for heavy metal ion remediation.* Journal of Nanoparticles Research, 2012. **14**: p. 1087.
106. F. Yasin, R.A. Boulos, B. Y. Hong, A. Cornejo, K. Swaminathan Iyer, L. Gao, H.T. Chua, C.L. Raston, *Microfluidic size selective growth of plladium nano-particles on carbon nano-onions.* Chemistry Communication, 2012. **48**: p. 10102-10104.
107. F. Banhart, Ph. Redlich, P.M. Ajayan, *The migration of metal atoms through carbon onions.* Chemical Physics Letters, 1998. **292**: p. 554-560.

Chapter 2

Preparation and Characterization of Carbon Nano-onions by Nanodiamond Annealing and Functionalization by Radio-frequency Ar/O_2 Plasma

ABSTRACT

Carbon nanomaterials can be prepared by several methods having in common that need a carbon source and often require high energies. In this Chapter, we describe the synthesis and characterization of carbon nano-onions by annealing of commercially available nanodiamonds. Heat treatment of nanodiamonds at 1200ºC for 6 hours under argon atmosphere afforded small round nano-onion particles of 3-4 nm diameter and 5-6 graphitic shells. The prepared CNOs were visualized by HRTEM and showed the characteristic XRD and Raman features. The results have been compared with a sample prepared by annealing at 1600ºC. Functionalization using RF plasma generates a facile way to introduce oxygen moieties into the surface of synthesized CNO. Xray photoemission spectroscopy (XPS) results showed that oxygen-containing groups like C-O, C=O and O-C=O were introduced unto the surface of CNOs. Raman spectroscopy clearly shows the change of $I_D/_G$ ratios as indicated in the conversion of sp^2 to sp^3 as a result of functionalization in the surface of CNO.

2.1 INTRODUCTION

The first method to synthesize carbon nano-onions (CNOs) by intense electron beam irradiation of amorphous carbon as precursor was described by Ugarte in 1992, which also marks the discovery of CNOs [1]. Following this report, many techniques were tried for efficient and gram-scale production of CNOs such as arc-discharge [2-4], chemical vapor deposition (CVD) [5, 6] and radio frequency/microwave plasma [7, 8]. As mentioned in the Introduction, these methods have some drawbacks relating with purity and quantity of the final product. For instance, arc-discharge often yields other carbon nanoparticles like carbon nanotubes, the diameter is not homogenous and the purification methods are destructive to the quality of CNOs.

Kuznetsov [9] proposed a precise way to produce homogenous and small onions approximately with size diameter of 5-8 carbon shells using ultra dispersed nanodiamonds (NDs) by vacuum annealing at high temperatures. This technique produces high yields of pure and small CNOs since it does not require any other catalyst and by adjusting the size distribution of the starting NDs before annealing it is possible to tune the size distribution of CNOs. Furthermore, this process could be scaled-up and useful for many applications. The detailed molecular dynamics simulation of the formation of NDs to CNOs are described by Tomita [10, 11] who proposed that the heating treatment graphitized the NDs from the surface to the inner core until fully hollow CNOs are formed. However, the onset temperature of the start of graphitization of NDs until it is fully transformed to CNOs is not clear and different values can be found in the literature. Obraztsova et al. [12] observed that at around 1400 K (1127˚C) the first traces of graphitic layer started to appear with almost full transformation at 1800 K (1527˚C) but they have noticed reconfigured CNOs into a highly ordered hexagonal structure. On the other hand, Qiao et al. [13] synthesized CNOs by annealing

NDs for 1 h at temperatures between 1100 and 1200˚C in an argon atmosphere. Their study revealed that CNOs begins to form at temperatures around 1100-1200˚C. Additionally, some literature claimed the onset of graphitization around 850˚C with full conversion to CNOs around 1200˚C [14].

The applications of carbon nano-onions have been limited due to the hydrophobic nature of carbon. To improve their solubilities, several functionalizations have been made either covalent [15-20] or non-covalent i.e. incorporated in composite materials [21-23]. One of the most popular methods is the chemical oxidation using strong oxidants like HNO_3 and H_2SO_4 which, in the case of nanotubes, can damage the structure and the conductivity decreases [24].

Plasma-based techniques are a new and attractive way to functionalize materials due to its simplicity and also because they are contaminant-free method. No harsh chemicals were used, it is environmentally friendly and safe and extremely easy to handle and operate. This method induces less damage on the structure of the material since the excited molecules produced during the plasma discharge attack the C=C bond creating open ends and defect sites as primary sites for functionalization [25]. Scheme 2.1 shows the possible reaction mechanisms of plasma treatment for activation/functionalization in a carbon surface with graphitic layers. As in multi-walled carbon nanotubes, the C=C bonds of CNOs are expected to be vulnerable to plasma activation with the formation of oxidized sites on the surface that can be the initial sites for further modifications [26] .

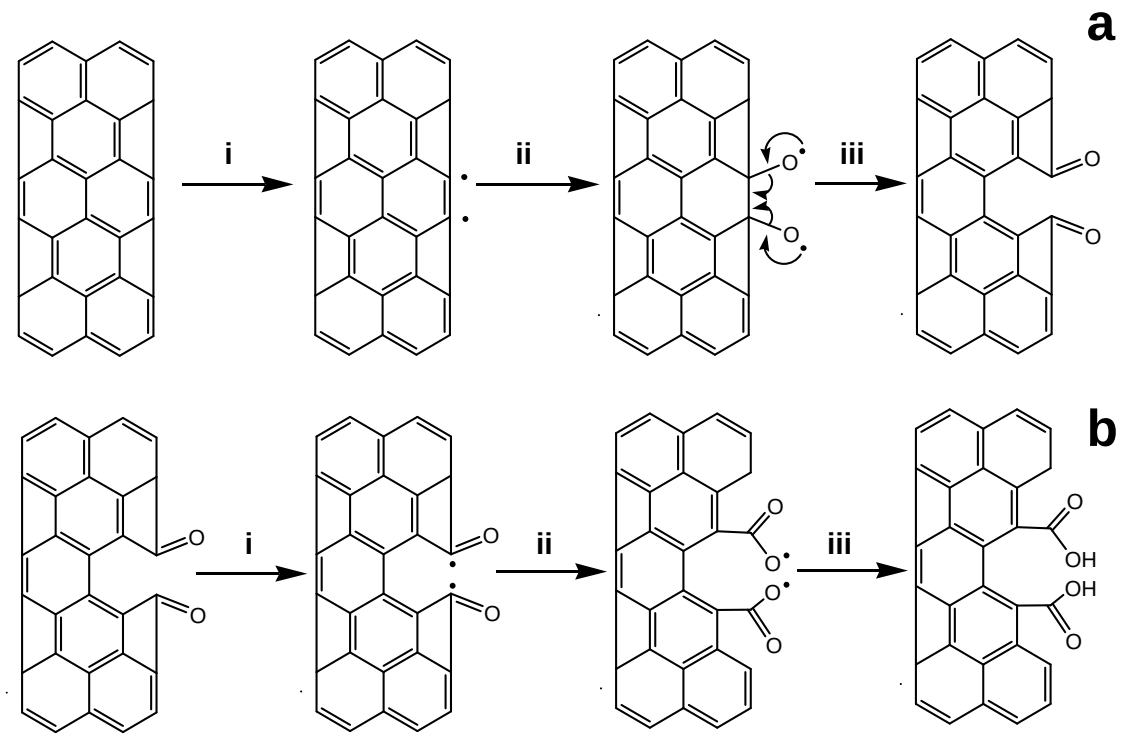

Scheme 2.1: Examples of possible oxidation mechanism of graphitic layers by Ar/O_2 microwave-surface wave plasma treatment: (a) generation of C=O bonds and (b) O-C=O bonds. i: plasma, ii: oxygen transfer, iii: hydrogen transfer (adapted from [26]).

In this Chapter, we describe the synthesis and characterization of carbon nano-onions by annealing of commercially available nanodiamonds. The prepared particles were further functionalized using a radio frequency (RF) plasma in Ar/O_2 atmosphere to introduce oxygenated groups on the surface of the CNOs [27]. The results on the synthesis are compared with a CNO sample kindly donated by Prof. Luis Echegoyen (University of Texas at El Paso).

2.2 EXPERIMENTAL SECTION

Nanodiamonds (particle size : <10 nm) were obtained from TCI Europe BV and used as received. The annealing process was carried out on a quartz tubular furnace (HST 12/600, Carbolite, UK) able to heat up until 1200˚C (Figure 2.1).

Figure 2.1: Photograph of the annealing tubular furnace.

Preparation: In the first attempt (**CNO-1**), 200 mg of nanodiamonds were loaded in a ceramic quartz boat and transferred to the furnace. The air in the furnace was removed by purging with nitrogen gas for several minutes. Annealing of nanodiamonds was performed at 1100˚C under nitrogen atmosphere at a flow rate of 3 L min^{-1} and with a heating ramp of 50˚C min^{-1}. The final temperature was kept for over a period of 3 h, and then the material was slowly cooled to room temperature.

A second attempt (**CNO-2**) was tried using 300 mg of nanodiamonds. The sample was loaded in a quartz boat and transferred to the furnace chamber. The air in the furnace was first removed by purging with argon for several minutes. The annealing was performed at 1200˚C under argon atmosphere at a flow rate 0.05 L min^{-1} at a heating ramp of 50˚C min^{-1}. The final temperature was maintained for 6 h and then the annealed sample was slowly cooled at room temperature.

Characterization: The annealed samples were characterized using high resolution transmission electron microscopy on a Jeol 2011 instrument (from the Servei de Microscòpia of Universitat Autónoma de Barcelona) operated at 200 kV and adapted

with diffraction patterns to visualize the structural form of the product before and after annealing. Samples were prepared in copper grids with a carbon layer and CNO samples were dispersed in ethanol.

Raman spectra were recorded in a RENISHAW inVia instrument equipped with 514 nm, 633 nm and 785 nm lasers exciting at 514 nm in 1-10% energy. A glass slide was used to hold the samples. X-ray diffraction (XRD) was performed using a Siemens D5000 diffractometer (Bragg-Brentano parafocusing geometry and vertical θ-θ goniometer) fitted with a curved graphite diffracted beam monochromator. The angular 2θ diffraction range was between 5˚ and 130˚. The data were collected with an angular step of 0.05˚ at 3 s per step and sample rotation. A low background Si (510) wafer was used as sample holder. $Cu_{k\alpha}$ radiation was obtained from a copper X-ray tube operated at 40 kV and 30 mA.

Purification. Prior to the plasma treatment, sample of synthesized CNO-2 was subjected for further purification procedure in which 50mg were boiled in 30% hydrogen peroxide for 3hrs. The insoluble particles were gathered and dried under vacuum at 50˚C. The treatment in peroxides was applied to remove amorphous carbon particles in the surface of CNOs. Peroxides are selective oxidizer, it easily etches low crystalline particles such as amorphous carbons but not with particles with better graphitized like CNOs [28].

Radio Frequency (RF) Plasma Treatment. RF plasma treatment was carried out in a Diener Electronic GmbH Femto SRCE plasma instrument equipped with PCCE control as shown in Figure 2.2. The low pressure plasma reactor consists of three main components: the vacuum chamber, the vacuum pump and a high frequency generator for plasma creation. A low pressure is created in the chamber by means of a vacuum

pump at a pressure as low as 0.3 mbar and then mixture of Ar/O_2 is fed into the chamber continuously flowing to expel other contaminants for 2 min before the main treatment. The working pressure was set at 0.4 mbar and when this pressure is achieved the generator is switched on and the process gas in the chamber is ionized. 40 mg of p-CNO-2 or purified CNO-2 sample were loaded in Pyrex® glass container and mounted into the rotary drum of the plasma machine. The plasma system receives continuously fresh gas while contaminated gas is removed. Ar and O_2 concentration in the reaction were 75% and 25%, respectively. The plasma treatment was carried out for 5 min at a power of 30 W and 60 W and after this time, another 5 min was set to let the gas flush and vent the chamber. The treated sample was removed and examined by X-Ray Photoemission Spectroscopy (XPS) (conducted at ICN2 facilities in Barcelona, Spain) and RAMAN spectroscopy. Ex-situ XPS experiments were performed at room temperature with a SPECS PHOIBOS 150 hemispherical analyzer at 10eV pass energy using monochromatic Al Kα (1486.74 eV) radiation as excitation source in a base pressure of 10^{-10} mbar.

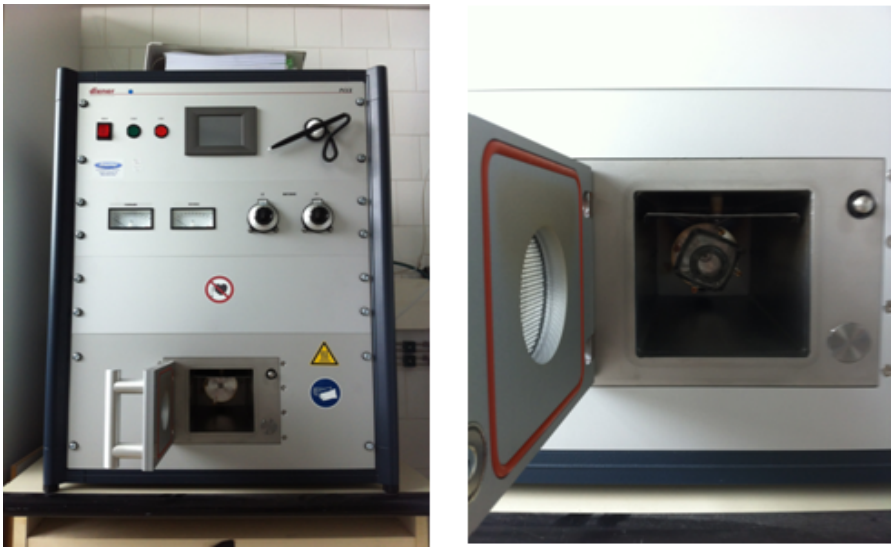

Figure 2.2: Photograph of the RF plasma activation reactor. The sample is loaded in the compartment displayed in the right.

2.3 RESULTS AND DISCUSSION

Preparation and Characterization of CNOs by nanodiamond annealing. The structural transformation of ND to CNOs was first confirmed by direct visual observation. As shown in Figure 2.3, there was a significant change of color of the starting material after annealing at high temperature. The percent of recovery after annealing for **CNO-1** and **CNO-2** were (179 mg) 89.5% and (230 mg) 76.6%, respectively.

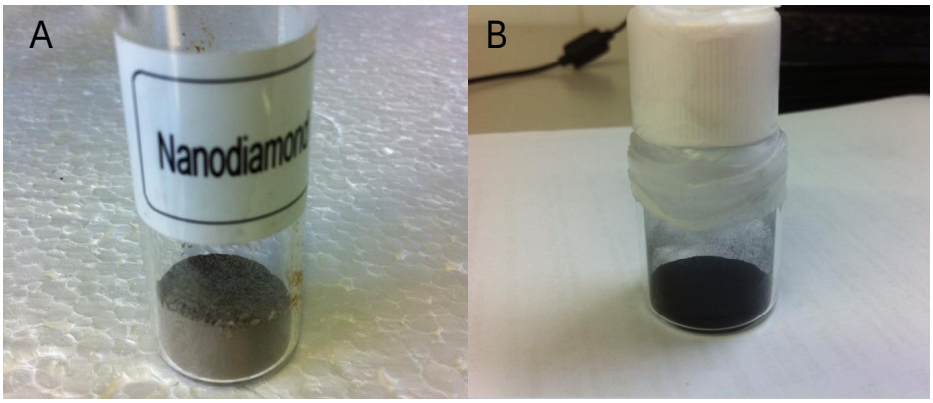

Figure 2.3: Transformation of the starting sample of (A) nanodiamonds to (B) CNOs after thermal annealing.

The transformation of nanodiamonds to carbon nano-onions was studied using high resolution transmission electron microscopy (HRTEM) (Figure 2.4). The HRTEM images of nanodiamonds (NDs) showed the presence of the typical crystal lattice of diamond formed by parallel planes separated by ~0.19 nm, in good agreement with literature reports [29] (Figure 2.4A). Inspection of HRTEM images of **CNO-1** in Figure 2.4C showed ND particles not completely transformed into CNOs in which a graphitic shell composed of 2-3 layers is present around a ND core with a slightly increased interlayer distance of 0.21 nm. Evidently is the result of the low temperature and short annealing time used in this process. Exposure of ND to the maximum temperature allowed by the furnace at 1200˚C for longer times (6 h) generated essentially spherical

CNO particles of 3-4 nm diameter with no presence of ND (**CNO-2**). These particles were formed by an average of 5-6 graphitic shells with distances between the carbon layers around of 0.35 nm and indicate that these annealing conditions are adequate to form small diameter CNOs from NDs (Figure 2.4D). As can be seen from figure 2.4B, the sample received from UTEP shows reconstructed hexagonal structures in the CNOs due to the fusion of graphitic layers [30] and this is also due to the annealing at higher temperatures (1600ºC).

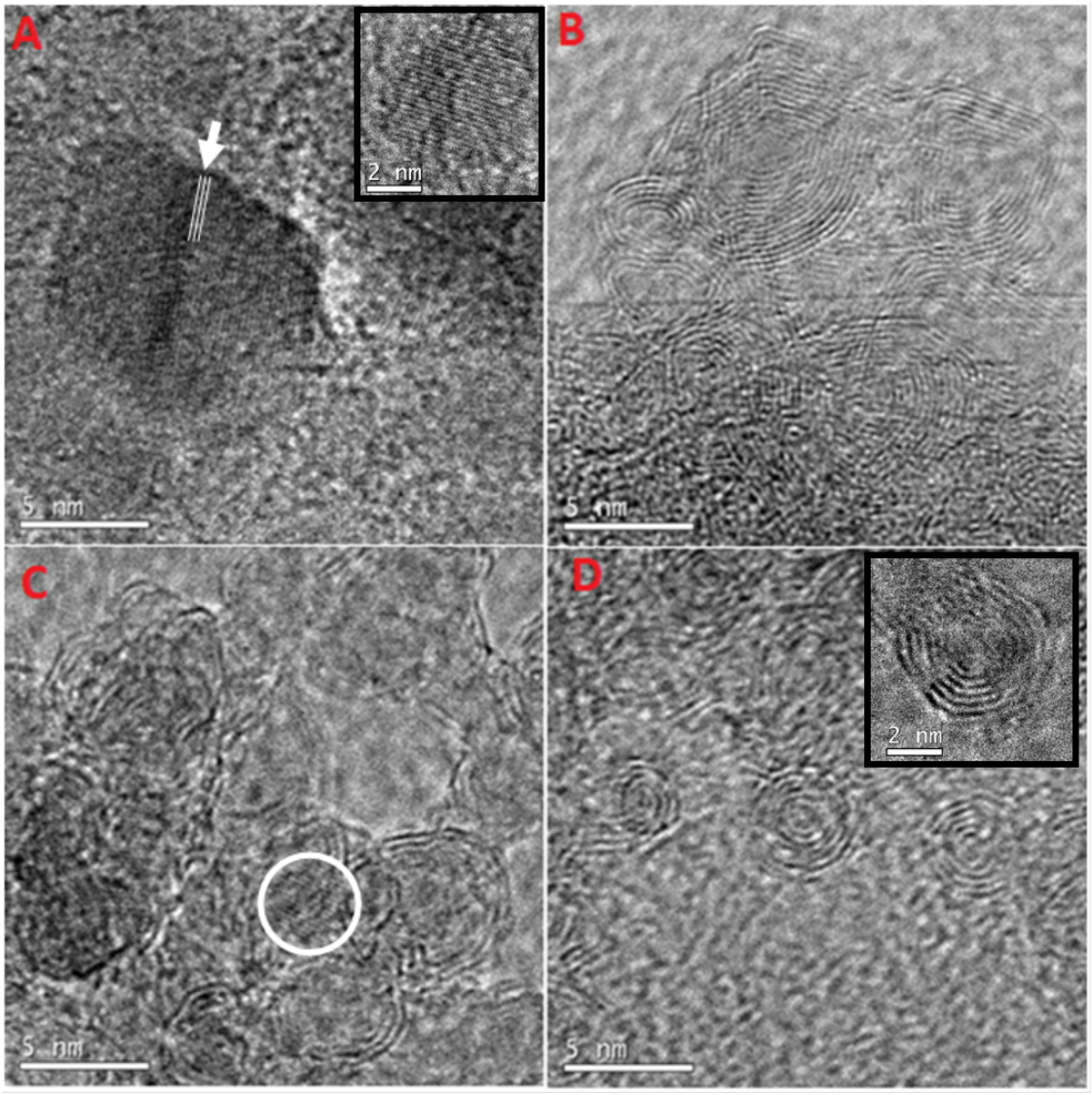

Figure 2.4: HRTEM images of A) NDs from TCI, B) CNO from UTEP, C) **CNO-1** and D) **CNO-2**.

XRD data was used to follow the transformation of NDs to CNOs (Figure 2.5). NDs have three characteristic peaks at 2θ values of 43.0º, 75º and 90º corresponding to the (111), (220) and (311) planes of sp^3-bonded diamond, respectively. On the other hand, the diffraction pattern of CNOs show two main peaks, one corresponding to sp^2 graphitic layers at 2θ values of 25º (002 plane) and a second broad peak at 43.7º (100 plane), which can be overlapped by the (111) peak of ND [11]. Figure 2.2 shows the diffraction patterns obtained for the starting NDs and the products resulting from annealing (**CNO-1** and **CNO-2**). In principle, the XRD signal can be generated from the coinciding scattering of many crystal planes and is thus proportional to the crystal volume of the whole sample. Therefore, in the case where large ND particles are not fully graphitized they would strongly contribute to the overall XRD signal and even small NDs that were fully transformed to sp^2 carbon will be overshadowed. This phenomenon was clearly observed in **CNO-1** in which the presence of peaks at 43º, 75º and 90º indicate that it contains a large amount of untransformed NDs, although a small peak of (002) plane for graphitic carbon at 25º is observed. In contrast, in **CNO-2** the peaks at 75º and 90º are absent, indicating the total transformation of NDs to CNOs. This diffraction pattern is similar to that of the CNO sample received from UTEP with peaks at 25º and 43.7º. The difference in peak intensities arises from the morphology of the particles, which is in turn a result of the annealing temperature, as seen above in HRTEM.

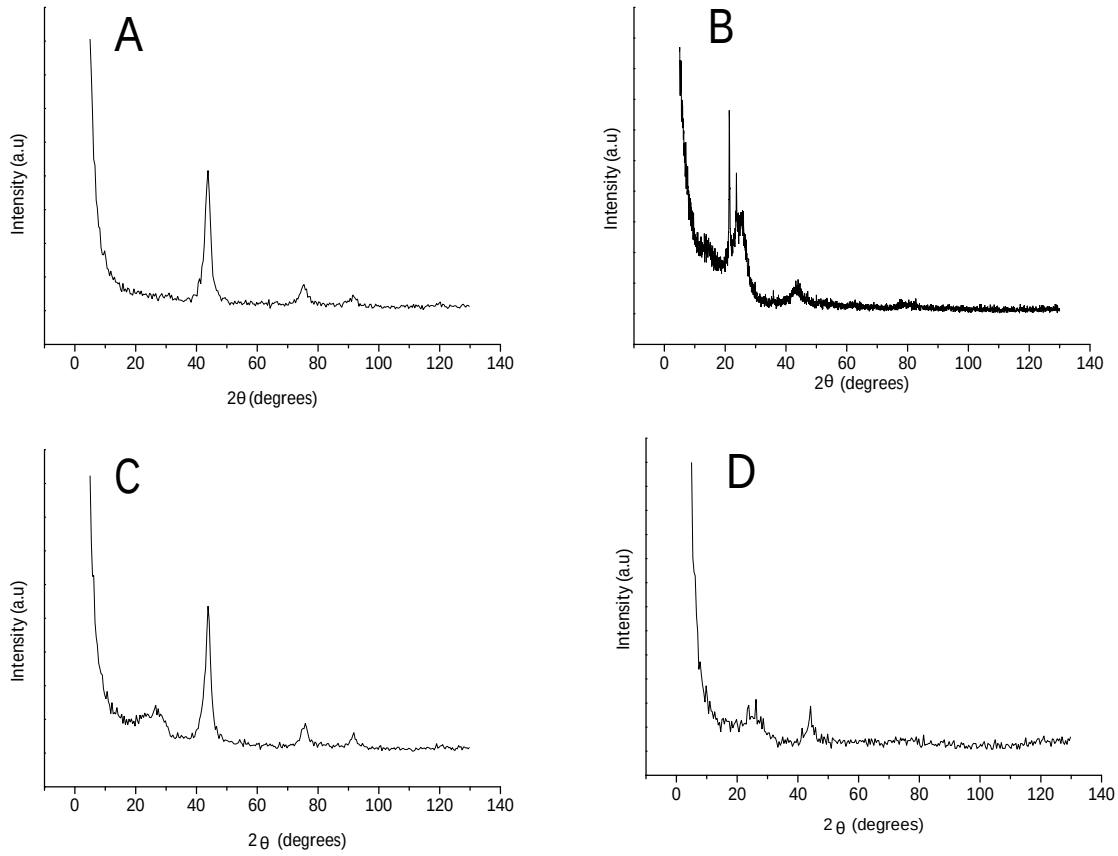

Figure 2.5: XRD patterns of A) NDs, B) CNO from UTEP, C) **CNO-1** and D) **CNO-2**.

Raman spectroscopy is a very useful technique to characterize carbon structures that complements XRD and HRTEM, especially for the presence of the so-called D and G bands. The G band (~1580 cm^{-1}) is due to the sp^2 bonded carbons and indicates the presence of the graphitic layer. The D band (~1340 cm^{-1}) is related with defect modes and is very sensitive to any disruption between the configurations of the carbon material. The transformation of ND to CNO is observed in the results of Raman spectra presented in Figure 2.6. ND spectrum shows a sharp peak at 1329 cm^{-1} (close to bulk diamond which appears at 1332 cm^{-1}) that corresponds to the sp^3 C-C bonds of the crystal lattice of ND. This peak is not of the same nature as found in synthesized CNOs, which appeared shifted to higher wavelengths and broader due to a larger crystal lattice spacing as observed in XRD and HRTEM. On the other hand, the peak at 1600 cm^{-1} is associated with adsorption of water molecules [31] and is shifted to a lower wavelength

as a result of the transformation to CNOs. Meanwhile, the ratio of the D and G bands indicate a change of structure of ND to CNO. The Raman spectrum of **CNO-1** shows two bands at 1340 and 1587 cm^{-1} with an I_D/I_G ratio of 1.07. Annealing at higher temperature for longer times as in **CNO-2**, gave a spectrum with well resolved peaks and I_D/I_G = 0.94 due to a stronger G-band peak (1584 cm^{-1}) that indicates that sp^3 carbons of the ND are converted to sp^2. Finally, **CNO-UTEP** samples showed a G-band peak in similar position as **CNO-2** with higher I_D/I_G ratio (1.11), suggesting that a high temperature annealing could also introduce defects into the surface of CNOs.

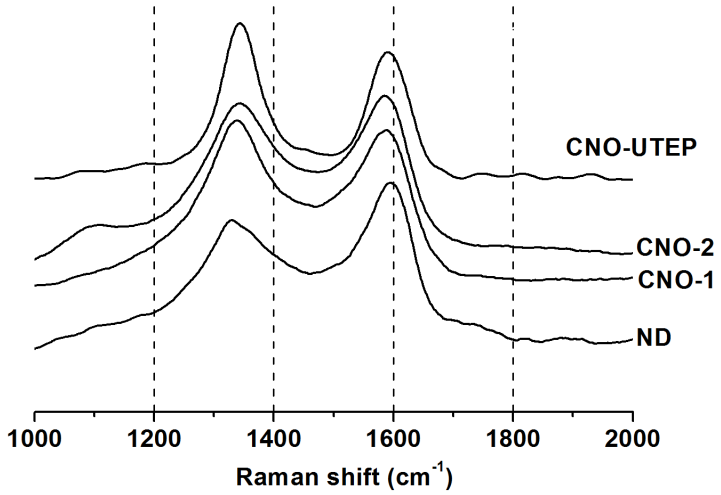

Figure 2.6: Raman spectra of CNO-1, CNO-2 and the sample received from UTEP.

RF Plasma Functionalization and XPS analysis. The possibility to use RF plasma for functionalization of CNOs was then investigated. For this, samples of **CNO-2** were treated with Ar/O_2 plasma for 5 min and the product was characterized by XPS and Raman spectroscopy (Scheme 2.2)

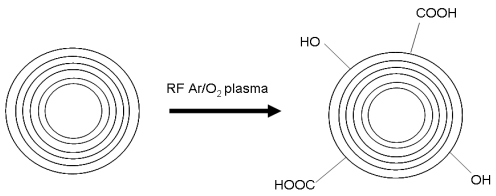

Scheme 2.2: RF plasma functionalization of CNOs.

The chemical modification of the surface of CNOs arising from the plasma treatment was analyzed by XPS. XPS is a surface sensitive technique used to identify the functional groups attached to the surface of the material. Figure 2.7 shows the XPS survey spectra of the pristine **CNO-2**, purified **CNO-2** and plasma treated samples together with the total percentages of carbon and oxygen. In all spectra, the distinctive existence of carbon and oxygen can be observed, even in pristine CNOs. The oxygen peak becomes more visible in the purified and treated samples as shown in the Figure 2.7b to e. Purification using hydrogen peroxide in the sample of CNOs did not only remove amorphous carbon but also reveals oxygen functionalization into the surface. Table 2.1 shows the normalized C and O atomic compositions of the different samples analyzed.

Table 2.1. XPS analysis of pristine **CNO-2** (**p-CNO-2**) and purified **CNO-2** before and after plasma treatment. The percents of each element were normalized to 100%.

	C 1s				O 1s		
Sample	peak 1 sp^2 (%)	peak 2 sp^3 (%)	peak 3 C-O (%)	peak 4 O-C=O (%)	H_2O (%)	C-O (%)	O-C=O (%)
p-CNO-2 (A)	50.48	34.77	13.71	1.04	34.42	27.57	38.01
purified CNO-2 (B)	49.65	33.87	14.80	1.68	13.90	46.24	39.86
CNO- 2 30W (C)	56.00	33.06	10.94	0	17.47	46.95	35.58
CNO- 2 60W (D)	49.92	35.01	13.77	1.3	13.25	36.54	50.21
p-CNO-2 60W (E)	48.79	35.52	13.94	1.46	0.00	41.45	58.55

Sample	C (%)	O (%)
p-CNO-2 (a)	89.20	10.80
purified CNO-2 (b)	78.94	21.06
CNO- 2 30W (c)	83.13	16.87
CNO- 2 60W (d)	84.75	15.25
p-CNO-2 60W (e)	88.16	11.84

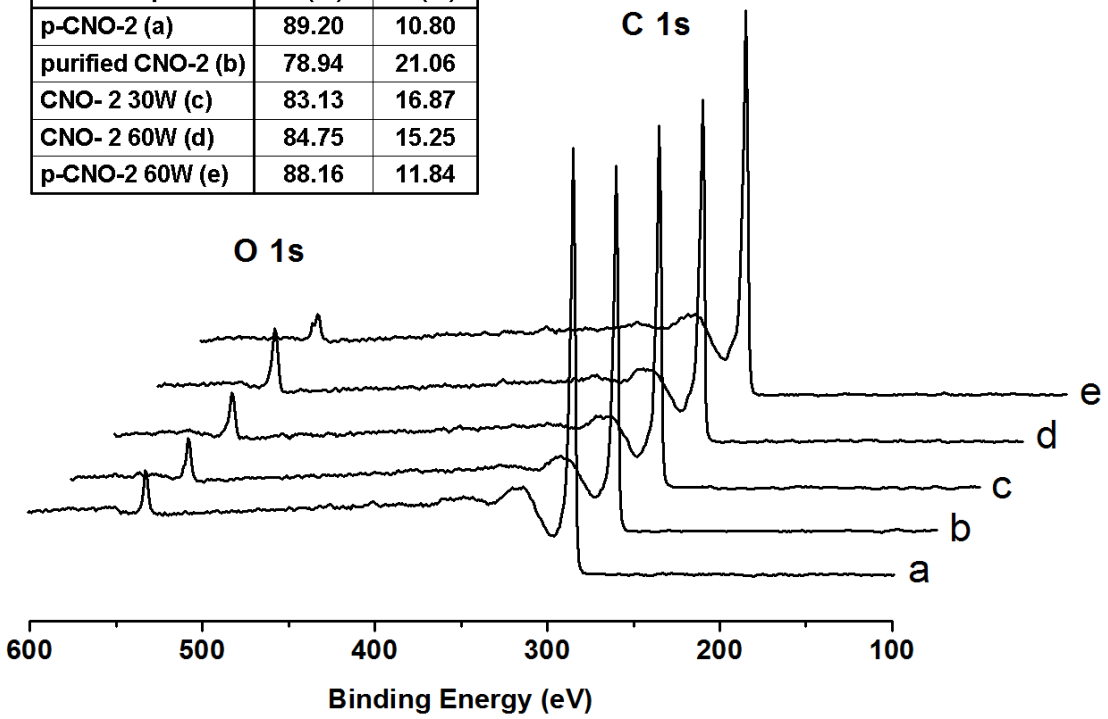

Figure 2.7: XPS survey spectra and elemental composition of (a) pristine **CNO-2**, (b) purified **CNO-2**, (c) purified **CNO-2** treated at 30 W, (d) purified **CNO-2** treated at 60 W and (e) pristine **CNO-2** treated at 60 W.

For CNOs before purification and plasma treatment, oxygen atoms come from air oxidation on the surface of CNO and humidity, which is about 10.80% (Figure 2.7a). There is a significant increase in the oxygen concentration after purification with hydrogen peroxide, doubling the value of the percent of oxygen of pristine CNO (21.06%) indicating that this step can oxygenate the surface of CNOs (see below for further discussion) (Figure 2.7b). Treating the sample with plasma after purification removes unstable oxygen groups attached into the surface of purified CNOs. Since plasma can be used for both etching and functionalization, unbounded and unstable moieties are removed as indicated by the decrease in %O content in **CNO-2** at 30W (Figure 2.7c) and 60W (Figure 2.7d). In the case of samples of pristine **CNO-2** directly treated with plasma at 60W showed a minimal increase of oxygen content (about 1%),

which clearly indicates that plasma treatment is a mild treatment to functionalize the CNO surfaces.

Further information on the nature of the functional groups on the CNO surface was obtained from the analysis of high-resolution XPS spectra. Figure 2.8 shows the deconvolution of the C1s peak of each analyzed sample. The assigned peak 1 at 284.9 eV is attributed to the graphitic structure (C=C) and sp^2 carbons. Peak 2 centered at 286.2 eV is related with the sp^3-hybridized carbon atoms (C-C). The peaks at 287.7 eV (peak 3) and 289.4 eV (peak 4) correspond to the C-O and O-C=O functionalities, respectively. An additional peak at 291.5 eV, related to π-π^* transition levels associated with free electrons between the graphitic planes [27], can be seen in some of the samples. After the purification (Figure 2.8b), there was a decrease in sp^2 and sp^3 signals (49.65% and 33.87%) accompanied by an increase in C-O and O-C=O (14.6 % and 1.68%) as compared to pristine **CNO-2** (Figure 2.8A), indicating that purification introduced oxygen functionalities into the surface of CNO. Moreover, the π-π^* peak is only present in pristine CNO not in purified CNO, which clearly indicates that the graphitic plane has been damaged decreasing the movement of free electrons. In plasma treated samples (Figure 2.8c and Figure 2.9d), there is an increase of sp^2 carbon, especially when treated at 30W, with a very slight restoration of the presence of π-π^* peak at 60 W. On the other hand, direct treatment of CNOs with plasma (Figure 2.8e) showed an obvious decrease in sp^2 carbons and an increase in all other peaks, which also indicates a successful oxygen functionalization in the surface of CNO. As mentioned earlier in the introduction, sp^2-hybridized graphite-like carbons are susceptible to plasma activation. The summary of the percentage of each fraction peaks is also shown in Table 2.1.

Further analysis on the oxygen content of the samples was carried out based on the high resolution O1s spectra of the samples before and after treatment (Figure 2.9). It is interesting to note the presence of water in all samples (except for pristine **CNO-2** treated at 60W), indicating a susceptibility to environment moisture, especially for pristine CNO. This water contents decreases when purified and treated with plasma and when pristine CNO was treated with plasma, a very hydrophobic surface seems to be generated thus moisture cannot affect the surface of CNO (Figure 2.9e).

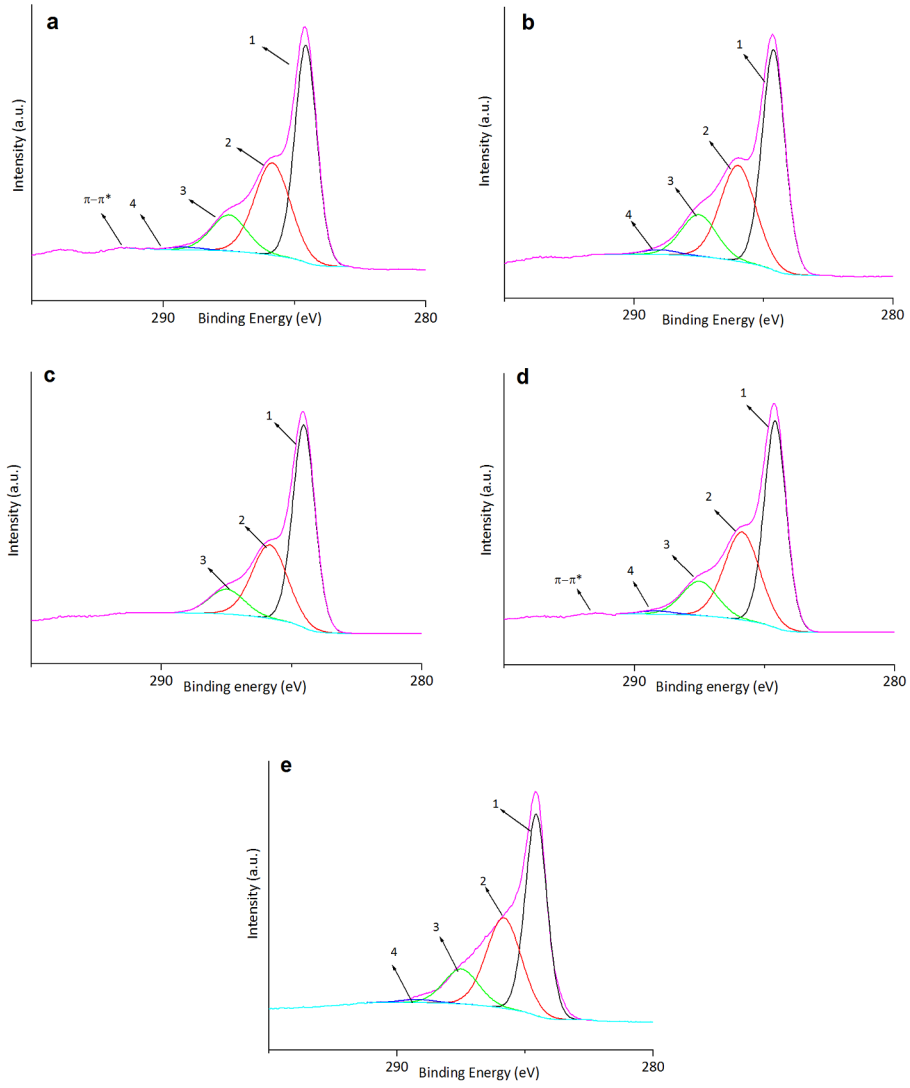

Figure 2.8: High resolution XPS C 1s spectra of (a) pristine **CNO-2**, (b) purified **CNO-2**, (c) purified **CNO-2** treated at 30 W, (d) purified **CNO-2** treated at 60 W and (e) pristine **CNO-2** treated at 60 W.

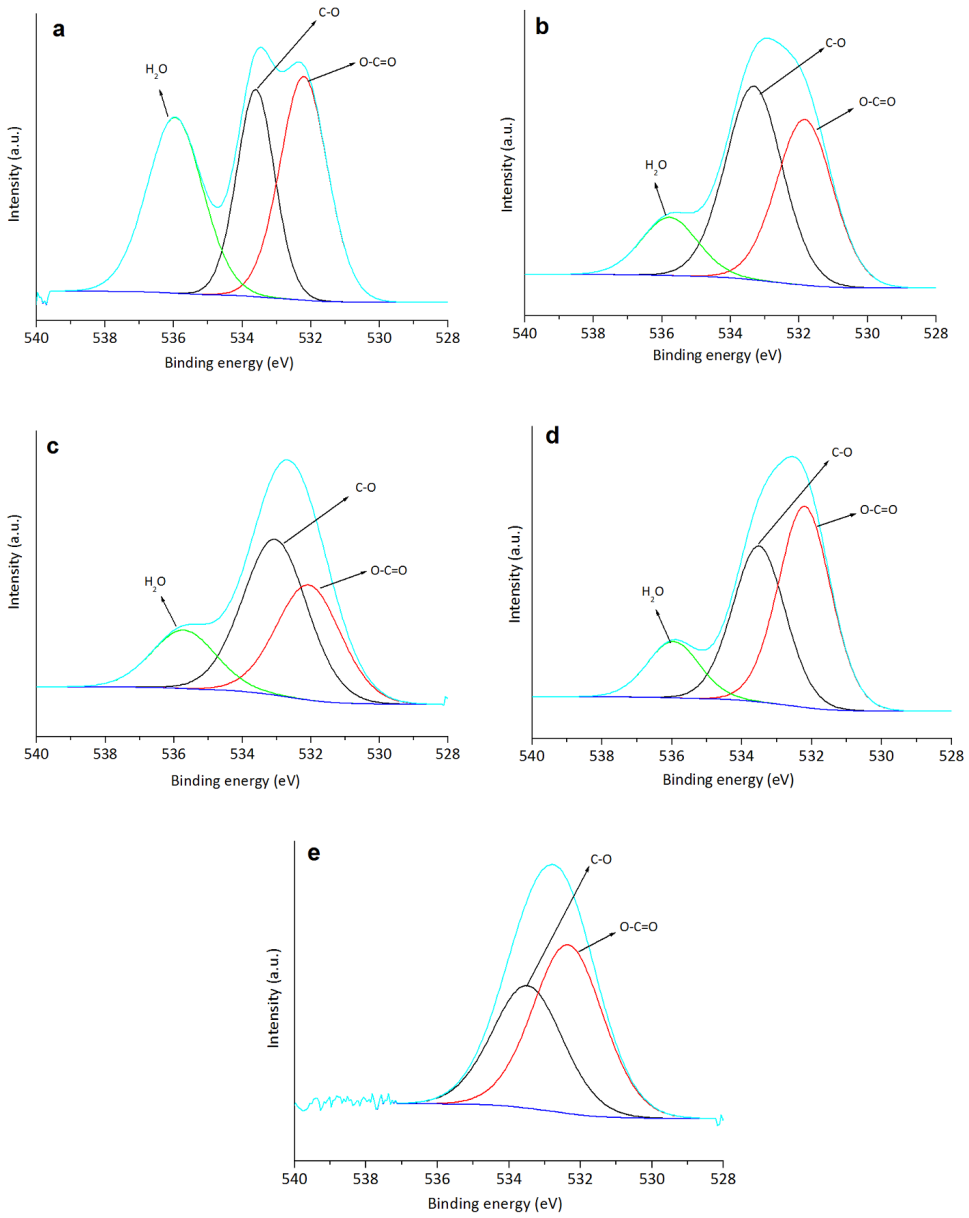

Figure 2.9: High resolution XPS O 1s spectra of (a) pristine **CNO-2**, (b) purified **CNO-2**, (c) purified **CNO-2** treated at 30 W, (d) purified **CNO-2** treated at 60 W and (e) pristine **CNO-2** treated at 60 W.

Raman spectroscopy was used to support the results in XPS for the change of sp^2-hybridized graphitic plane C=C to sp^3 carbon C-C before and after purification and plasma treatment as shown in Figure 2.10.

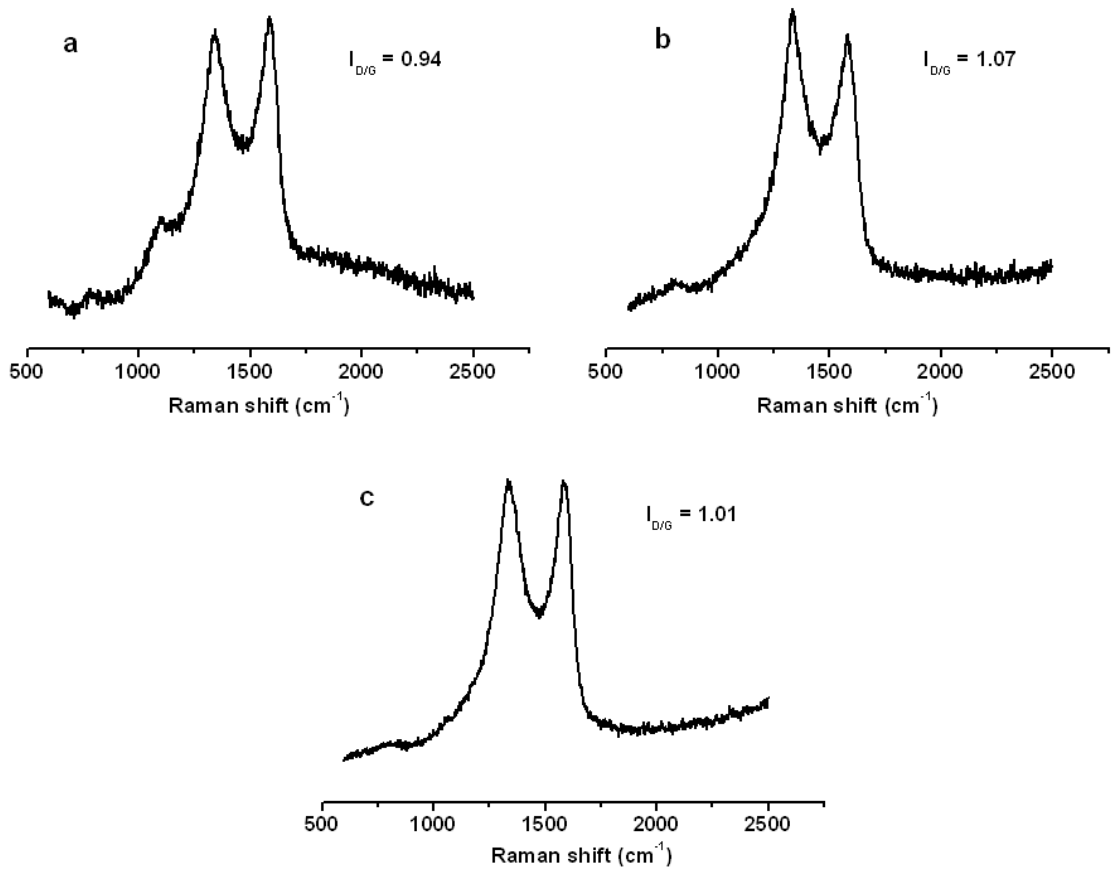

Figure 2.10: Raman spectra of a) pristine **CNO-2**, (b) purified **CNO-2**, (c) purified **CNO-2** treated at 60 W.

The high sensitivity of Raman techniques to the disorder surface of CNO before and after purification and plasma treatment are clearly shown in Figure 2.10, as revealed in the presence of the D and G bands. Pristine CNO showed lower $I_{D/G}$ ratio of 0.94 due to the stronger intensity peak of the graphitic plane (sp^2) C=C as indicated in the intensity signal of G band ~1584 cm^{-1} and lower disorder plane (sp^3) C-C of D band ~1337 cm^{-1} which, correlates well with the XPS findings. After the purification, some of the sp^2 were disrupted and converted to sp^3, thus there is a significant change in the $I_{D/G}$ ratio of 1.07. The sp^3 or D band has been enhanced due to the functionalization of the surface by purification as also reflected in XPS data. Furthermore, plasma treatment at 60W after purification improves the $I_{D/G}$ ratio of 1.01 due to the etching process or removal of unstable disordered plane in the surface exposing the graphitic layer of

CNOs as clearly stated in the XPS results. These results allow us to propose a mechanism similar to that represented in Figure 2.11 to account for the XPS and Raman results of the different treatments.

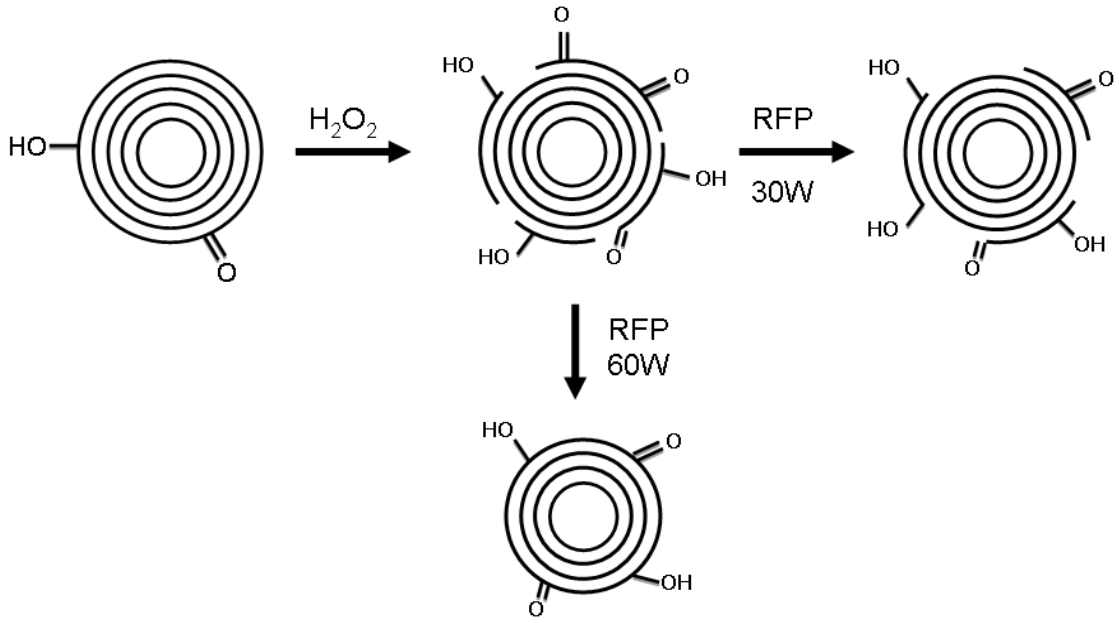

Figure 2.11: Possible surface transformations of **CNO-2** after purification and RF treatment.

CONCLUSIONS

CNOs have been prepared by annealing nanodiamonds at high temperatures. Heat treatment of ND at 1200ºC for 6 hours under argon atmosphere afforded small round CNO particles of 3-4 nm diameter and 5-6 graphitic shells. The CNO sample was characterized by HRTEM, XRD and Raman spectroscopy. Purification and plasma treated samples of CNOs generates oxygen functionalities into the surface which was extensively and specifically determined and analyzed using XPS and Raman spectroscopy.

REFERENCES

1. D. Ugarte, *Curling and closure of graphitic networks under electron beam radiation.* Nature, 1992. **359**(6397): p. 707-709.
2. N. Sano, H. Wang, M. Chhowalla, I. Alexandrou, G. A. J. Amaratunga, *Nanotechnology: synthesis of carbon "onions" in water.* Nature, 2001. **414**: p. 506-507.
3. N. Sano, H. Wang, I. Alexandrou, M. Chhowalla, K.B.K. Teo, G.A.J. Amaratunga, *Properties of carbon onions produced by an arc discharge in water.* Journal of Applied Physics, 2002. **92**(5): p. 2783-2788.
4. R. Borgohain, J. Yang, J.P. Selegue, D.Y. Kim, *Controlled synthesis, efficient purification, and electrochemical characterization of arc-discharge carbon nano-onions.* Carbon, 2014. **66**: p. 272-284.
5. X. Wang, B. Xu, X. Liu, J. Guo, H. Ichinose, *Synthesis of Fe-included onion-like Fullerenes by chemical vapor deposition.* Diamond and Related Materials 2006. **15**: p. 147-150.
6. Y. Yang, X. Liu, Y. Han, W. Ren, B. Xu, *Ferromagnetic property and synthesis of onion-like fullerenes by chemical vapor deposition using Fe and Co catalysts supported on NaCl.* Journal of Nanomaterials, 2010. **2011**: p. 6 pages.
7. A. Du, X. Liu, D. Fu, P. Han, B. Xu, *Onion-like fullerenes synthesis from coal.* Fuel, 2007. **86**(1-2): p. 294-298.
8. D. Fu, X. Liu, A. Du, P. Han, H. Jia, B. Xu, *Synthesis of nanostructured onion-like fullerenes by MW plasma.* Journal of Inorganic Materials, 2006. **21**(3): p. 576-582.
9. V.L. Kuznetsov, A. L. Chuvilin, Y. V. Butenko, I. Y. Mal'kov, V. M. Titov, *Onion-like carbon from ultra-disperse diamond.* Chemical Physics Letters, 1994. **222**(4): p. 343-348.
10. L. Hawelek, A. Brodka, S. Tomita, J.C. Dore, V. Honkimaki, A. Burian, *Transformation of nano-diamonds to carbon nano-onions studied by X-ray duffraction and molecular dynamics.* Diamond and Related Materials, 2011. **20**: p. 1333-1339.
11. O. Mykhaylyk, Y. M. Solonin, D. N. Batchelder, R. Brydson, *Transformation of nanodiamond into carbon onions: A comparative study by high-resolution transmission electron microscopy, electron energy-loss spectroscopy, x-ray diffraction, small-angle x-ray scattering, and ultraviolet Raman spectroscopy.* Journal of Applied Physics, 2005. **97**: p. 074302.
12. E.D. Obraztsova, M. Fujii, S. Hayashi, V.L. Kuznetsov, Yu.V. Butenko, A.L. Chuvilin, *Raman identification of onion-like carbon.* Carbon, 1998. **36**(5-6): p. 821-826.
13. Z. Qiao, J. Li, N. Zhao, C. Shi, P. Nash, *Graphitization and microstructure transformation of nanodiamond to onion-like carbon.* Scripta Materialia, 2006. **54**(2): p. 225-229.
14. Q. Zou, M. Wang, Y. Li, *Onio-like carbon synthesis by annealing nanodiamond at lower temperature and vacuum.* Journal of Experimental Nanoscience, 2010. **5**(5): p. 375-382.
15. Y. Gao, Y.S. Zhou, M. Qian, X. N. He, J. Redepenning, P. Goodman, H.M. Li, L. Jiang, Y. F. Lu, *Chemical activation of carbon nano-onions for high-rate supercapacitor electrodes.* Carbon, 2013. **51**(0): p. 52-58.
16. L. Zhou, C. Gao, D. Zhu, W. Xu, F. F. Chen, A. Palkar, L. Echegoyen, E. S. Kong, *Facile functionalization of multilayer fullerenes (carbon nano-onions) by*

nitrene chemistry and "grafting from" strategy. Chemistry European Journal, 2009. **15**: p. 1389-1396.

17. A.S. Rettenbacher, B. Elliot, J.S. Hudson. A. Amirkhanian, L. Echegoyen, *Preparation and functionalization of multilayer fullerenes (carbon nano-onions).* Chemistry a European Journal, 2006. **12**: p. 376-387.
18. A.S. Rettenbacher, M.W.Perpall, L. Echegoyen, J.S. Hudson, D.W. Smith Jr., *Radical addition of a conjugated polymer to multilayer fullerenes (carbon nano-onions).* Chemistry of Materials, 2007. **19**: p. 1411-1417.
19. K. Flavin, M.N. Chaur, L. Echegoyen, S. Giordani, *Functionalization of multilayer fullerenes (carbon nano-onions) using diazonium compounds and "Click" chemistry.* Organic Letters, 2010. **12**(4): p. 840-843.
20. A. Molina-Ontoria, M. N. Chaur, M.E. Plonska-Brzezinska, L. Echegoyen, *Preparation and characterization of soluble carbon nano-onions by covalent functionalization, employing a Na-K alloy.* Chemistry Communication, 2013. **49**: p. 2406-2408.
21. J. Breczko, K. Winkler, M.E. Plonska-Brzezinska, A. Villalta-Cerdas, L. Echegoyen, *Electrochemical properties of composites containing small carbon nano-onions and solid polyelectrolytes.* Journal of Materials Chemistry, 2010. **20**: p. 7761-7768.
22. M.E. Plonska-Brzezinska, J. Mazurczyk, B. Palys, J. Breczko, A Lapinski, A.T. Dubis, L. Echegoyen, *Preparation and characterization of composites that contain small carbon nano-onions and conducting polyaniline.* Chemistry a European Journal, 2012. **18**: p. 2600-2608.
23. A. Lapinski, A.T. Dubis, M.E. PLonska-Brzezinska, J. Mazurczyk, J. Breczko, L. Echegoyen, *Vibrational spectroscopic study of carbon nano-onions coated with polyaniline.* Physica Status Solidi C, 2012. **9**(5): p. 1210-1212.
24. J.P. Boudou, J.I. Paredes, A. Cuesta, A. Martinez-Alonso, J.M.D. Tascon, *Oxygen plasma modification of pitch-based isotropic carbon fibres.* Carbon, 2002. **41**: p. 41-56.
25. M.V. Naseh, A.A. Khodadadi, Y. Mortazavi, F. Pourfayaz, O. Alizadeh, M. Maghrebi, *Fast and clean functionalization of carbon nanotubes by dielectric barrier discharge plasma in air compared to acid treatment.* Carbon, 2010. **48**: p. 1369-1379.
26. C. Chen, B. Liang, A. Ogino, X. Wang, M. Nagatsu, *Oxygen functionalization of multiwall carbon nanotubes by microwave-excited surface-wave plasma treatment.* Journal of Physical Chemistry, 2009. **113**: p. 7659-7665.
27. B. Zhao, L. Zhang, X. Wang, J. Yang, *Surface functionalization of vertically-aligned carbon nanotube forests by radio-frequency Ar/O2 plasma.* Carbon, 2012. **50**: p. 2710-2716.
28. M. Bystrzejewski, M.H. Rummeli, T. Gemming, H. Lange, A. Huczko, *Catalyst-free synthesis of onion-like carbon nanoparticles.* New Carbon Materials, 2010. **25**(1): p. 8 pages.
29. J. Xiao, G. Ouyang, P. Liu, C.X. Wang, G.W. Yang, *Reversible nanodiamond-carbon onion phase transformations.* Nano Letters, 2014. **14**: p. 3645-3652.
30. S. Tomita, T. Sakurai, H. Ohta, M. Fujii, S. Hayashi, *Structure and electronic properties of carbon nano-onions.* Journal of Chemical Physics, 2001. **114**(17): p. 7477-7482.
31. V.N. Mochalin, O. Shenderova, D. Ho, Y. Gogotsi, *The properties and applications of nanodiamonds.* Nature Nanotechnology, 2012. **7**: p. 11-23.

Chapter 3

Supramolecular Dispersion of Carbon Nano-onions Based on Crown ether/ammonium Interactions

ABSTRACT

In this chapter, we explore the possibility of crown ether/ammonium interactions for the dispersion of CNOs in water using biocompatible polymers. CNOs were functionalized by reaction of diazotized 4-aminobenzo-18-crown-6. In the presence of biocompatible polymers containing pendant amino groups, such as aminated carboxymethyl cellulose (CMC-NH_2) and poly-L-lysine, the modified CNOs formed dispersions in water at acidic pH. Of them, the dispersion of CNO-18C6 and CMC-NH_2 at pH 4 was stable after several months at room temperature. Precipitation of the CNO-18C6 under basic conditions and in the presence of excess K^+ cation indicates that the ammonium/crown ether interactions are the major driving force in the formation of the CNO dispersions.

3.1 INTRODUCTION

Carbon nanomaterials are generally highly aggregated and poorly soluble in most common organic solvents. This does not only hinders to a great extent the possibility of chemical functionalization to prepare new materials but also limits some applications in which the preparation of stable dispersions is desirable, for example to prepare thin films [1]. Like other carbon allotropes, CNOs are not exempted of chemical inertness and lack of solubility and have therefore been generally underexploited until recently [2]. Modification in the surface of CNOs facilitates an increase of solubility in different solvents [3]. Some of these covalent functionalizations include 1,3-dipolar cycloaddition [4, 5], oxidation reactions with strong acids [3], fluorination [6, 7], polymerization [8] and reaction with diazonium compounds [9].

Supramolecular interactions have been previously employed to prepare soluble CNOs (Figure 3.1). The covalent functionalization of CNOs by metal-ligand interactions was first described by Palkar et al [10]. In their work, CNOs were modified with pyridyl units and then used as axial ligands to form a complex with the central zinc atom of Zn-porphyrin. This strategy generated water soluble self-assembled nanoporous networks of CNO−porphyrin nanohybrids. The preparation of these complexes is also possible using other metals such as platinum and palladium and may have potential applications in the field of catalysis and hydrogen storage.

Our group recently reported the solubilization of CNOs by host-guest interactions [11]. Initially, CNOs were oxidized followed by amidation reaction with β-cyclodextrin amine. Subsequently, the CNO-cyclodextrin derivative was allowed to interact with a guest polymer prepared by grafting ferrocene units into a hydrophilic dextran polymer (Fc-Dex). The formation of inclusion complexes between β-

cyclodextrin and Fc molecules caused an improvement in the solubility of CNOs aqueous solutions as revealed by dynamic light scattering and zeta-potential measurements. These dispersions precipitated back upon addition of a competitive guest such as adamantanecarboxylic acid, demonstrating the importance of the host-guest interactions in the formation of the dispersed CNOs.

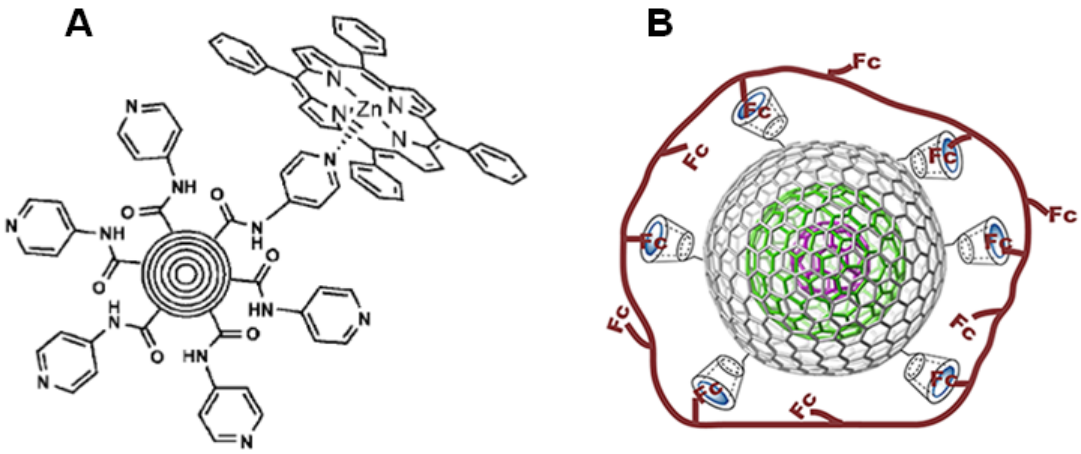

Figure 3.1: Supramolecular structures based on CNOs. A) CNO-porphyrin nanohybrid; B) CNO-cyclodextrin/Fc polymer complex.

The supramolecular interactions between amines and crown ethers are well known and have been widely described in the literature [12-14]. Crown ethers are macrocyclic compounds in which -CH_2CH_2O- groups repeat in regular order (Figure 3.2). The name arises from the resemblance of these molecules to a crown and, depending on the size of the ring and the number of oxygen atoms, they are called 12-crown-4, 15-crown-5, and 18-crown-6, etc. They can capture positively charged ions like metal and ammonium ions because the negatively charged electrons of the oxygen atoms point inward and attract and catch the ion. These interactions have been widely used to construct different supramolecular architectures such as rotaxanes and catenanes [14, 15]. Among the many types of crown ethers, benzocrown ethers are ideal as ammonium receptor molecules [16]. These receptors contain more rigid catechol groups

instead of the oxoethyl residue and the presence of the aromatic ring allows the functionalization of these receptors to obtain more complex systems[17].

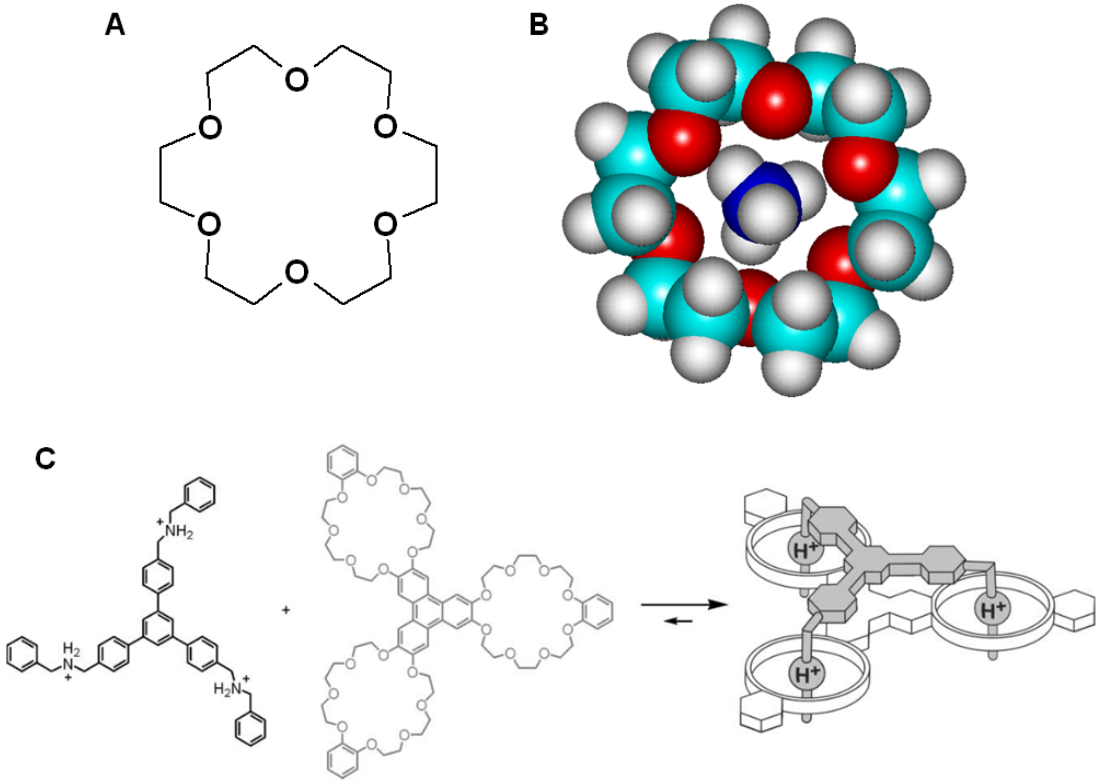

Figure 3.2: Molecular formula of 18-crown-6 (A) and energy minimized structure of the 18-crown-6 complex with ammonium cation (B). Crown ether/ammonium based rotaxane (C) (from ref [17]).

In this chapter, we explore the possibility to use crown ether/ammonium interactions for the dispersion of CNOs in water using biocompatible polymers. For this, we describe the functionalization and characterization of pristine CNOs with benzo-18-crown-6 (CNO-18C6) and study their interaction with biocompatible polymers containing pendant amino groups such as aminated carboxymethyl cellulose (CMC-NH_2) and poly-L-lysine.

3.2 EXPERIMENTAL SECTION

Materials. All chemicals and solvents used were commercially available and used without further purification. 4-aminobenzo-18-crown-6, isopentyl nitrite, carboxymethyl cellulose (MW 70 kDa) and poly-L-lysine hydrobromide (MW = 150,000-300,000) were purchased from Sigma. Water was purified using a Milli-Q-water purification system (Millipore) to a resistivity of 18.2 MΩ.cm then filtered through a 0.22 μM filter. CNOs were kindly provided by Prof. Luis Echegoyen (University of Texas at El Paso).

Instrumentation. Raman spectra were recorded with an Invia Renishaw using a 514 nm laser line from an Ar laser. The samples were loaded in glass slides. Fourier Transform Infrared (FTIR) spectra (KBr pellets) were recorded in a Jasco FT/IR-600 PLUS spectrometer. Thermal gravimetric analysis (TGA) experiments were carried out in a Mettler Toledo TGA/SDTA851 instrument. Typically, 1-2 mg of CNOs was loaded in the sample holder and the material was heated up at rate of 10˚C min^{-1} in air, while the weight was recorded continuously. High resolution transmission electron microscopy (HRTEM) images were acquired using a Jeol model 2011 operated at 200 kV equipped with an energy dispersive spectrometer (EDS) coupled to an Oxford Inca detector. Dispersed samples were deposited on Cu grids with a carbon layer. Zeta-potentials and hydrodynamic diameters were measured using a Malvern Instruments Zetasizer 3000 HSa particle sizer.

Synthesis of CNO-18C6. The synthetic procedure for the functionalization of CNOs by reaction with diazonium salts was similar to that described elsewhere [9].

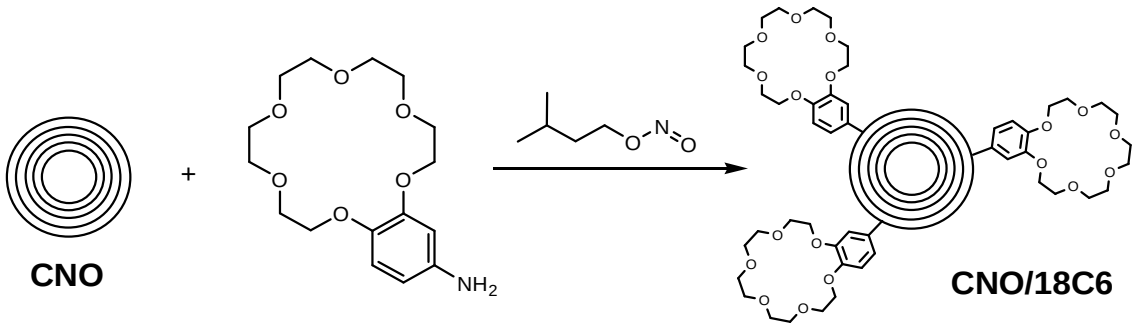

Scheme 3.1: Synthesis of CNO-18C6.

Briefly, 50 mg of pristine CNOs were initially dispersed in dimethyl formamide (50 mL) by tip sonication for 30 min. To this dispersion, 5 mmol of 4-aminobenzo-18-crown-6 were added followed by the addition of isopentyl nitrite (10 mmol) under an inert atmosphere. The reaction was stirred overnight at 60˚C and allowed to cool at room temperature. The CNO-18C6 was separated from the reaction mixture by centrifugation followed by successive washing with DMF. The solid was redispersed in toluene and methanol, washed and the black product was dried under vacuum (Yield: 47 mg).

Preparation of aminated-carboxymethyl cellulose (CMC-NH_2).

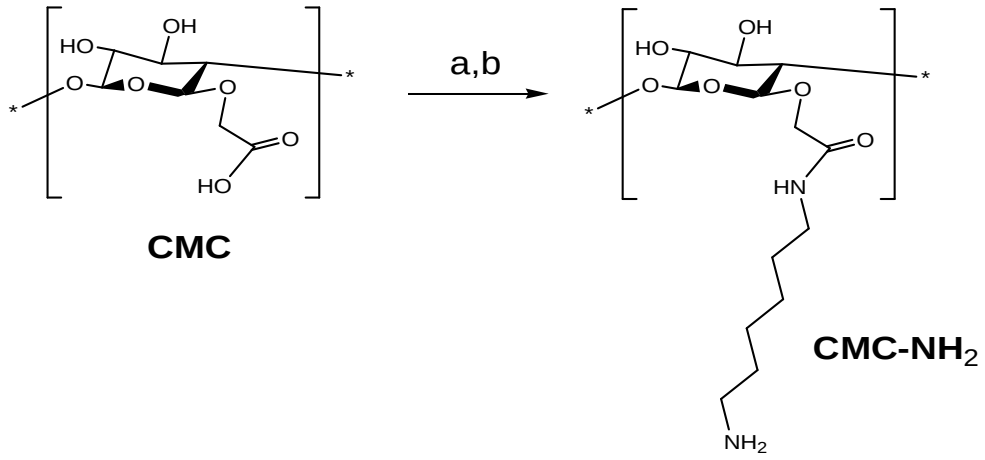

Scheme 3.2: a) EDC; b) 1,6-diaminohexane.

One-gram of CMC was dissolved in 10 mL of acetate buffer pH 5 then 3 mL of 0.2 M EDC was added and stirred for 30 min at 4ºC. 1,6-diaminohexane was then added (3g) into the mixture and stirred overnight at room temperature. To precipitate the CMC-NH_2, analytical grade ethanol was added into the mixture and then quickly stored at -20˚C in the freezer. The precipitate was repeatedly washed with cold ethanol and dried under vacuum at 40˚C. The presence of amino groups in the modified CMC-NH_2 was evidenced by FTIR and by the ninhydrin test.

Interaction of CNO/18C6 with the aminated polymers. Aqueous solutions of CMC-NH_2 (5 mg/mL) and poly-L-lysine (2% w/v) were prepared at different pH. CNO-18C6 (1mg) was added to 2 mL of the above solutions and the mixture was sonicated for 15 min. The supramolecular dispersions were then stored at room temperature in order to study their stability.

3.3 RESULTS AND DISCUSSION

The overall procedure for the supramolecular solubilization of CNO-18C6 is showed in Figure 3.3. The initial step involves the in-situ diazotization reaction under inert atmosphere to create CNO-18C6, which was slightly soluble in water. Afterwards, the polymers of CMC-NH_2 or poly-L-lysine in aqueous solutions were tested as supramolecular dispersive agents at different pH for CNO-18C6. In principle, at lower pH the amine group of the polymers must be protonated to give a positive ammonium cation that interact via ion-dipole with the crown ether residues attached to CNO.

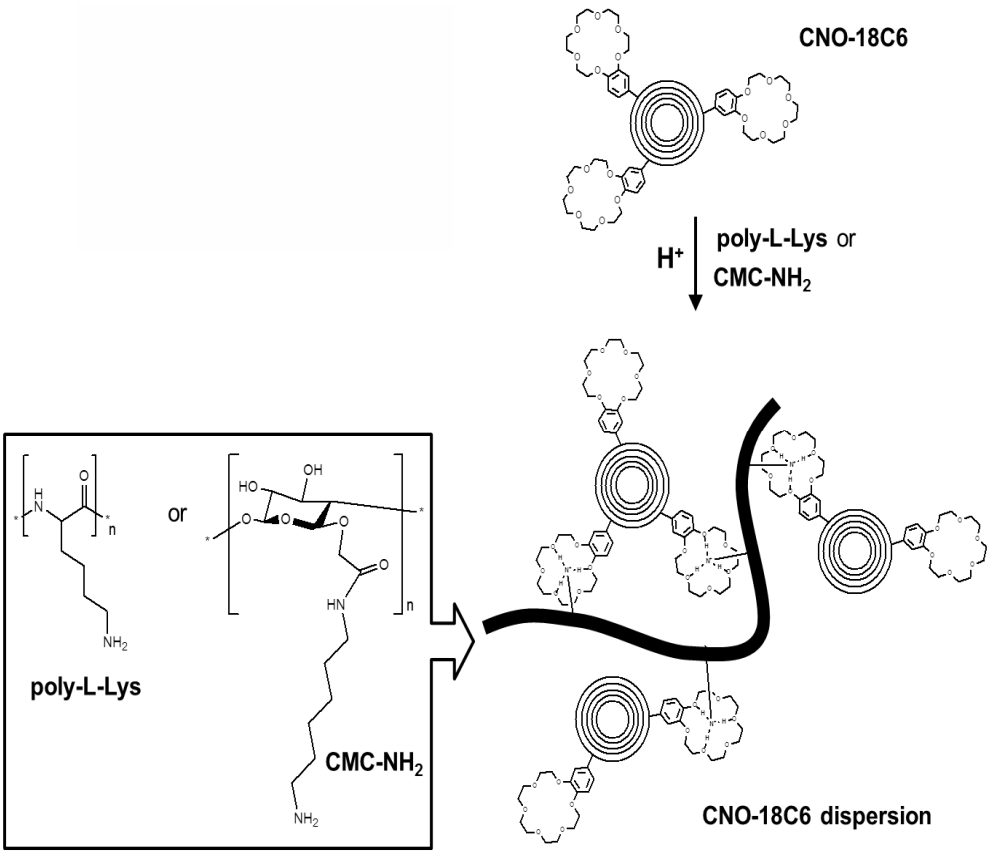

Figure 3.3: Strategy employed for the supramolecular solubilization of CNOs via crown ether/ammonium interactions.

Characterization of CNO-18C6. Evidence of the functionalization of CNOs by benzo-18-crown-6 was obtained from Raman spectroscopy and TGA measurements. The Raman spectrum (Figure 3.4) of the pristine CNOs shows the D band at 1318 cm^{-1}, while the G band appears at 1578 cm^{-1} with an I_D/I_G ratio of 1.4. Attachment of the benzo-18-crown-6 moieties provoked a shift of the D band to 1338 cm^{-1} and of the G band to 1568 cm^{-1}. These shifts can be attributed to the presence of disordered carbon structures and loss of symmetry due to incorporation of the benzo-18-crown-6 moieties to unsaturated carbon−carbon bond and indicate the successful modification of the surface of the CNOs. More notably, the I_D/I_G ratio in CNO-18C6 was found to be very close to 1. This increase of the D-band intensity has been observed in other covalently modified CNOs and is due to the increase of sp^3-hybridized carbon atoms.

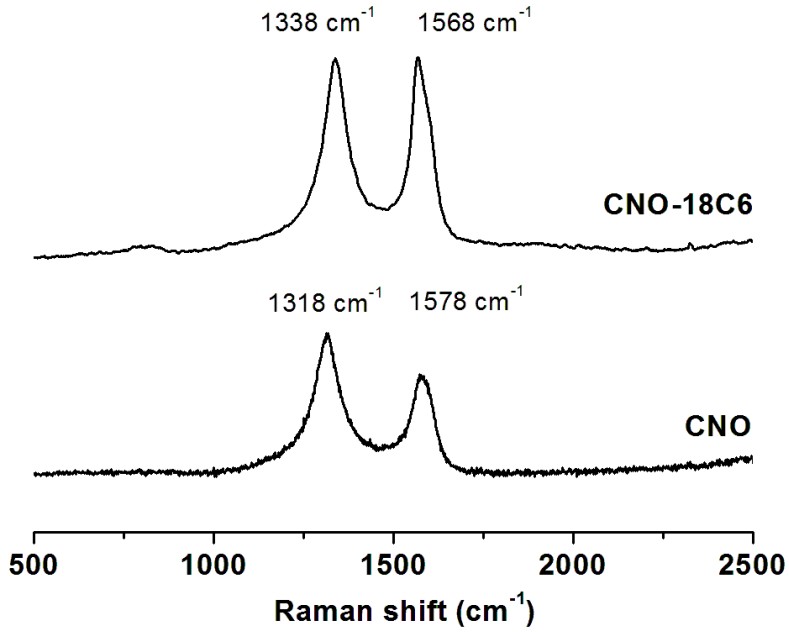

Figure 3.4: Raman spectra of CNO and CNO-18C6.

TGA was used to determine the degree of modification of benzo-crown ether groups in CNO-18C6. This analysis is based on the fact that the temperature required for the evaporation of the CNO-bound functional groups is considerably lower than that of the CNOs, allowing the selective removal of the functional groups in a TGA scan and thus the quantification of the degree of substitution. As shown in Figure 3.5 the TGA scan of modified CNO exhibits a first weight loss of 17% at 340ºC corresponding to the loss of the attached benzo-18-crown-6 ether from the surface of CNOs and a final decomposition at 746˚C. Interestingly, the covalent modification enhanced by ~30ºC the thermal stability of the CNOs. From the results of TGA, the average number of functional groups per CNO can be calculated [5]. Based on the HRTEM images of CNO-18C6 (Figure 3.6), they contain ~6 graphitic shells. Considering that each shell contains $60 \times n^2$ atoms, where n is the shell number, the sixth shell should then contain 2160 carbon atoms and the total number of carbon atoms in the CNO is 5460 with an average molecular weight of $5460 \times 12 = 65520$ g mol^{-1}. Translating the weight loss of

17% in CNO-18C6 into moles indicates that there are ~42 benzo-18-crown-6 groups per CNO (~1 per every 51 carbon of the outer shell).

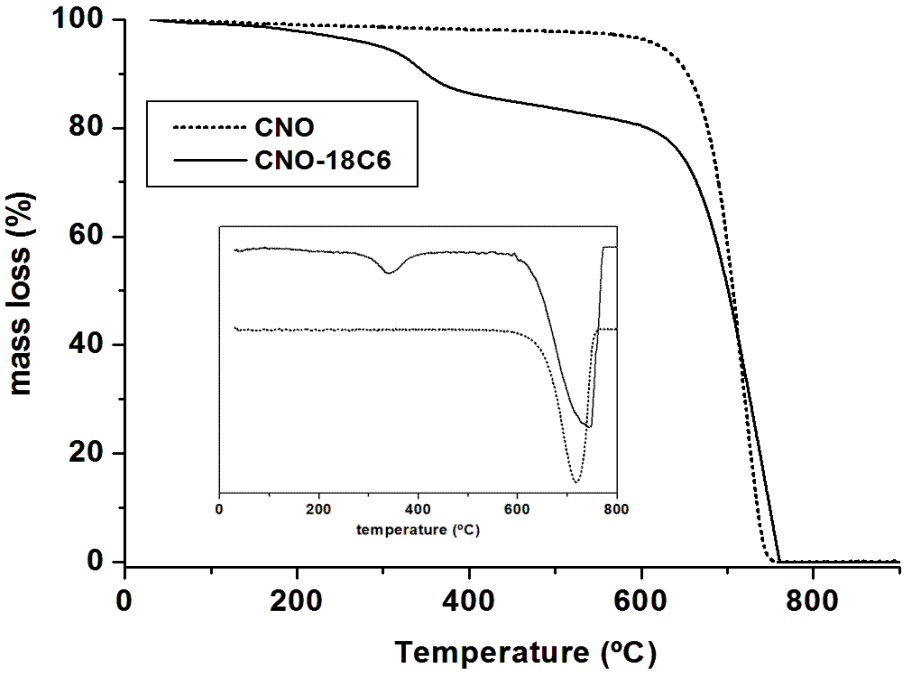

Figure 3.5: TGA curves for CNO (····) and CNO-18C6 (—). The corresponding first derivative curves are shown in the inset.

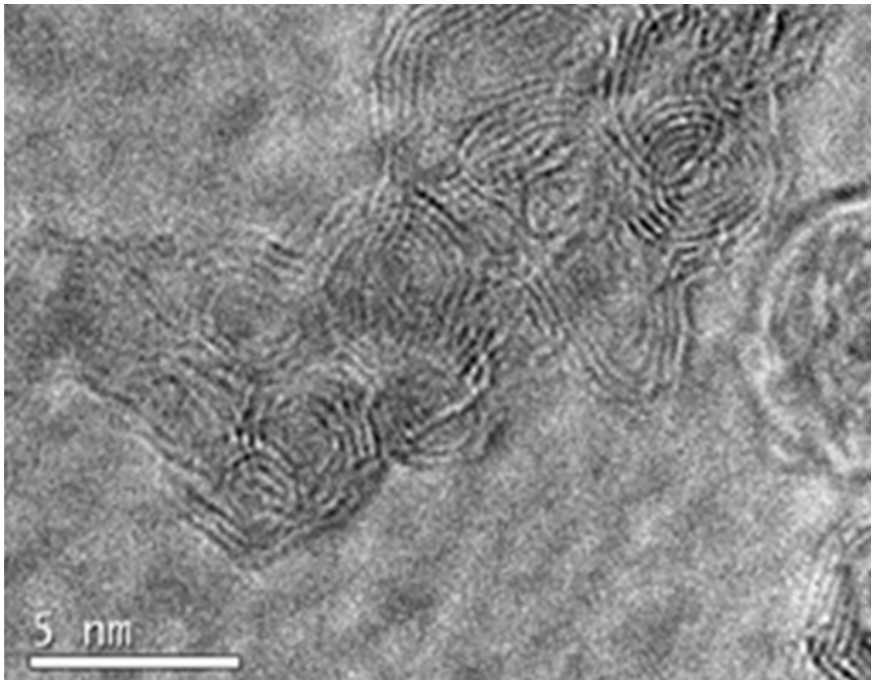

Figure 3.6: HRTEM image of CNO-18C6.

Interaction of CNO-18C6 with CMC-NH_2 and PLL. Linear polysaccharide polymers tend to adopt a random coil conformation in diluted aqueous solution [18]. This is important so that the pendant amino groups are available for the interaction with CNO-18C6.

Similarly, the proper conformation of poly-L-lysine in solution is determinant for a good dispersion of CNOs in solution. The conformation structure of poly-L-lysine in solution can be regulated by the nature of the solvent and by adjusting the pH as presented and there are two main conformations that can be found (Figure 3.7). The α helix is a spiral structure in which the peptide bonds form an intra-chain hydrogen bond network that stabilizes the structure and the lateral residues point outwards and are in contact with the solvent. This structure can be more opened as in the case of the P_{II} helix. On the other hand, the β-sheet is a more rigid pseudo-planar structure in which the hydrogen bonds associate between the strands and the side chains of the amino acids alternate above and below the sheet.

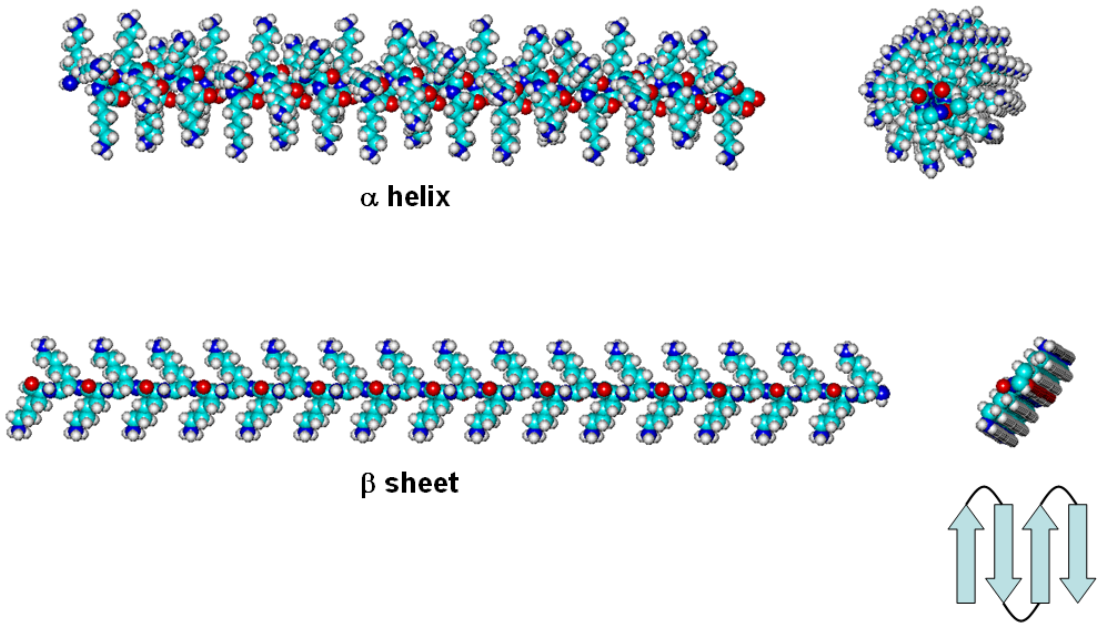

Figure 3.7: Energy minimized structures of the possible conformations of poly-L-Lys.

It can be expected that the α and P_{II} helix conformations would give a good dispersion of CNOs since they are more flexible structures and the amino groups of the side chains are more available for interaction. The conformations present in solution can be determined using infrared spectroscopy by analyzing the position of the amide bands. The amide I band stretches from 1600 to 1690 cm^{-1}, the amide II from 1500 to 1580 cm^{-1} and the amide III from 1220 to 1330 cm^{-1}. The nature or sensitivity of these amide stretching bands is related with the final folding structures of poly-L-lysine in solution. Usually, the presence of amide I in the range 1625–1640 cm^{-1} is dominated by β-sheet and strand conformations, while α and P_{II} helix make the band appear at higher wavenumbers (1643-1654 cm^{-1}). Amide II from α and P_{II} helix can be found at 1543–1552 cm^{-1} and aggregated β-sheets appear at 1530 cm^{-1}. Finally, the amide III band above 1200 cm^{-1} is much weaker and mostly originated by β conformations, while α and P_{II} helix give bands above 1290 cm^{-1} [19].

Poly-L-lysine has a pK_a value of ~10 [20]. This means that at neutral and slightly acid medium it should be fully protonated. Figure 3.8 shows the FTIR spectrum of poly-L-lysine at pH 4. The peaks appearing at 1644 and 1547 cm^{-1}, corresponding to amide I and II stretchings, respectively, indicate that the α and P_{II} helix are the dominant conformations, while the presence of the weak peak at 1244 cm^{-1} indicates a small contribution of the β sheet.

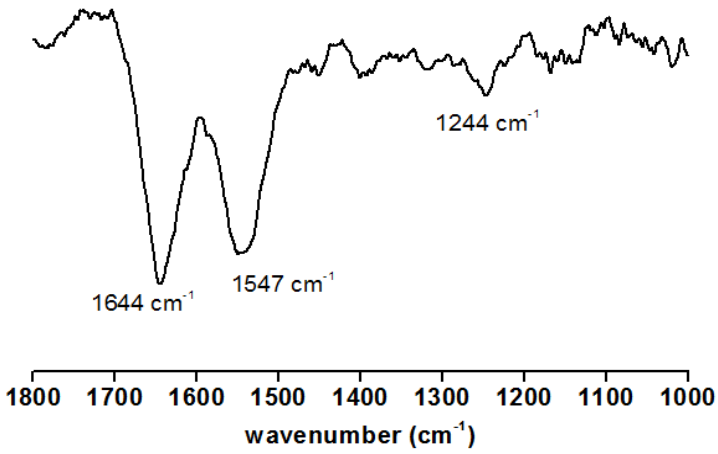

Figure 3.8: FTIR of Poly-L-lysine at pH 4.

Figure 3.9 shows photographs of CNO and CNO-18C6 dispersions obtained after sonication in the absence or presence of the aminated polymers at different pH values. As expected, CNO rapidly sediment in water and in poly-L-Lys but, interestingly, CNOs dispersed in CMC-NH_2 solution to form a suspension that is stable for a few hours. The reason for this behavior is not clear, but it is evident that there is some kind of interaction between the surface of the CNOs and the polymer. On the other hand, more stable dispersions of CNO-18C6 were obtained in the presence of the aminated polymers. In particular, the dispersion of CNO-18C6 and CMC-NH_2 at pH 4 was still clearly visible after several months at room temperature.

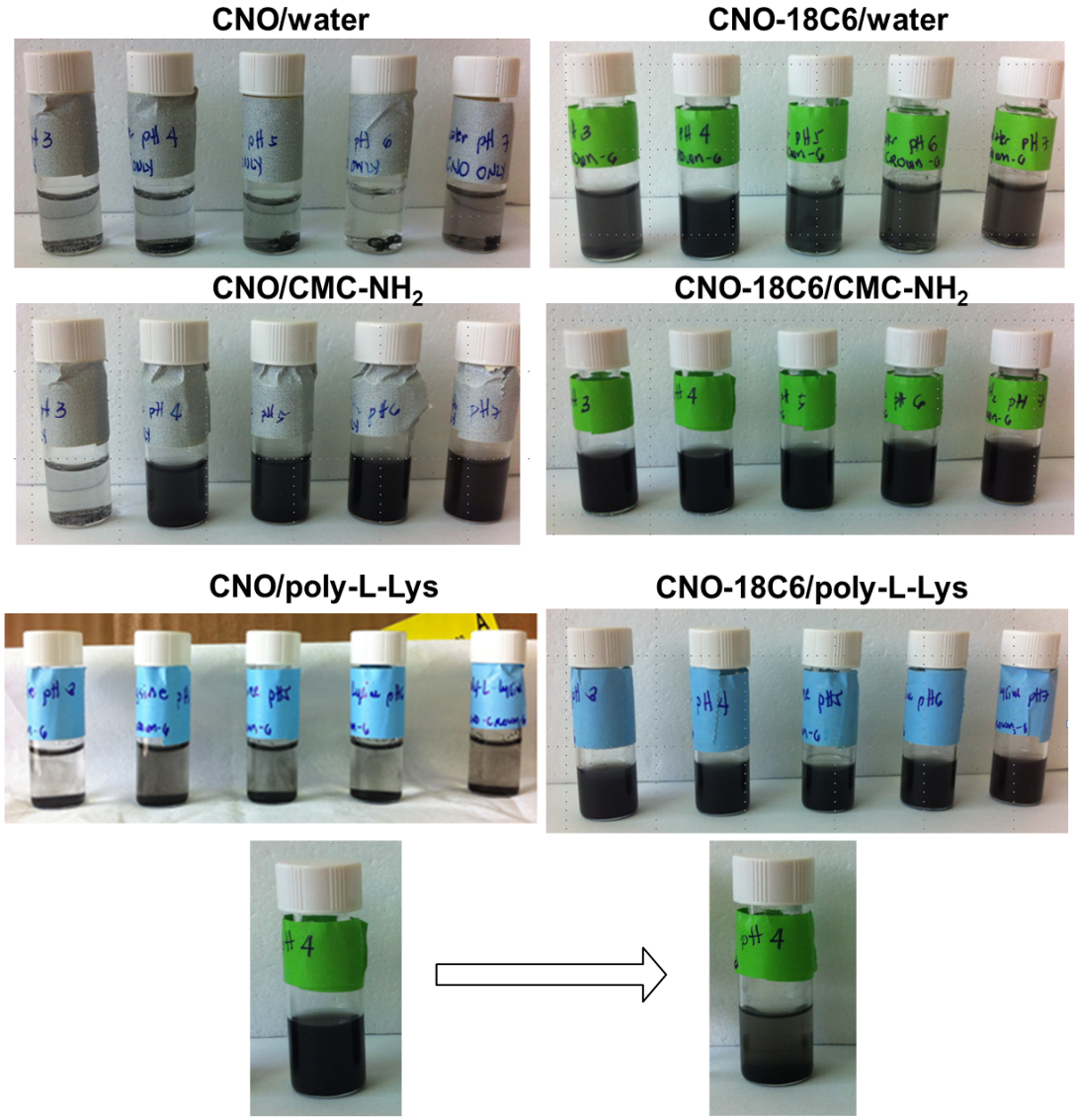

Figure 3.9: *Top*: Photographs of the different dispersions obtained at different pH (3 to 7) in aqueous solution with CNOs (left) and CNO-18C6 (right) the absence or presence of the aminated polymers. *Bottom*: Dispersion of CNO-18C6 in the presence of CMC-NH_2 at pH 4 after several months at room temperature.

When the pH of the CNO-18C6/CMC-NH_2 system was increased, a rapid precipitation of CNO-18C6 occurred due to the deprotonation of the aminated polymer (Figure 3.10). On the other hand, addition of an excess of K^+ to CNO-18C6/CMC-NH_2 at pH 4 induced the formation of a fine precipitate of CNO-18C6. This process was much slower than the precipitation due to the pH change and is due to competition of the K^+ cation with the pendant $–NH_3^+$ groups for the crown ether moiety. These results

indicate that the ammonium/crown ether interactions are the major driving force in the formation of the CNO dispersions.

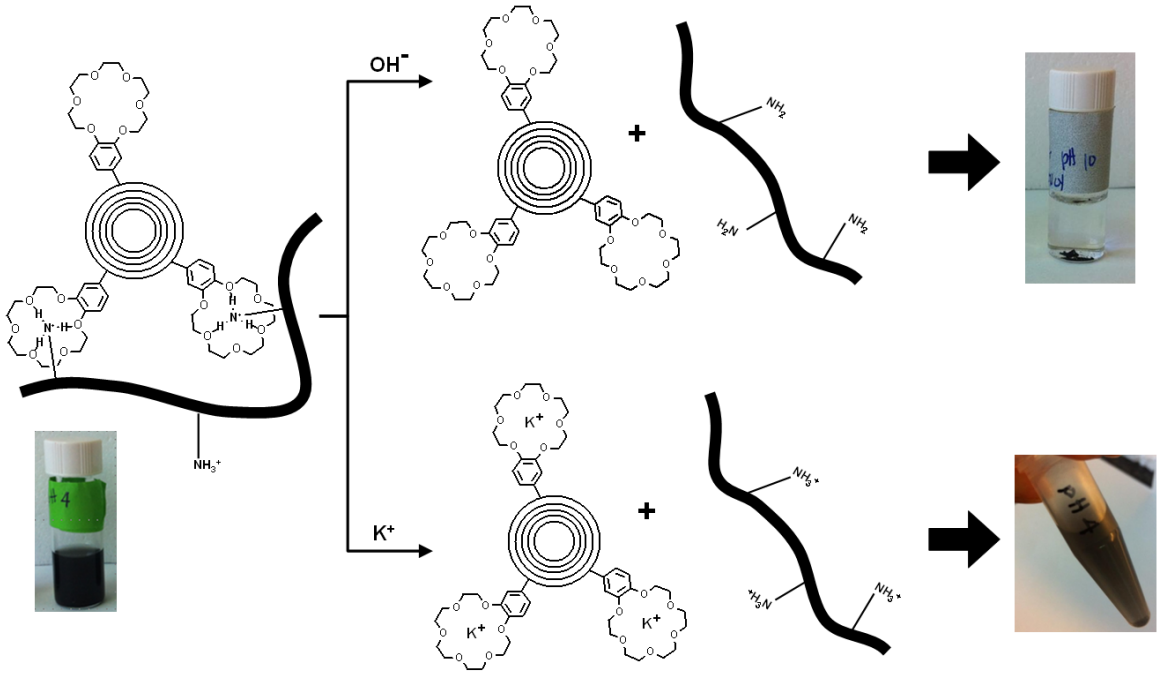

Figure 3.10: Effect of pH increase (top) and addition of K^+ cations (0.1 M K_2SO_4, bottom) on the CNO-18C6/CMC-NH_2 system.

CONCLUSIONS

In this chapter, we have explored the possibility to use crown ether/ammonium interactions for the dispersion of CNOs in solution using biocompatible polymers. CNOs were functionalized by reaction of diazotized 4-aminobenzo-18-crown-6. In the presence of biocompatible polymers containing pendant amino groups, such as aminated carboxymethyl cellulose and poly-L-lysine, the modified CNOs formed dispersions in water at acidic pH. Of them, the dispersion of CNO-18C6 and CMC-NH_2 at pH 4 was stable after several months at room temperature. Precipitation of the CNO-18C6 under basic conditions and in the presence of excess K^+ cation indicates that the ammonium/crown ether interactions are the major driving force in the formation of the CNO dispersions.

REFERENCES

1. J.L. Delgado, M. A. Herranz, N. Martin, *The nanoforms of carbon.* Journal of Materials Chemistry, 2008. **18**: p. 1417-1426.
2. S. Iijima, *Helical microtubules of graphitic carbon.* Nature, 1991. **354**: p. 56-58.
3. A. Molina-Ontoria, M. N. Chaur, M.E. Plonska-Brzezinska, L. Echegoyen, *Preparation and characterization of soluble carbon nano-onions by covalent functionalization, employing a Na-K alloy.* Chemistry Communication, 2013. **49**: p. 2406-2408.
4. V. Georgakilas, D.M. Guldi, R. Signorini, R. Bozio, M. Prato, *Organic functionalization and optical properties of carbn nano-onions.* Journal of American Chemical Society, 2003. **125**: p. 14268-14269.
5. C. Cioffi, A. Palkar, F. Melin, A. Kumbhar, L. Echegoyen,M. Melle-Franco, F. Zerbetto, G. Rahman, C. Ehli, V. Sgobba, D. Guldi, M. Prato, *A carbon nano-onion-ferrocene donor-acceptor system:synthesis, characterization and properties.* Chemistry a European Journal, 2009. **15**: p. 4419-4427.
6. A. Palkar, F. Melin, C.M. Cardona, B. Elliot, A.K. Naskar, D.D. Edie, A. Kumbhar, L. Echegoyen, *Reactivity differences between carbon nano onions (CNOs) prepared by different methods.* Chemistry an Asian Journal, 2007. **2**: p. 625-633.
7. A.S. Rettenbacher, M.W.Perpall, L. Echegoyen, J.S. Hudson, D.W. Smith Jr., *Radical addition of a conjugated polymer to multilayer fullerenes (carbon nano-onions).* Chemistry of Materials, 2007. **19**: p. 1411-1417.
8. L. Zhou, C. Gao, D. Zhu, W. Xu, F. F. Chen, A. Palkar, L. Echegoyen, E. S. Kong, *Facile functionalization of multilayer fullerenes (carbon nano-onions) by nitrene chemistry and "grafting from" strategy.* Chemistry European Journal, 2009. **15**: p. 1389-1396.
9. K. Flavin, M.N. Chaur, L. Echegoyen, S. Giordani, *Functionalization of multilayer fullerenes (carbon nano-onions) using diazonium compounds and "Click" chemistry.* Organic Letters, 2010. **12**(4): p. 840-843.
10. A. Palkar, A. Kumbhar, A.J. Athans, L. Echegoyen, *Pyridyl-functionalized and water-soluble carbon nano onions: Firts supramolecular complexes of carbon nano onions.* Chemistry of Materials, 2008. **20**: p. 1685-1687.
11. E. Wajs, A. Molina-Ontoria, T.T. Nielsen, L. Echegoyen, A. Fragoso, *Supramolecular Solubilization of cyclodextrin-modified carbon nano-onions by host-guest interactions.* Langmuir, 2015. **31**: p. 535-541.
12. A. Späth, B. König, *Molecular recognition of organic ammonium ions in solution using synthetic receptors.* Beilstein Journal of Organic Chemistry, 2010. **6**(32).
13. F. Wang, C. Chen, Y.Zhang, D. Fu, *Crystal structure and dielectric property of supramolecular macrocyclic [(NDPA)(18-crown-6)]2+(DMA)+3ClO4 assemblies.* Chinese Chemical Letters, 2015. **26**: p. 31-35.
14. G.W. Gokel, W.M. Leevy, M.E. Weber, *Crown Ethers: Sensors for Ions and Molecular Scaffolds for Materials and Biological Models.* Chemical Reviews, 2004. **104**(5): p. 2723-2750.
15. B. Zheng, F. Wang, S. Dong, F. Huang, *Supramolecular polymers constructed by crown ether-based molecular recognition.* Chemical Society Reviews, 2012. **41**: p. 1621-1636.

16. M.C.T. Fyfe, J.F. Stoddart, *(Supra)molecular systems based upon crown ethers and secondary dialkylammonium ions.* Advance Supramolecular Chemistry, 1999. **5**: p. 1-53.
17. V. Balzani, A. Credi, S. Silvi, M. Venturi, *Artificial nanomachines based on interlocked molecular species: recent advances.* Chemical Society Reviews, 2006. **35**: p. 1135-1149.
18. J. Kadokawa, T. Arimura, Y. Takemoto, K. Yamamoto, *Self-assembly of amylose-grafted carboxymethyl cellulose.* Carbohydrate Polymers, 2012. **90**: p. 1371-1377.
19. A. Mirtic, J. Grdadolnik, *The structure of poly-L-lysine in different solvents.* Biophysical Chemistry, 2013. **175-176**: p. 47-53.
20. H.M. Eckenrode, H. Dai, *Nonlinear Optical Probe of Biopolymer Adsorption on Colloidal Particle Surface: Poly-L-Lysine on Polystyrene Sulfate Microsphere.* Langmuir, 2004. **20**(21): p. 9202-9209.

Chapter 4

Simultaneous detection of nitrite and ascorbic acid at carbon nano-onion modified glassy carbon electrodes

ABSTRACT

In this work we have evaluated two possible different surfaces for simultaneous detection of two analytes. The electrochemical properties of the stable layer of pristine carbon nano-onion (CNO) in the surface of glassy carbon electrode (GCE) in ferrricyanide solution were verified in cyclic voltammetry. The glassy carbon electrode modified carbon nano-onions (GCE/CNO) with electrografted ortho-aminophenol (*o*-AP) and physically adsorbed thionine have been used for the simultaneous detection of nitrite and ascorbic acid. By utilizing cyclic voltammetry and by tuning alternately the desired potentials in DC amperometry, the modified surfaces exhibited fast response and able to detect the presence of nitrite and ascorbic acid. For simultaneous detection of nitrite and ascorbic acid, two well-separated voltammograms peaks were obtained and the corresponding peak separations between nitrite and ascorbic acid were +750mV and +200 mV respectively. The modified surface with GCE/CNO showed enhanced electrocatalytic behaviour as compared to GCE modified only with o-AP and thionine as shown in their amperometric results. Furthermore, the CNO-modified surface showed good reproducibility and stability through time.

4.1 INTRODUCTION

Nitrite and ascorbic acid (AA) are two of the most widely used additive compounds in products for human consumption. They are controlled substances and thus there is an increasing interest for their analysis [1-5]. Ascorbic acid has been recognized as an important food stabilizer to improve nutritional value and prevent autooxidation of products [6, 7]. Although ascorbic acid toxicity is very rare; a high dose can lead to stomach upset and diarrhea [8]. On the other hand, nitrite is a useful preservative in food industry to enhance color and extend the shelf life of processed meats. However, nitrite ions can react with amines to form nitrosamines, which are well known carcinogenic substances [9, 10].

Various methods have been proposed for the detection of AA and nitrite such as chromatography [11-13], spectroscopic techniques [14-16] and electrochemical analysis [17-23]. However, these molecules can be directly oxidized in the surface of conventional electrodes at high overpotentials (Figure 4.1). Many new materials have been suggested to overcome this problem and among these is the use of carbon nanomaterials. They had been utilized due to their good electrocatalytic properties that may result in a lowering of oxidation potentials [24-32]. Like for example, Zhu et al. [31], prepared modified poly(amidoamine) dendrimer- carbon nanotubes for the determination of nitrite held at +0.73V as oxidation potential in chronoamperometry. Using nanodiamond powder electrode for the analysis of nitrite was investigated by Chen et al. [32] in which the oxidation of nitrite appears around +1.05V using cyclic voltammetry (CV) and differential pulse voltammetry (DPV). On the other hand, the oxidation of ascorbic acid on the prepared ZnO-decorated reduced graphene oxide electrode exhibited at around +0.2V [26]. While using poly(xanthurenic

acid)/multiwalled carbon nanotubes for electrochemical determination of ascorbic applied a potential at +0.3 V in linear sweep voltammetry (LSV) and amperometry [24].

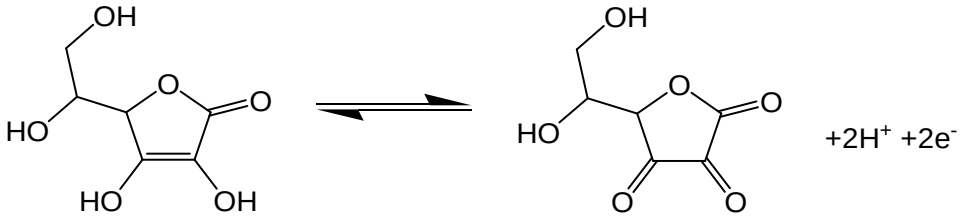

$$NO_2^- + H_2O \rightarrow NO_3^- + 2H^+ + 2\ e^-$$

Figure 4.1: Oxidation reactions of AA and nitrite.

As we have seen in previous chapters, CNOs are attractive candidates for the development of electrochemical detection systems due to their morphological and electrical properties. To the best of our knowledge, there is only one example of application of CNOs in electrochemical detection of small molecules [33]. A mixture of carbon CNO/poly(diallyldimethylammonium chloride)- composites were deposited on a gold electrode then the electrochemical properties of the surface were tested for the ability to detect dopamine in the presence of uric and ascorbic acid. Their findings showed good selectivity and sensitivity of the modified electrodes.

Diazonium salts ($R\text{-}N{\equiv}N^+\ X^-$) are a class of organic compounds prepared by the treatment of aromatic amines with sodium nitrite in the presence of a mineral acid. Electrochemical grafting for covalent modification of conductive surfaces by electrochemical reduction of aryl diazonium salts was first investigated by Pinson using isolated tetrafluoroborate salts [34] and further extended to *in situ* generated diazonium cations [35]. This method can be applied to a wide variety of surfaces such as carbon (including nanotubes and diamond), metals and metal oxides and provide an easy and

efficient way to covalently modify the surface of these materials [35-37]. The mechanism of the reaction involves the formation of an aryl radical produced upon one-electron reduction of the diazonium salt that then reacts with the surface to form a covalent bond (Figure 4.2). In our group, we have exploited this technique to construct various types of electrochemical sensors based on *ortho*-aminophenol (*o*AP) films on glassy carbon surfaces [38-41].

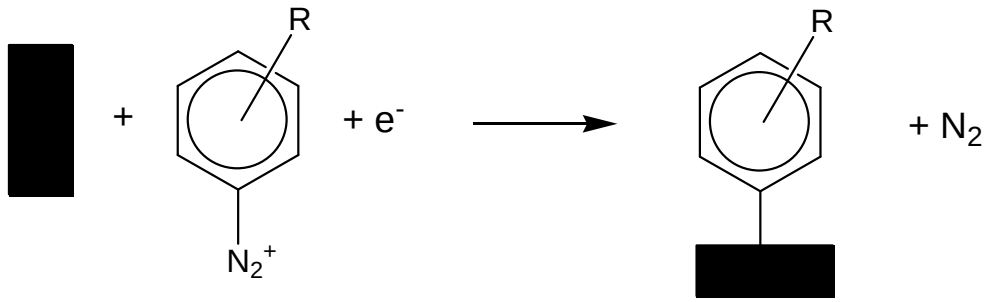

Figure 4.2: Modification of surfaces by electrografting of diazonium salts.

On the other hand, thionine is a thiazine derived aromatic dye containing two –NH2 groups and generally used for dyeing. Thionine is also an electrochemical redox indicator being colorless in reduced form and violet when oxidized. Several studies have been conducted, particularly on carbon nanotubes, in which thionine was directly absorbed and attached to the surface creating a strong supramolecular π-π interaction [28, 42-44].

In this chapter, we describe the electrocatalytic behavior of electrografted *ortho*-aminophenol (*o*AP) and physically adsorbed thionine in a modified CNO-glassy carbon electrode (GCE/CNO). We used pristine CNOs that were directly casted on GCE surface before the covalent functionalization using in-situ electrochemical grafting of *o*AP. We also study, for the first time, the absorption of thionine to the surface of CNO and use these surfaces for the simultaneous detection of AA and nitrite.

4.2 EXPERIMENTAL SECTION

Reagents and Instrumentation. The CNO sample was kindly provided by Dr. Luis Echegoyen (Department of Chemistry, University of Texas at El Paso). Dimethylformamide (DMF), L-ascorbic acid, 2-nitro-4-aminophenol, $NaNO_2$ and thionine were obtained from Sigma-Aldrich and used as received. All other chemicals used in buffer solutions preparation were of analytical-reagent grade. All solutions were prepared with milliQ water.

Tip sonicator (amplitude 60%, cycle 0.5, Ultraschallprocessor UP200S) was used to mechanically disperse CNOs in 10 mL DMF. All electrochemical measurements were carried out using an Autolab model PGSTAT 12 potentiostat/galvanostat controlled with the general purpose electrochemical system (GPES) software (Eco Chemie, The Netherlands), equipped with BASi C-3 Stand (RF-1085) three-electrode cell. This configuration contains a bare or chemically modified glassy carbon electrode (BAS model MF-2012, 3.0 mm diameter) as working electrode, a platinum wire as counter electrode and an $Ag/AgCl_{(sat)}$ as reference electrode. All potentials were recorded with respect to this electrode. A magnetic stirrer provided the convective transport during the amperometric experiments.

Purification, Dispersion and Deposition of CNOs. The as-received sample of CNOs was subjected for purification procedure in which 5 mg were boiled in 30% hydrogen peroxide for 2 hours and then 1 hour in milliQ water. The insoluble particles were gathered and dried under vacuum at 100ºC. The treatment in peroxides was applied to remove amorphous carbon particles in the surface of CNOs. Two-milligrams of purified CNOs were dispersed in 10 mL dimethyl formamide (DMF) and subjected to tip sonication for 30 min to obtain a homogenous solution.

Prior to the deposition of CNOs, the glassy carbon electrode was polished to a mirror finish with 0.3 μM alumina slurries, cleaned and sonicated in milliQ water for 5 min and then dried under a stream of nitrogen gas.

To obtain a thin layer of CNOs on the surface of the electrode, the homogenized CNO solution in DMF (2 μL) was dropped into the cleaned electrode. The deposition of CNOs was achieved in successive cycles of drop casting and then dried with hot air at about 150ºC. The procedure was repeated until the desired thickness of CNOs in the surface of the GCE was obtained. Then the electrode was washed with milliQ water and dried with nitrogen gas to be ready to use. The modified electrodes were characterized by Environmental Scanning Electron Microscopy (ESEM, FEI Company Inc., Quanta 600) at high vacuum at 25 kV in 10 mm working distance and cyclic voltammetry.

Electrochemical grafting of *o*AP on GCE/CNO. 2-nitro-4-aminophenyl films were prepared on GCE/CNO electrodes using essentially the same method as described in reference [14]. A cold mixture of 2-nitro-4-aminophenol and $NaNO_2$ (both 10 mM) was treated with 0.5 M HCl (degassed with N_2) for 10 min in an electrochemical cell. GCE/CNO electrodes were immersed and the potential was cycled from 0 V to -0.6 V at 100 mV/s for 60 scan cycles. The generated 2-nitrophenol film was rinsed and sonicated in milliQ water (5 min). For complete reduction of the nitro group the electrode was subjected to 5 potential scans between -0.1 and -0.85 V at 100 mV/s in 0.1 M H_2SO_4. The electrodes were washed with milliQ water then subsequently subjected to potential scanning between -0.1 and 0.6 V for 10 cycles at 100 mV/s in phosphate buffer (0.1 M, pH 7.4) to remove the physically adsorbed compounds.

The characterization of the *o*AP film in the GCE/CNO was carried out by cyclic voltammetry between -0.4 to 0.6 V at different scan rates in phosphate citrate buffer pH

3.5. O_2-free nitrogen was used to remove oxygen from the solution and a continuous flow of nitrogen was maintained during the voltammetric measurements. All experiments were carried out at ambient temperature. The same procedure was done with bare GCE that served as a control.

Preparation of thionine modified GCE/CNO electrode. The prepared electrode of GCE/CNO was immersed in a 2 mg/mL thionine solution for several hours for optimization (1hour, 2h, 3h, 4h and 5h) and then washed thoroughly with phosphate citrate buffer pH 3.5 for 30 min at temperature with convective stirring to remove the unbound thionine molecules. The modified GCE/CNO/thionine was activated though successive voltammetric cycling between -0.3 and 1.0 V at 100 mV/s at 10 scan cycles in the blank phosphate citrate buffer pH 3.5. The same procedure was done with bare GCE that served as a control.

Detection of nitrite and ascorbate with GCE/CNO/*o*AP and GCE/CNO/thionine electrodes. The modified electrode surfaces with electrografted oAP were used for the detection of nitrite and ascorbic acid. DC amperometric measurements were performed at 0.750 V or 0.200 V for the detection of nitrite and ascorbic acid, respectively, in an electrochemical cell containing 5 mL phosphate citrate buffer pH 3.5 in the presence of a constant concentration of 10 µM of either nitrite or ascorbic acid, depending on the desired analyte to be detected.

The background current was measured under stirring conditions at 350 rpm. Subsequently, successive injections of 50 µL of 1 mM nitrite or ascorbic acid have been added to the cell and the current response was continuously recorded. The same procedures were done in GCE/CNO/thionine. Control experiments were carried out on GCE/*o*AP or GCE/thionine electrodes under the same conditions for comparison.

4.3 RESULTS AND DISCUSSION

Deposition of CNOs on glassy carbon electrodes

Figure 4.3 shows the ESEM images of bare GCE and modified GCE with CNO, A and B respectively. As can be seen in the images revealed that the morphology of bare GCE is very different from the modified GCE/CNO. The GCE has been properly covered with CNO and the surface has a markedly rough and porous characteristic.

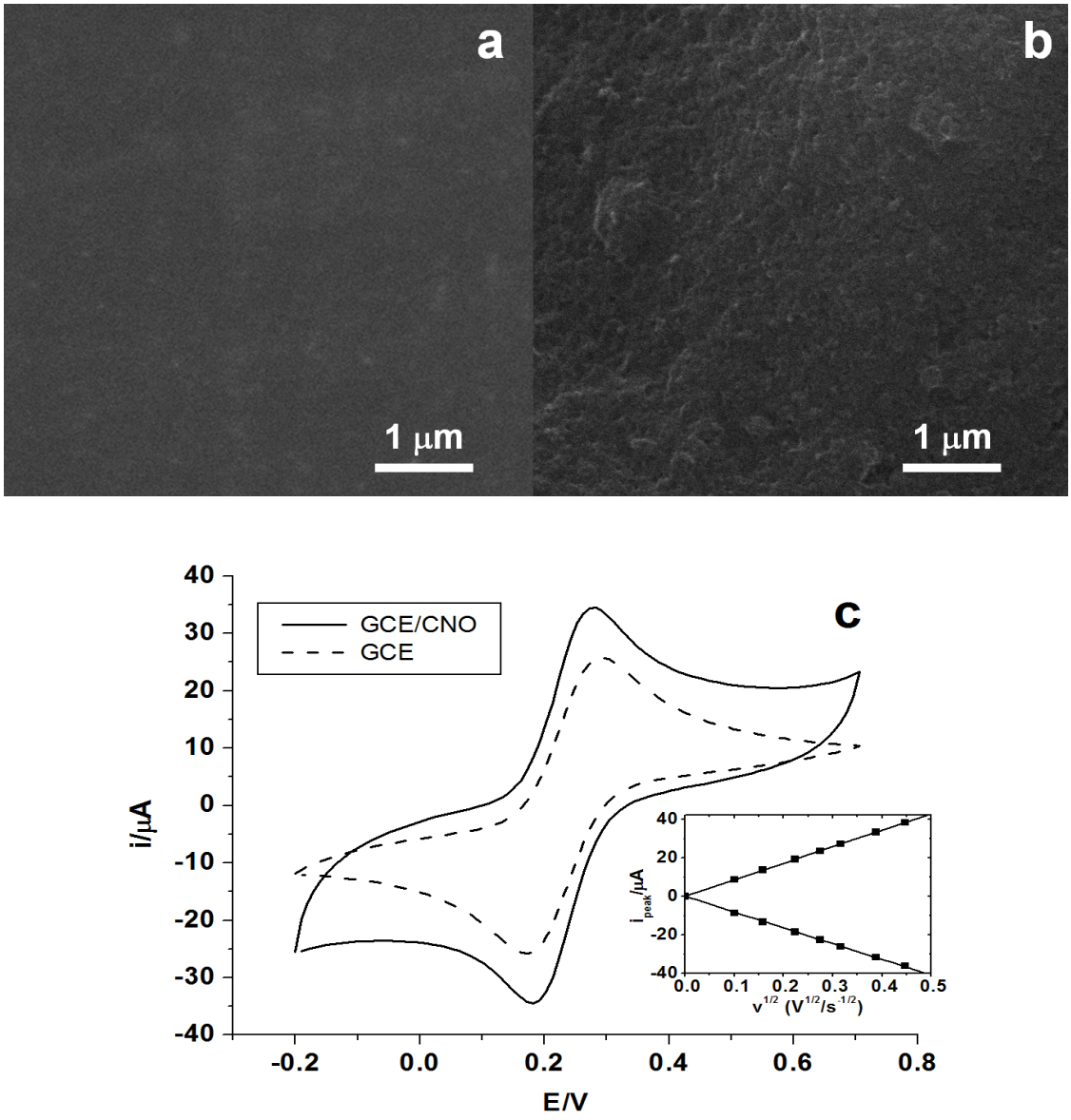

Figure 4.3: ESEM images of GCE (a) and GCE/CNO (b) and their corresponding cyclic voltammetry in 1 mM $[Fe(CN)_6]^{3-}$ in 0.1 M KCl at scan rate 0.1 Vs^{-1} (c) inset: plot of the peak currents *vs*. scan rate for GCE/CNO.

The electroactive surface area of GCE/CNO was determined by cyclic voltammetry (CV) using $[Fe(CN)_6]^{3-}$ in KCl as electroactive marker. As shown in Figure 4.3c, GCE/CNO showed a notable higher peak current signal as compared to bare GCE due to the increased active area provided by the deposition of CNOs in the transducer surface. The electroactive surface area of GCE/CNO modified electrodes was determined using the Randles-Sevcik equation [45]:

$$i_p = 2.69\times10^5 A D^{1/2} n^{3/2} v^{1/2} c$$

Where i_p is the peak current, A is the electroactive surface (cm^2), D is the diffusion coefficient of $[Fe(CN)_6]^{3-}$ in dilute aqueous solution, n is the number of transferred electrons by $[Fe(CN)_6]^{3-/4-}$ (n = 1), v is the scan rate in V s^{-1} and c is the concentration of the marker (1×10^{-6} mol/cm^3). Based from this equation, by plotting the values of i_p versus $v^{1/2}$ (shown in the inset Figure 4.3c), the calculated electroactive surface of modified GCE/CNO is 0.56 cm^2 whereas bare GCE only have 0.43 cm^2 active surface area. This suggests also that the addition of CNO into the surface improves the effective surface active areas thus electrochemical properties of the surface has been enhanced.

It was also observed that the deposited purified CNOs showed a good mechanical stability in aqueous solution. Treatments such as repetitive washings with water, immersion in aqueous solutions for a long time and even mild sonication did not cause removal of deposited material from the surface of GCE as proven by electrochemical measurements and reproducibility results (data not shown).

Electrochemical characterization of *o*AP and thionine modified GCE/CNO electrodes

The *o*AP modified electrodes were prepared in two steps by electrografting the *in situ* prepared diazonium salt of 2-nitro-4-aminophenol followed by potential reduction in acidic medium (Scheme 4.1)

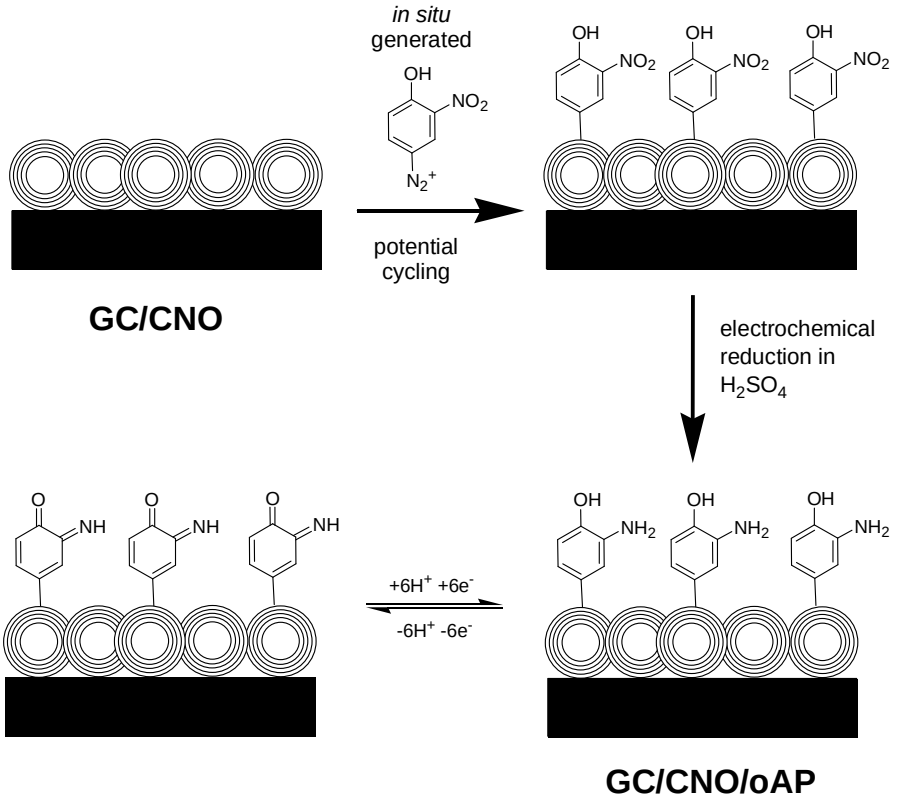

Scheme 4.1: Preparation of GC/CNO/*o*AP electrodes.

The cyclic voltammograms of GC/CNO/*o*AP modified electrodes at different scan rates showed the typical quasi-reversible signal associated with the oxidation and reduction of electrografted *oAP* at $E_{1/2}$ = -3 mV vs Ag/AgCl (Figure 4.4). As observed, the voltammetric response of GCE/CNO/*o*AP electrodes presents higher current intensities than the corresponding GCE/*o*AP prepared in a similar way although the $E_{1/2}$ is essentially the same. This enhancement in the current signal is consistent with the

results presented in Figure 1c associated to an increase in electrode area in the presence of CNOs.

The surface coverage of *o*AP in the surface of GCE/CNO/*o*AP was evaluated from the equation $\Gamma = Q/nFA$, where Q is the charge associated with the *o*AP oxidation peak (area under the curve corrected for the baseline) at a low scan rate (10 mV s^{-1}), n is the number of exchanged electrons (n = 2), F is the Faraday's constant and A is the area of the electrode. The calculated value of Γ was 2.71 × 10^{-10} mol cm^{-2}, which is about 2 times higher than that obtained for the grafting of *o*AP on GCE.

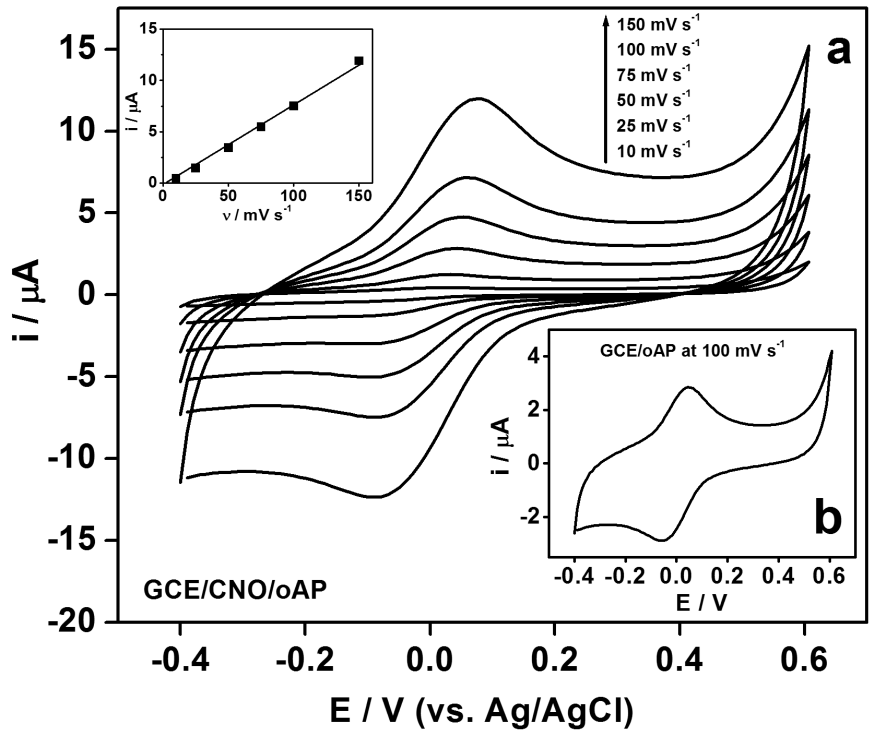

Figure 4.4: Cyclic voltammograms at different scan rates of electrografted *o*AP on GCE/CNO (a) and GCE (b) in phosphate citrate buffer pH 3.5.

Thionine was immobilized on GCE/CNO electrodes by spontaneous adsorption (Scheme 4.2). CNOs have a higher surface area than and, as expected, a higher amount

of thionine could be absorbed onto the modified GCE/CNO surface. The rough and porous surface layer of GCE/CNO evidenced in the ESEM images would maximize the access of thionine deposited as thin film which leads to a more stable surface.

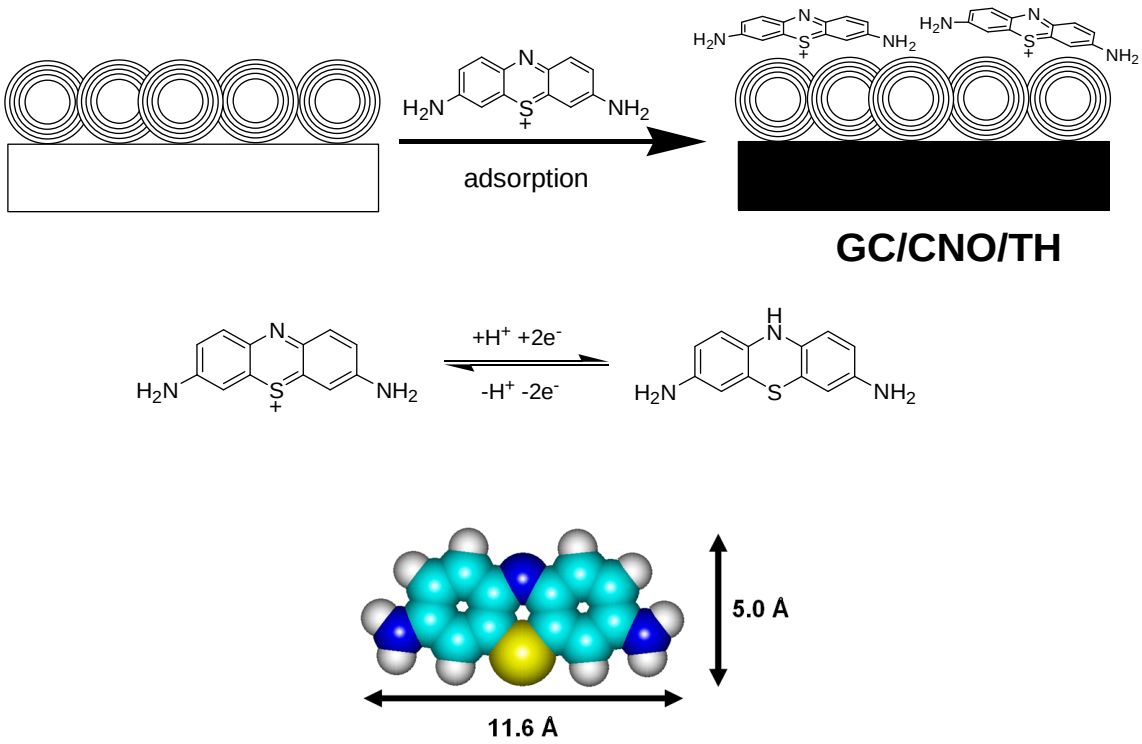

Scheme 4.2: Top: Preparation of GC/CNO/TH electrodes. Bottom: Redox reaction of thionine and dimensions.

The adsorption of thionine was studied as a function of time by cyclic voltammetry on both surfaces (Figure 4.5). As can be seen, the redox signals of thionine increase with time and remain essentially constant after three hours on the GCE/CNO surface. This time was thus used in further experiments. In the case of GCE, the saturation is achieved after two hours and the redox response is markedly lower, indicating a weak interaction of thionine with the bare surface.

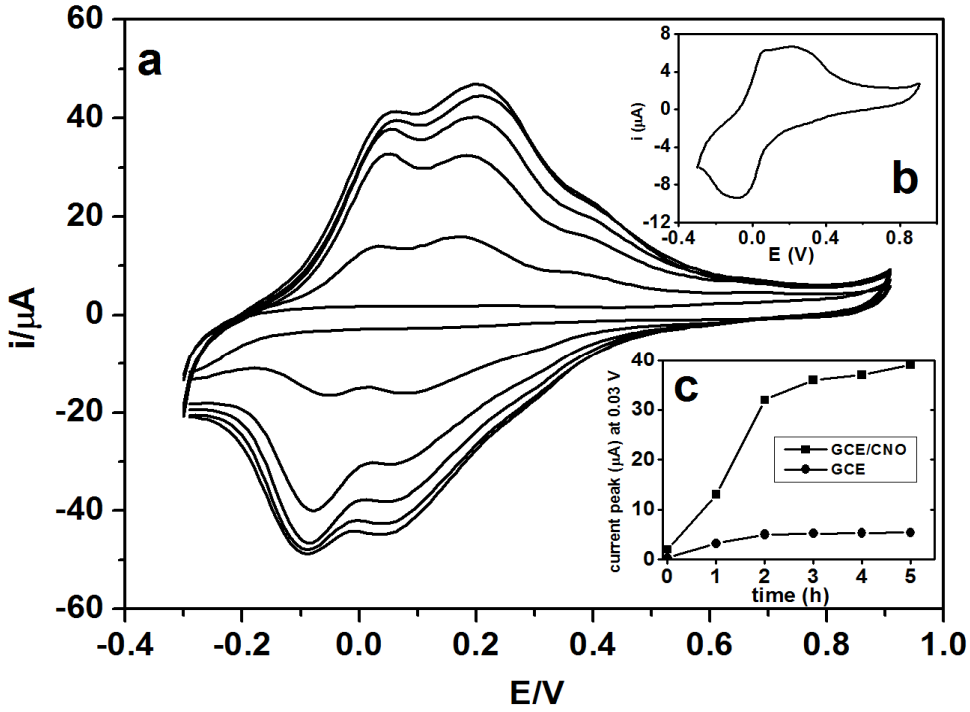

Figure 4.5: a) Cyclic voltammograms of thionine at different incubation times (0, 1, 2, 3, 4, 5 h) on GCE/CNO. (b) Cyclic voltammogram of thionine at bare GCE after 3 h of incubation. c) Dependence of the anodic current signal at 0.03 V with time for both surfaces. Scan rate: 50 mVs^{-1} in phosphate citrate buffer pH 3.5.

Figure 4.6 shows the cyclic voltammograms of thionine modified GC/CNO surface at different scan rates. The voltametric response of thionine is characterized by broad successive peaks in both anodic and cathodic scans, indicating the electrochemical activity of adsorbed thionine [28, 44, 46]. The current responses showed a linear relationship with scan rate, indicating surface confinement of thionine. After continuous potential cycling, the electrochemical characteristics of thionine were stable, indicating a strong interaction with the CNO surface. The surface coverage of thionine in the surface of GCE/CNO was 1.81×10^{-10} mol cm^{-2}. This surface coverage is about 6 times higher than that observed of GCE/thionine. Considering the dimensions of thionine (58 $Å^2$) and assuming a planar stacking on the CNO-surface, the theoretical coverage of thionine on GCE/CNO would be 2.77×10^{-10} mol cm^{-2} and therefore about 65% of the surface is actually covered. This is not surprising, considering the roughness of the

CNO-modified surface that could hinder the formation of a perfectly adsorbed monolayer.

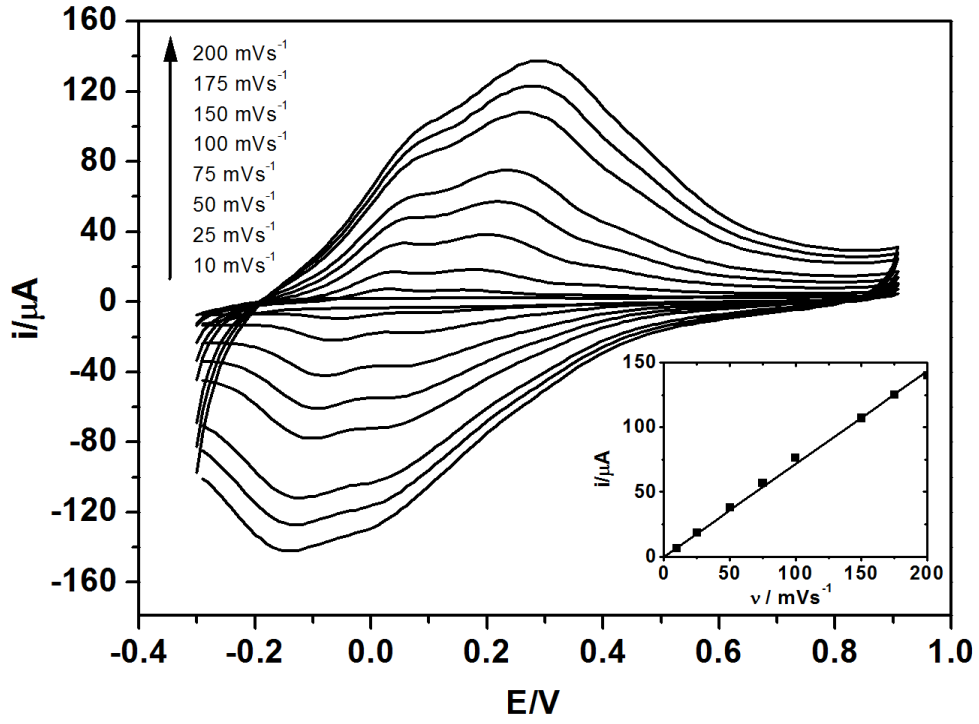

Figure 4.6: Cyclic voltammograms of adsorbed thionine in GCE/CNO at different scan rates in phosphate citrate buffer pH 3. Inset: current vs. scan rate plot.

Electrochemistry of nitrite and ascorbic acid at GCE and GCE/CNO

The electrochemical response of AA and nitrite at GCE is characterized by irreversible anodic signals at 0.12 and 0.89 V (Figure 4.7). Interestingly, at GCE/CNO electrodes both oxidation processes are favored and shifted to less positive potentials (0.09 and 0.80 V for AA and nitrite). Thus, the overpotential for the oxidation of nitrite is reduced by 0.11 V, indicating that the presence of CNOs favors the electron transfer reactions (Figure 4.8).

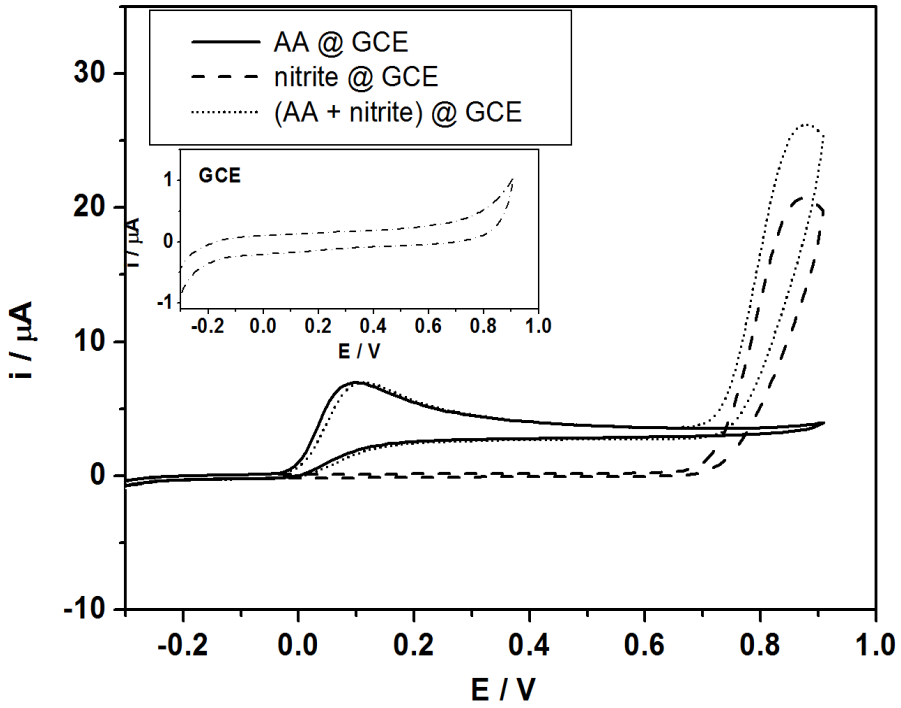

Figure 4.7: Cyclic voltammograms at bare GCE in the presence of 100 µM nitrite, 100 µM ascorbate and a mixture of both (100 µM each). Scan rate 100 mV/s in phosphate citrate pH 3.5.

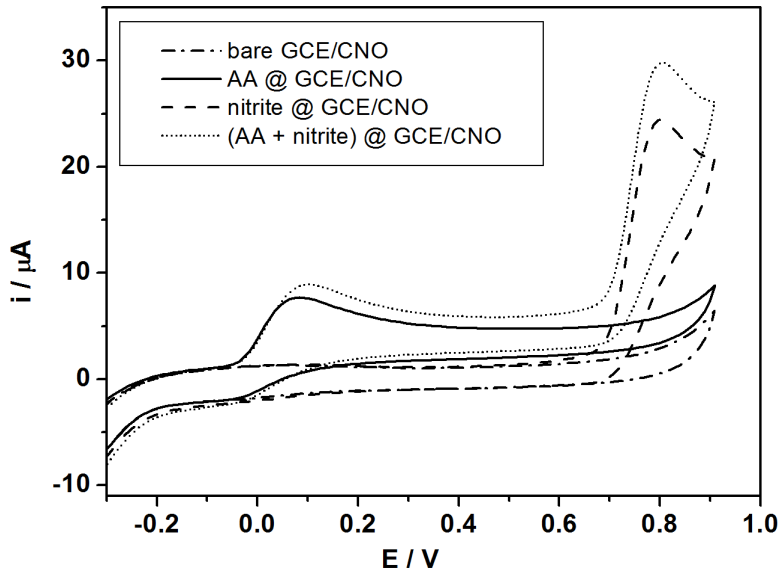

Figure 4.8: Cyclic voltammograms at GCE/CNO in the presence of 100 µM nitrite, 100 µM ascorbate and a mixture of both (100 µM each). Scan rate 100 mV/s in phosphate citrate pH 3.5.

Electrochemical detection of nitrite and ascorbic acid at GCE/CNO/*o*AP electrode

In order to evaluate the electrocatalytic activity of modified GCE/CNO/*o*AP surface towards the oxidation of AA and nitrite, cyclic voltammograms were recorded in phosphate citrate buffer pH 3.5 in the absence and presence of 100 µM NO_2^- and/or 100 µM AA as shown in Figure 4.9.

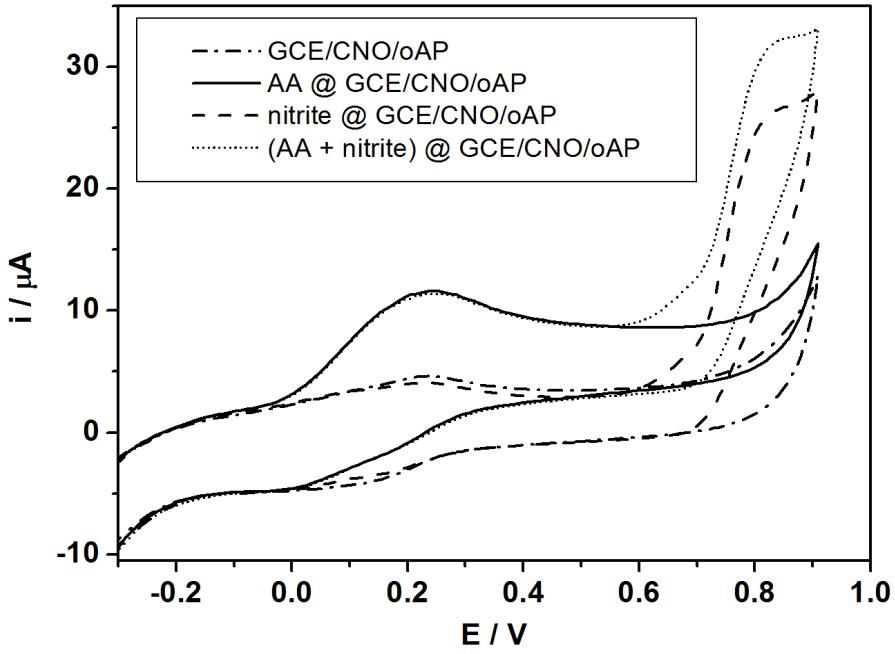

Figure 4.9: Cyclic voltammograms at GCE/CNO/*o*AP in the presence of 10 µM nitrite, 10 µM ascorbate and a mixture of both (10 µM each). Scan rate 100 mV/s phosphate citrate buffer pH 3.5.

Upon the addition of nitrite on modified GCE/CNO/*o*AP, there is an irreversible oxidation peak at 0.78 V which corresponds to the two-electron oxidation process of NO_2^- to NO_3^-. This peak potential is negatively shifted ~20 mV with respect to GCE/*o*AP indicating that the presence of CNO reduced the overpotential and also enhances the oxidation current. In the case of the presence of AA, there is also a noticeable enhancement of the anodic peak around 0.2 V, which shows that the surface

is sensitive to the addition of AA. Therefore, the modified GCE/CNO/*o*AP surface has the capability to oxidize ascorbate and nitrite at different potentials.

This surface was then used to detect ascorbic acid and nitrite by amperometric measurements at different potentials but in the same electrode. The amperometric measurements were done with either the presence of nitrite or ascorbic acid added into the buffer solution prior to the addition of the other analyte in order to know if the presence of the other analyte in the solution would somehow affect the current response. As can be seen in Figures 4.10a and 4.10b, the current responses rapidly achieved a steady current with the successive additions of 10 µM of each analyte indicating a fast electrochemical response.

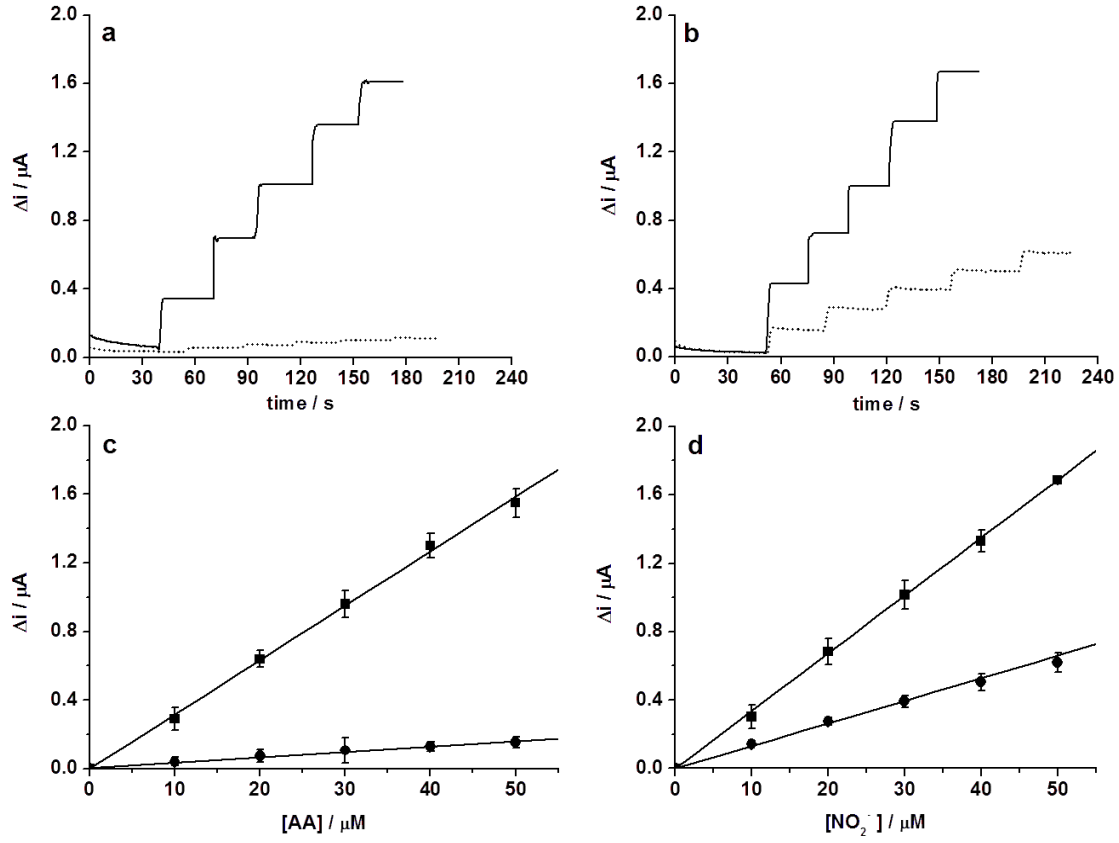

Figure 4.10: Amperometric responses at GCE/CNO/*o*AP (—, ■) and GCE/*o*AP (·····,●) for: (a) addition of 10 µM AA in the presence of 10 µM nitrite at +200 mV; (b) the successive addition of 10 µM of nitrite in the presence of 10 µM AA at +750 mV; (c) and (d) corresponding calibration curves. The same modified electrodes were used in both cases for the detection of nitrite and ascorbic acid.

A linear relationship of the current responses with the concentration of nitrite and AA was observed over the ranges of 0-50 μM. The sensitivity for the detection of nitrite at GCE/CNO/*o*AP was 0.034 μA/μM with a correlation coefficient of 0.99. This value is almost 3 times more sensitive than GCE/*o*AP. The estimated limit of detection (LOD) of nitrite at GCE/CNO/*o*AP as obtained from the calibration curve was 1.82 μM which is 2 times lower as compared to GCE/*o*AP. For the detection of ascorbate the sensitivity of the electrode is about 0.024 μA/μM which are 8 times more sensitive than GCE/*o*AP and the LOD was 2.32 μM, about 3 times lower than the GCE/*o*AP. Hence, the incorporation of CNO gave enhanced performance in terms of sensitivity and lower limit of detection compared to GCE with *o*AP system.

Electrochemical detection of nitrite and ascorbic acid at GCE/CNO/thionine electrode

Figure 4.11 shows the cyclic voltammograms of GCE/CNO/thionine modified electrodes with the absence and presence of 100 μM NO_2^- and/or 100 μM AA in phosphate citrate buffer pH 3.5. Similarly to the *o*AP modified electrodes, upon addition of both analytes, the corresponding anodic signals appear in the voltammograms although the background signal corresponding to adsorbed thionine is higher.

Figure 4.12 shows the amperometric current responses and calibration curves in the modified GCE/CNO/thionine and GCE/thionine. In this case, the sensitivity for the detection of nitrite was 0.045 μA/μM (2 times more sensitive than GCE/thionine) with a LOD of 1.89 μM (6 times lower LOD than GCE/thionine). For the determination of ascorbate the sensitivity was 0.043 μA/μM (9 times higher than GCE/thionine) and the LOD was 0.66 μM (2 times lower than GCE/thionine).

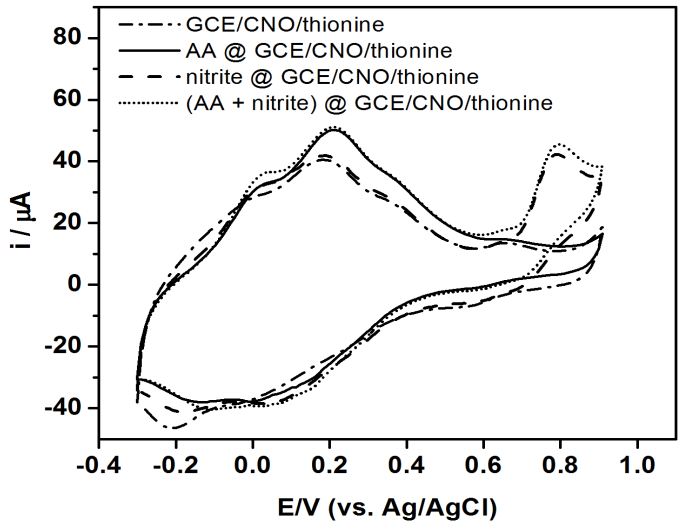

Figure 4.11: Cyclic voltammograms at GCE/CNO/thionine in the presence of 100 µM nitrite, 100 µM ascorbate and a mixture of both (100 µM each). Scan rate 100 mV/s in phosphate citrate buffer pH 3.5.

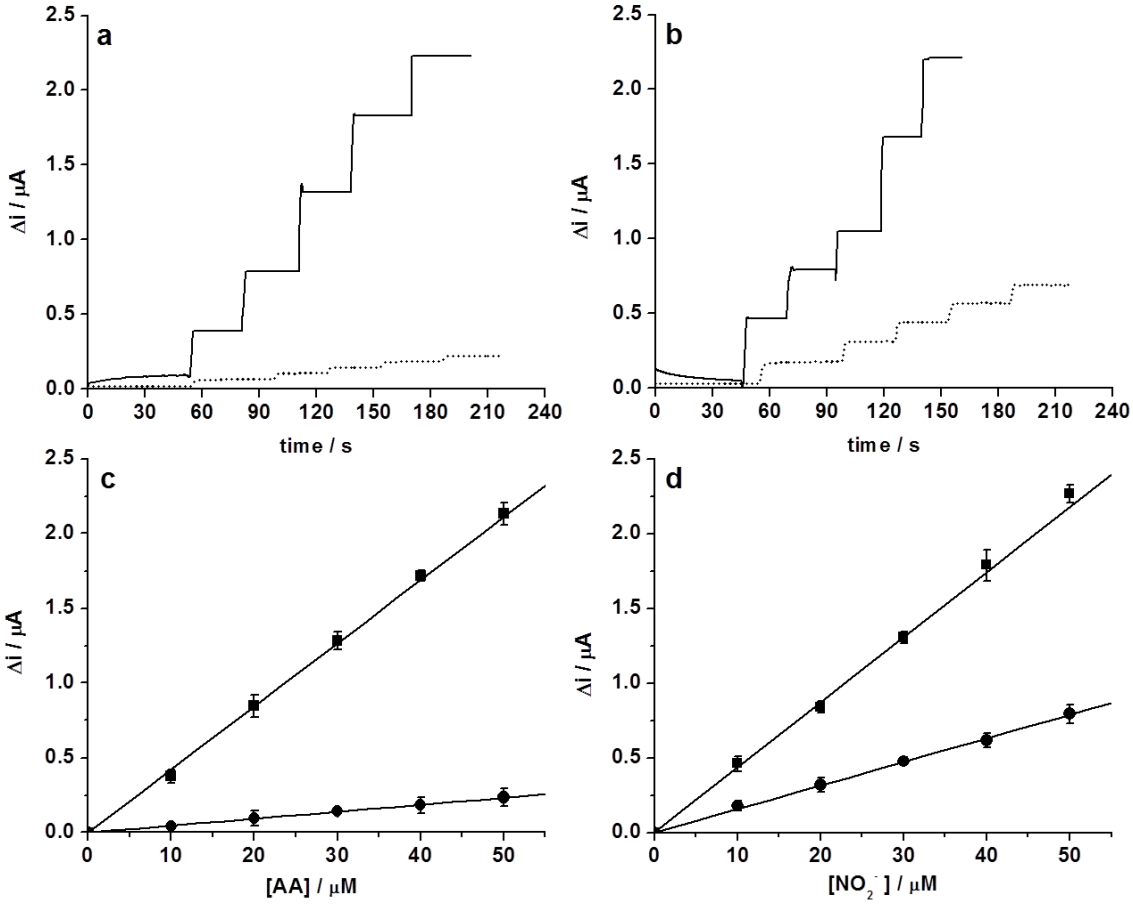

Figure 4.12: Amperometric responses at GCE/CNO/thionine (—, ■) and GCE/thionine (·····,●) for: (a) addition of 10 µM AA in the presence of 10 µM nitrite at +200 mV; (b) the successive addition of 10 µM of nitrite in the presence of 10 µM AA at +750 mV; (c) and (d) corresponding calibration curves. The same modified electrodes were used in both cases for the detection of nitrite and ascorbic acid.

Reproducibility studies

The electrochemical measurements were repeated 5 times each for the detection of nitrite and ascorbic acid with the same electrode. The relative standard deviation of the current responses for GCE/CNO/*o*AP with nitrite was 3.2% and 3.9% for ascorbic acid. For GCE/CNO/thionine with nitrite and ascorbic acid were 2.8%. These low relative deviations derived from the responses indicate that both modified surfaces of GCE/CNO/*o*AP and GCE/CNO/thionine had good operational reproducibility. The stability of modified surface of GCE/CNO/*o*AP and GCE/CNO/thionine were found stable for over a month and retaining 90% of the initial response when stored at 4^0C.

CONCLUSIONS

Carbon nano-onions (CNOs) were used to modify glassy carbon electrodes followed either by covalent functionalization of *ortho*-aminophenol (*o*AP) through in-situ electrochemical grafting of diazonium salt or by physical adsorption of thionine. These electrodes were used for the detection of nitrite and ascorbic acid at different potentials, simultaneously. The prepared surface of GCE/CNO was characterized in ESEM for the morphology and structure of the surface, and then electrochemically characterized using cyclic voltammetry. Electrochemical grafting of *o*AP and adsorption of thionine were successful showing the reversible peaks in their corresponding cyclic voltammograms. DC amperometry measurements were used to probe the electrocatalytic capability of the modified surface of GCE/CNO/*o*AP and GCE/CNO/thionine for the detection of nitrite and ascorbic acid. Nitrite was detected at potential +750mV higher than the potential of ascorbic acid at +200mV. Both results showed excellent enhancement in the current response and lower limit of detection as compared to GCE/*o*AP and GCE/thionine controls.

REFERENCES

1. M.J. Moorcroft, J. Davis, R.G. Compton, *Detection and determination of nitrate and nitrite: a review.* Talanta, 2001. **54**: p. 785-803.
2. K. Matsumoto, K. Yamada, Y. Osajima, *Ascorbate electrode for determination of L-ascorbic acid in food.* Analytical Chemistry, 1981. **53**(13): p. 1974-1979.
3. A.M Pisoschi, A.F. Danet, S. Kalinowski, *Ascorbic Acid Determination in Commercial Fruit Juice Samples by Cyclic Voltammetry.* Journal of Automated Methods and Management in Chemistry, 2008. **2008**: p. 8 pages.
4. J. Umah, A. O. Ketiku, M.K.C. Sridhar *Nitrate, Nitrite and Ascorbic Acid Content of Commercial and Home - Prepared Complementary, Infant Foods.* African Journal of Biomedical Research, 2003. **6**(1): p. 15-20.
5. C.F. Cheng, C.W. Tsang, *Simultaneous determination of nitrite, nitrate and ascorbic acid in canned vegetable juices by reverse-phase ion-interaction HPLC.* Food Additives and Contaminants, 1998. **15**(7): p. 753-758.
6. A.G Frenich, M. E. H. Torres , A. B. Vega , J. L. M. Vidal , P. P. Bolaños, *Determination of Ascorbic Acid and Carotenoids in Food Commodities by Liquid Chromatography with Mass Spectrometry Detection.* Journal of Agricultural Food Chemistry, 2005. **53**(19): p. 7371-7376.
7. K.M Phillips, M. T. Tarrago´ -Trani, S. E. Gebhardt , J. Exler, K. Y. Patterson, D. B. Haytowitz, P. R. Pehrsson, J. M. Holden, *Stability of vitamin C in frozen raw fruit and vegetable homogenates.* Journal of Food Composition and Analysis, 2010. **23**: p. 253-259.
8. M. Levine, S. C. Rumsey, R. Daruwala, J. B. Park, Y. Wang, *Criteria and Recommendations for Vitamin C Intake.* Journal of American Medical Association, 1999. **281**(15): p. 1415-1423.
9. R.A. Scanlan, *Formation and occurrence of nitrosamines in food.* Cancer Research, 1983. **43**: p. 2435s-2440s.
10. J.S. Griesenbeck, M. D. Steck, J. C. Huber, J. R. Sharkey, A. A. Rene, J. D. Brender, *Development of estimates of dietary nitrates, nitrites, and nitrosamines for use with the short willet food frequency questionnaire.* Nutrition Journal, 2009. **8**(16).
11. D.C. Siu, A. Henshall, *Ion chromatographic determination of nitrate and nitrite in meat products.* Journal of Chromatography A, 1998. **804**(1-2): p. 157-160.
12. I. Shah, A. Petroczi, R. A. James , D. P. Naughton, *Determination of Nitrate and Nitrite Content of Dietary Supplements Using Ion Chromatography.* Journal of Analytical Bionalytical Techniques, 2013.
13. Z. Gazdik, O. Zitka, J. Petrlova , V. Adam, J. Zehnalek, A. Horna, V. Reznicek , M. Beklova, R. Kizek, *Determination of Vitamin C (Ascorbic Acid) Using High Performance Liquid Chromatography Coupled with Electrochemical Detection* Sensors, 2008. **8**: p. 7097-7112.
14. A.H. Qader, *Spectrophotometric determination of nitrite in curing meat samples.* Applied Science Report, 2013. **3**(3): p. 153-156.
15. R. Shanmugam, S. Sornambikai, N. S. Karthikeyan, K. Sathiyanarayanan, A. S. Kumar, *A Simple Colorimetric Screening of Nitrite Using Iodide in an Acidic pH Solution.* Austin Journal of Analytical and Pharmaceutical Chemistry, 2014. **1**(6).
16. H. Yang, J. Irudayaraj, *Rapid determination of vitamin C by NIR, MIR and FT-Raman techniques.* Journal of Pharmacy and Pharmacology, 2002. **54**(9): p. 1247-1255.
17. M. Badea, A. Amine, M. Benzine, A. Curulli, D. Moscone, A. Lupu, G. Volpe, G. Palleschi, *Rapid and Selective Electrochemical Determination of Nitrite in Cured Meat in the Presence of Ascorbic Acid.* Microchimica Acta, 2004. **147**(1-2): p. 51-58.
18. H. Karimi-Maleh, M. Moazampour, M. Yoosefian, A. L. Sanati, F. Tahernejad-Javazmi, M. Mahani, *An Electrochemical Nanosensor for Simultaneous*

Voltammetric Determination of Ascorbic Acid and Sudan I in Food Samples. Food Analytical Methods, 2014. **7**(10): p. 2169-2176.

19. A. Amine M. Badea, G. Palleschi, D. Moscone, G. Volpe, A. Curulli, *New electrochemical sensors for detection of nitrites and nitrates.* Journal of Electroanalytical Chemistry, 2001. **509**: p. 66-72.
20. W. Okiei, M. Ogunlesi, L. Azeez, V. Obakachi, M. Osunsanmi, G. Nkenchor, *The Voltammetric and Titrimetric Determination of Ascorbic Acid Levels in Tropical Fruit Samples.* International Journal of Electrochemical Science, 2009. **4**: p. 276-287.
21. S. Skrovankova, J. Mlcek, J. Sochor, M. Baron, J. Kynicky, T. Jurikova, *Determination of Ascorbic Acid by Electrochemical Techniques and other Methods.* International Journal of Electrochemical Science, 2015. **10**: p. 2421-2431.
22. H. Ibrahim, I. Habib, *Anodic striping voltammetric determination of nitrite using caron paste electrode.* Americal Journal of Analytical Chemistry, 2011. **2**: p. 284-288.
23. A.B. Florou, M. I. Prodromidis, M. I. Karayannis, S. M. Tzouwara-Karayanni *Flow electrochemical determination of ascorbic acid in real samples using a glassy carbon electrode modified with a cellulose acetate film bearing 2,6-dichlorophenolindophenol* Analytica Chimica Acta, 2000. **409**: p. 113-121.
24. K. Lin, P. Yeh, S. Chen, *Electrochemical Determination of Ascorbic Acid Using Poly(Xanthurenic Acid) and Multi-Walled Carbon Nanotubes.* International Journal of Electrochemical Science, 2012. **7**: p. 12752-12763.
25. K.S. Ngai, W. T. Tan, Z. Zainal, R. M. Zawawi, M. Zidan, *Voltammetry Detection of Ascorbic Acid at Glassy Carbon Electrode Modified by Single-Walled Carbon Nanotube/Zinc Oxide* International Journal of Electrochemical Science, 2013. **8**: p. 10557-10567.
26. M.J. Nithya, *Electrochemical sensing of ascorbic acd on ZnO-decorated reduced graphene oxide electrode.* Biosensors and Bioelectronics, 2015. **6**(1): p. 1-9.
27. B.R. Kozub, N.V. Rees, R.G. Compton, *Electrochemical determination of nitrite at a bare glassy carbon electrode; why chemically modify electrodes?* Sensors and Actuators B: Chemical, 2010. **143**(2): p. 539-546.
28. K. Zhao, H. Song, S. Zhuang, L. Dai, P. He, Y. Fang, *Determination of nitrite with the electrocatalytic property to the oxidation of nitrite on thionine modified aligned carbon nanotubes.* Electrochemistry Communications, 2007. **9**: p. 65-70.
29. Y. Sahraoui, S. Chaliaa, A. Maaref, A. Haddad, N. Jaffrezic-Renault, *An Electrochemical Nitrite Sensor Based on a Multilayer Film of Polyoxometalate.* Journal of Sensor Technology, 2013. **3**: p. 84-93.
30. J.K. Goh, W.T. Tan, F.T. Lim, N.A.M. Maamor, *Electrochemical oxidation of ascorbic acid mediated by carbon nanotubes /Li+ / carbon paste modified soild electrode.* The Malaysian Journal of Analytical Sciences, 2008. **12**(2): p. 480-485.
31. N. Zhu, Q. Xu, S. Li, H. Gao, *Electrochemical determination of nitrite based on poly(amidoamine) dendrimer-modified carbon nanotubes for nitrite oxidation* Electrochemistry Communications, 2009. **11**: p. 2308-2311.
32. L.H. Chen, J.B. Zang, Y.H. Wang, L.Y. Bian *Electrochemical oxidation of nitrite on nanodiamond powder electrode.* Electrochimica Acta, 2008. **53**(8): p. 3442-3445.
33. J. Breczko, M.E. Plonska-Brzezinska, L. Echegoyen, *Electrochemical oxidation and determination of dopamine in the presence of uric and ascorbic acids using a carbon nano-onion and poly(diallyldimethylammonium chloride) composite.* Electrochimica Acta, 2012. **72**: p. 61-67.
34. M. Delamar, R. Hitmi, J. Pinson, J. M. Saveant, *Covalent Modification of Carbon Surfaces by Grafting of Functionalized Aryl Radicals Produced from Electrochemical Reduction of Diazonium Salts* Journal of American Chemical Society, 1992. **114**: p. 5883-5884.

35. S. Baranton, D. Belanger, *Electrochemical Derivatization of Carbon Surface by Reduction of in Situ Generated Diazonium Cations.* Journal of Physical Chemistry B, 2005. **109**: p. 24401-24410.
36. R. Polsky, J.C. Harper, D.R. Wheeler, S. M. Dirk, D.C. Arango, S.M. Brozik, *Electrically addressable diazonium-functionalized antibodies for multianalyte electrochemical sensor applications* Biosensors and Bioelectronics, 2008. **23**: p. 757-764.
37. A. Kowalczyk, A. Nowicka, R. Jurczakowski, M. Fau, A. Krolikowska, Z. Stojek, *Construction of DNA biosensor at glassy carbon surface modified with 4-aminoethylbenzenediazonium salt.* Biosensors and Bioelectronics, 2011. **26**(5): p. 2506-2512.
38. H.M. Nassef, A. Radi, C.K. O'Sullivan, *Electrocatalytic oxidation of hydrazine at o-aminophenol grafted modified glassy carbon electrode: Reusable hydrazine amperometric sensor* Journal of Electroanalytical Chemistry, 2006. **592**: p. 139-146.
39. H.M. Nassef, A. Radi, C.K. O'Sullivan, *Electrocatalytic sensing of NADH on a glassy carbon electrode modified with electrografted o-aminophenol film* Electrochemistry Communications, 2006. **8**(11): p. 1719-1725.
40. H.M. Nassef, L. Civit, A. Fragoso, C.K. O'Sullivan, *Amperometric sensing of ascorbic acid using a disposable screen-printed electrode modified with electrografted o-aminophenol film.* Analyst, 2008. **133**(12): p. 1736-1741.
41. H.M. Nassef, A. Radi, C.K. O'Sullivan, *Simultaneous detection of ascorbate and uric acid using a selectively catalytic surface.* Analytica Chimica Acta, 2007. **583**(1): p. 182-189.
42. C. Deng, J. Chen, Z. Nie, M. Yang, S. Si *Electrochemical detection of nitrite based on the polythionine/carbon nanotube modified electrode.* Thin Solid Films, 2012. **520**: p. 7026-7029.
43. Q. Li, J. Zhang, H. Yan, M. He, Z. Liu, *Thionine-mediated chemistry of carbon nanotubes* Carbon 2004. **42**: p. 287-291.
44. A. Salimi, A. Noorbakhsh, S. Soltania, *Electroless Deposition of Thionin onto Glassy Carbon Electrode Modified with Single Wall and Multiwall Carbon Nanotubes: Improvement of the Electrochemical Reversibility and Stability.* Electroanalysis, 2006. **18**(7): p. 703-711.
45. A. Wang X. Zhou, Y. Pan, C. Yu, Y. Zou, Y. Zhou, Q. Chen, S. Wu *Facile synthesis of a Co3O4@carbon nanotubes/polyindole composite and its application in all-solid-state flexible supercapacitors.* journal of materials Chemistry A, 2015. **3**: p. 13011-13015.
46. L. Meng, P. Wu, G. Chen, C. Cai, Y. Sun, Z. Yuan *Low potential detection of glutamate based on the electrocatalytic oxidation of NADH at thionine/single-walled carbon nanotubes composite modified electrode.* Biosensors and Bioelectronics, 2009. **24**: p. 1751-1756.

Chapter 5

Reactive carbon nano-onion modified glassy carbon surfaces as DNA sensors for human papillomavirus oncogene detection with enhanced sensitivity[1]

ABSTRACT

Glassy carbon electrodes were modified with small carbon nano-onions (CNOs) and activated by electro-grafting of diazonium salts bearing terminal carboxylic acid and maleimide groups. The CNO-modified surfaces were characterized by ESEM and AFM microscopy as well as by electrochemical techniques. The modified electrodes were used for the amperometric detection of a model DNA target sequence associated with the human papillomavirus by immobilizing short recognition sequences by amidation or thiol-maleimide reactions. The analytical parameters of the developed biosensors were compared with glassy carbon electrodes without CNOs. In both cases, the incorporation of CNOs resulted in an enhancement in sensitivity and a decrease in detection limits ascribed to a combination of large surface areas and enhanced electron transfer properties of the CNO-modified electrodes. These results offer promise for the construction of other CNO-based biomolecule detection platforms with enhanced sensitivities.

[1] This chapter has been published in J. P. Bartolome, L. Echegoyen, A. Fragoso, *Anal. Chem.* **2015**, *87*, 6744-6751.

5.1 INTRODUCTION

Carbon nano-onions (CNOs) were first reported by Ugarte in 1992 after irradiating a sample of carbon soot particles under an electron beam [1]. This allotrope of carbon is a multilayered fullerene concentrically arranged one inside the other. Their average sizes typically range from 5 nm to 40 nm in diameter [2] and, unlike other carbon allotropes, they remain relatively less explored [3, 4]. Similar to other carbon nanomaterials, CNOs are generally insoluble in organic and inorganic solvents. To improve the solubility and applicability, CNOs have been chemically functionalized using a wide range of reactions including cycloadditions [5, 6], amidations [6, 7], oxidations [8] or radical additions of diazonium compounds [9] as well as by means of supramolecular interactions [10, 11].

CNOs have been incorporated into polydimethylsiloxane, polyurethane and polymethyl-methacrylate matrices and the electromagnetic properties of these materials have been investigated [12]. Plonska and coworkers have fabricated a novel type of CNO-based composite containing poly(diallyl-dimethylammonium chloride) (PDDA) or chitosan [13]. The composite films were deposited on glassy carbon and the capacitance of the films was shown to be primarily related to the amount of CNOs incorporated into the layer of the filler. The low relaxation times exhibited by these composites indicate that they can operate as capacitors in short time windows. Recently, the electrochemical properties of CNO/PDDA composites deposited on gold were examined by voltammetric techniques and their ability to detect dopamine in the presence of uric and ascorbic acids was studied [14]. CNOs have also been incorporated in microsupercapacitors [15] to exploit their fast charging and discharging rates and have been used as additives in lubricants due to their tribological properties [16] and as catalysts [17].

More recently, some studies have focused on the possibility of using CNOs for biomedical applications [18] such as for cell imaging [19, 20] and have also shown low cytotoxicity and low inflammatory properties [21]. The covalent functionalization of oxidized CNOs (containing COOH groups) with biomolecules by using biotin-avidin interactions has been reported [22]. An amino-terminated monolayer was created on a gold surface and oxidized CNOs were covalently attached by amide bonds followed by reaction of biotin hydrazide with the remaining COOH groups. This Au/CNO/biotin surface was used to capture avidin, a process that was followed by surface plasmon resonance. To the best of our knowledge, this is the only report involving the use of CNO-modified surfaces to study biomolecular interactions.

Considering the previously demonstrated importance of the incorporation of carbon nanomaterials in transducer surfaces [23, 24] and the lack of reports on the use of CNOs for this purpose, we evaluate the possibility of using CNO-modified electrodes in biosensing applications. A stable dispersion of pristine CNOs was initially prepared and deposited on glassy carbon (GC) electrodes to form a mechanically stable GC/CNO surface that was further modified by electrochemical grafting of two different diazonium salts derived from 4-aminophenylacetic acid (PAA) and 4-aminophenylmaleimide (PM) (Scheme 5.1). The GCE/CNO/PAA and GCE/CNO/PM surfaces were evaluated as supports for the attachment of small biotinylated or thiolated DNA probes. These CNO-based biosensors were then used for the amperometric detection of human papillomavirus (HPV) [25] oncogene DNA sequences as a model system using a sandwich assay. The sensitivity and analytical performance of the developed GCE/CNO sensors were compared with those of diazonium modified electrodes in the absence of CNOs.

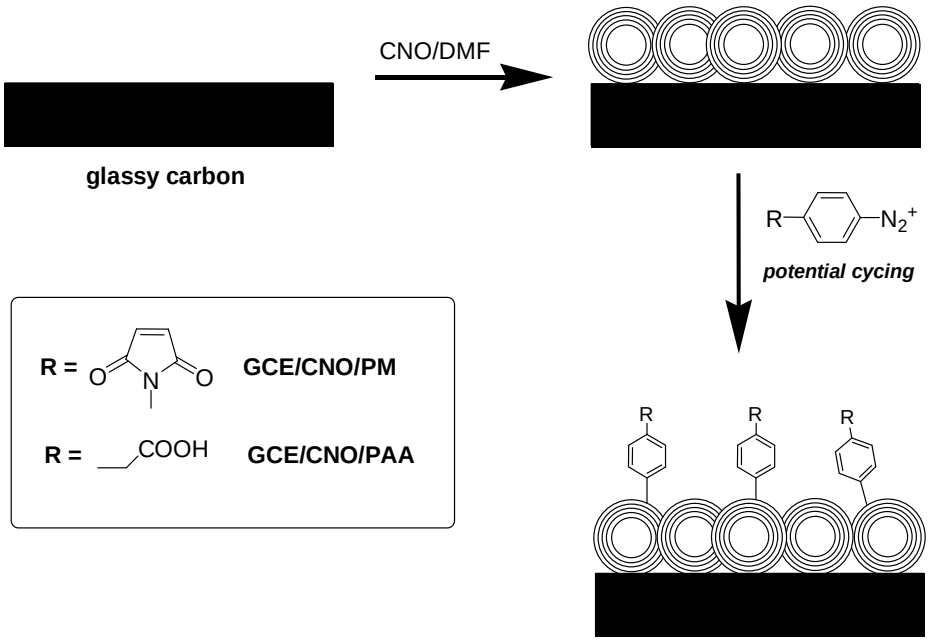

Scheme 5.1: Strategy employed for the modification of glassy carbon electrodes with CNOs and diazonium salts

5.2 EXPERIMENTAL SECTION

Reagents. CNOs were prepared as previously reported [6]. Dimethylformamide (DMF), N-(4-aminophenyl)- maleimide, 4-aminophenyl acetic acid, $NaNO_2$, tetrabutylammonium tetrafluoroborate (TBA-TFB), 6-ferrocenyl-1-hexanethiol (Fc-SH), acetonitrile, 1-ethyl-3-[3-dimethylaminopropyl]-carbo-diimide hydrochloride (EDC), N-hydroxysuccinimide (NHS), streptavidin from *Streptomyces avidini* and Tetramethylbenzidine (TMB) Liquid Substrate for ELISA were obtained from Sigma-Aldrich and used as received. HPV16E7-related 5'-biotinylated and 5'-thiolated DNA capture probe, target sequence and horseradish peroxidase (HRP) labelled reporter probe (21-mer) were purchased from Biomers.net (Ulm, Germany). The nucleotide sequences of these probes can be found elsewhere [26]. All other chemicals used in buffer solution preparations were of analytical-reagent grade. All solutions were prepared with milliQ water.

Instrumentation. A tip sonicator (amplitude 60%, cycle 0.5, Ultraschallprocessor UP200S) was used to mechanically disperse CNOs. All electrochemical measurements were obtained using an PC-controlled PGSTAT 12 Autolab potentiostat (Eco Chemie, The Netherlands), equipped with BASi C-3 Stand (RF-1085) three-electrode cell. This configuration contains a bare or modified glassy carbon electrode (BAS model MF-2012, 3.0 mm diameter) as the working electrode, a platinum wire as the counter electrode and a Ag/AgCl(sat) as the reference electrode. Impedance spectra were recorded over the frequency range of 10 kHz-0.1 Hz at a bias potential of +0.22 V and an ac amplitude of 5 mV. Transmission Electron Microscope images of CNOs dispersed in DMF were obtained on a Jeol 1011 instrument using a copper grid. Environmental Scanning Electron Microscopy (ESEM) was recorded in a Quanta 600 microscope (FEI Company Inc.) under high vacuum at 25 kV. The modified GCE were placed vertically in the sample chamber and analyzed at a 10 mm working distance. Atomic Force Microscopy (AFM) analyses were recorded using a Molecular Imaging model Pico SPM II (Pico+) instrument from Agilent Technologies in tapping mode using a 1 nm high resolution SHR150 tip from Budget Sensors. A freshly cleaved thin layer of highly-oriented pyrolytic graphite (from SPI) was used as substrate.

Deposition of CNOs on GC electrodes. Prior to the deposition of CNOs, the glassy carbon electrode was polished to a mirror finish with 0.3 μM alumina slurries, cleaned and sonicated in milliQ water for 5 min and then dried under a stream of nitrogen gas. Two-milligrams of purified CNOs were dispersed in 10 mL dimethylformamide (DMF) and subjected to tip sonication for 30 min to obtain a homogenous dispersion. To obtain a thin layer of CNOs on the surface of the electrode, the homogenized solution was sprayed onto the clean electrode for 2 s and then dried with hot air at about 150ºC (Scheme 5.1). The process was repeated 30 times and after every fifth cycle the

electrode was thoroughly washed with milliQ water and acetone then dried again. This method created a compact and mechanically stable layer of ~9 μm thickness as observed by ESEM.

Electrochemical grafting of diazonium salts on GCE/CNO. A stirred ice-cold solution of PAA or PM (2 mL, 10 mM) in 0.5 M HCl was treated with 2 mL of 10 mM $NaNO_2$ for 10 min in an electrochemical 10 mL glass cell. After stirring for 10 min the GCE/CNO electrode was immersed into the mixture and the potential was cycled between 0 and -0.6 V for 2, 5, 10, 20, 30, 40, 50 or 60 cycles at 0.1 V/s. The modified electrodes were then sonicated in milliQ water for 1 min to remove physically adsorbed compounds. The GC/CNO/PAA and GC/CNO/PM electrodes were studied by cyclic voltammetry (CV) using 1 mM $Fe(CN)_6^{3-/4-}$ in 0.1 M KCl as an electroactive probe. The electrografted PM group was reacted with 500 μM 6-ferrocenylhexanethiol for 2 h, followed by rinsing in acetonitrile and the GC/CNO/PM/Fc electrodes were characterized using CV in 0.1 M tetrabutylammonium tetrafluoroborate in acetonitrile. The surface coverage of Fc was calculated from the area of the anodic peak.

Biosensor construction and detection of HPV DNA sequences. GC/CNO/PAA: The carboxyl groups of PAA were activated with an aqueous mixture of EDC (0.2 M) and NHS (50 mM) for 30 min followed by immersion in 20 μg/mL solution of streptavidin in acetate buffer (pH 5) for 30 min at 4ºC. The remaining carboxyl groups were then blocked with 0.1 M ethanolamine hydrochloride (pH 8.5) for 30 min. The electrodes were washed in milliQ water and the 5'-biotinylated DNA capture probe (1 μM in milliQ water) was incubated for 30 min at room temperature. Afterwards, the target DNA (0, 2.5, 5, 10, 20, 50 nM) in Trizma hybridization buffer pH 7.38 was added and incubated for a further 30 min at 37ºC. After washing with Trizma the HRP-labeled

reporter probe (50 nM) was introduced and incubated for another 30 min to complete the DNA sandwich assay.

GCE/CNO/PM. A mixture of 1 μM of 5'-thiolated HPV16E7 DNA and 100 μM mercaptohexanol was co-immobilized for 30 mins (co-immobilization technique) or modified by sequential incubation of 1 μM thiolated DNA, washing with 0.01 M PBS pH 7.4 and incubation of 100 μM mercaptohexanol (sequential immobilization). Before the addition of the target DNA, the electrodes were washed with 0.1 M PBS pH 7.4. The target DNA and reporter probe were then incubated as described for the PAA surface.

Amperometric measurements were carried out in a 5 mL electrochemical cell containing 0.1 M PBS pH 6 and TMB Liquid Substrate (2:1 v/v final ratio) under stirring conditions at room temperature. The current was measured at 0.15 V after 2 min for a period of 1 min and the current vs. [DNA] calibration curves were constructed from triplicate measurements. The same modification and detection procedures were employed for GCE/PAA and GCE/PM electrodes as controls.

Clinical samples from cervical scraps, previously genotyped to determine the type of HPV subtype present, were obtained from, amplified and prepared as reported earlier [27] and incubated directly over the electrodes. Electrochemical detection was carried out as described above.

5.3 RESULTS AND DISCUSSION

Deposition of CNOs on glassy carbon surfaces. Tip sonication of a CNO suspension in DMF afforded a homogeneous dispersion with an average diameter 3.7 nm as revealed by TEM (Figure 5.1a). ESEM analysis of CNOs deposited on GCE after 30 spraying cycles (Figure 5.1b) indicated that the surface of GCE had been covered with a thin layer of CNOs when compared to the morphology of the bare GCE (not shown)

with a thickness of ~9 μm (Figure 5.1c). The deposited CNO layers showed good mechanical stability, particularly in aqueous solution. Treatments such as repetitive washings with water, immersion in aqueous solutions for a long time and even sonication for short periods of time did not cause any partial removal of material from the surface of the GCE, as revealed by electrochemical measurements. The morphology of the GC/CNO surface was also studied by AFM (Figure 5.1d). Round shaped structures of about 10 nm diameter were observed, consistent with the deposition of CNOs on the surface.

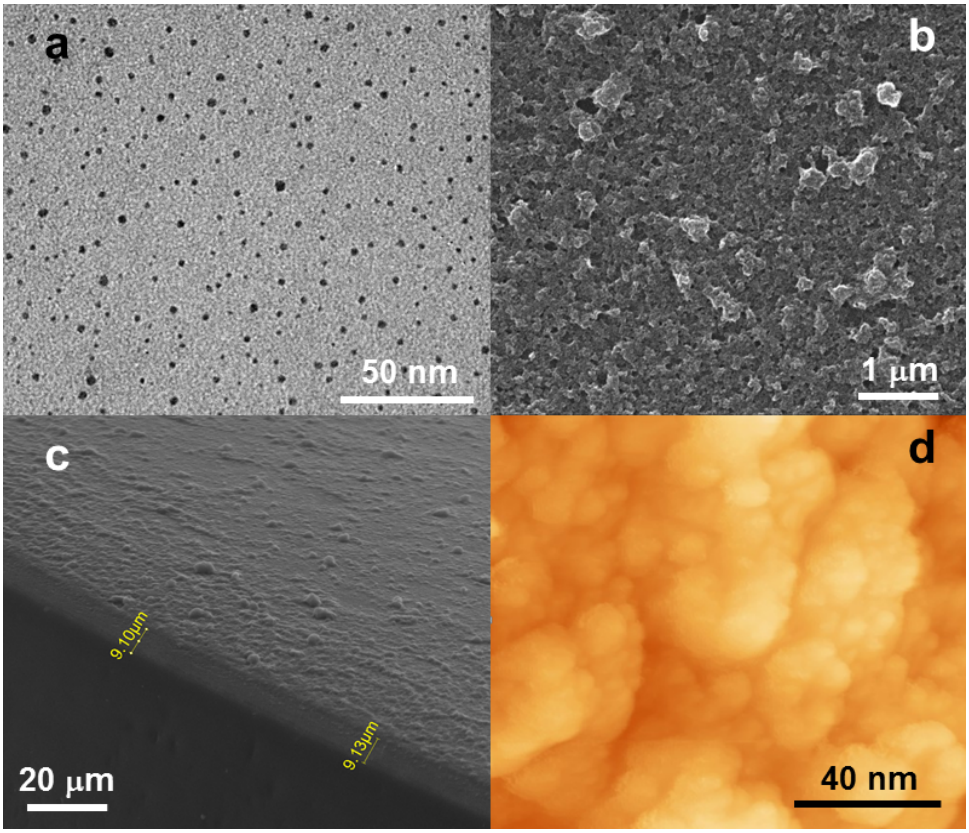

Figure 5.1: TEM image of dispersed CNOs in DMF after tip sonication (a). ESEM (b,c) and AFM (d) images of deposited CNO on GC.

Characterization of diazonium electrografting on GC/CNO. Phenylacetic acid (PAA). The presence of electrografted PAA moieties on the surface of modified GCE/CNO electrodes was monitored by CV in $Fe(CN)_6^{3-/4-}$ solutions. Carboxylic acid terminated surfaces are neutral at low pH due to the protonation of the carboxyl group

and result in a negative charge as the pH is raised (Scheme 5.2). Thus the electrochemical response of the anionic ferricyanide probe is sensitive to pH changes.

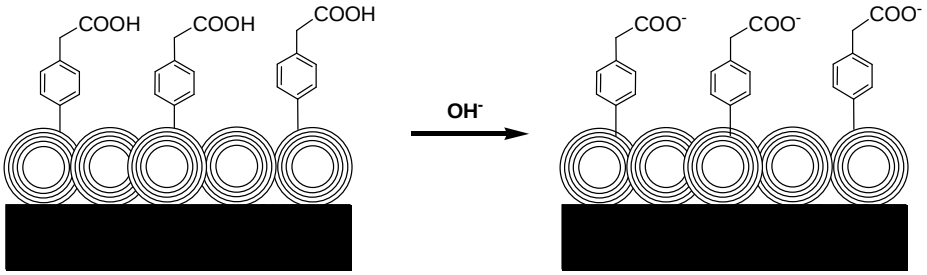

Scheme 5.2: Deprotonation of GC/CNO/PAA in basic media.

Figure 5.2a shows variations in the CV response of $Fe(CN)_6^{3-/4-}$ at the surface of modified GCE/CNO/PAA as the pH increases from 1 to 7. As expected, the CV response of $Fe(CN)_6^{3-/4-}$ solutions on modified GCE/CNO/PAA surfaces strongly depends on the pH of the solution. At acidic pH (pH 1), a quasirreversible redox signal is observed centered at $E_{1/2}$ = 0.28 V and a peak-to-peak separation ΔE = 95 mV, indicating that the surface is essentially neutral and does not effectively block the electron transfer process for the anionic $Fe(CN)_6^{3-/4-}$ probe. As the pH is raised, deprotonation of the COOH groups results in a surface negative that block the probe due to electrostatic repulsion. The dependence of anodic peak current as a function of pH showed an inflection point at pH 2.3, which corresponds to the interfacial pK_a of the modified GCE/CNO/PAA surface (Figure 5.2b). This value is about two orders of magnitude lower than the corresponding value for a GCE/PAA surface (pK_a = 4.7, Figure 5.2b, inset) and indicates that the presence of the CNO layer enhances the acidity of the PAA, presumably due to the electron withdrawing effect of the polyaromatic CNO structure. This property can be highly advantageous in the design of reactive surfaces as it facilitates its subsequent functionalization.

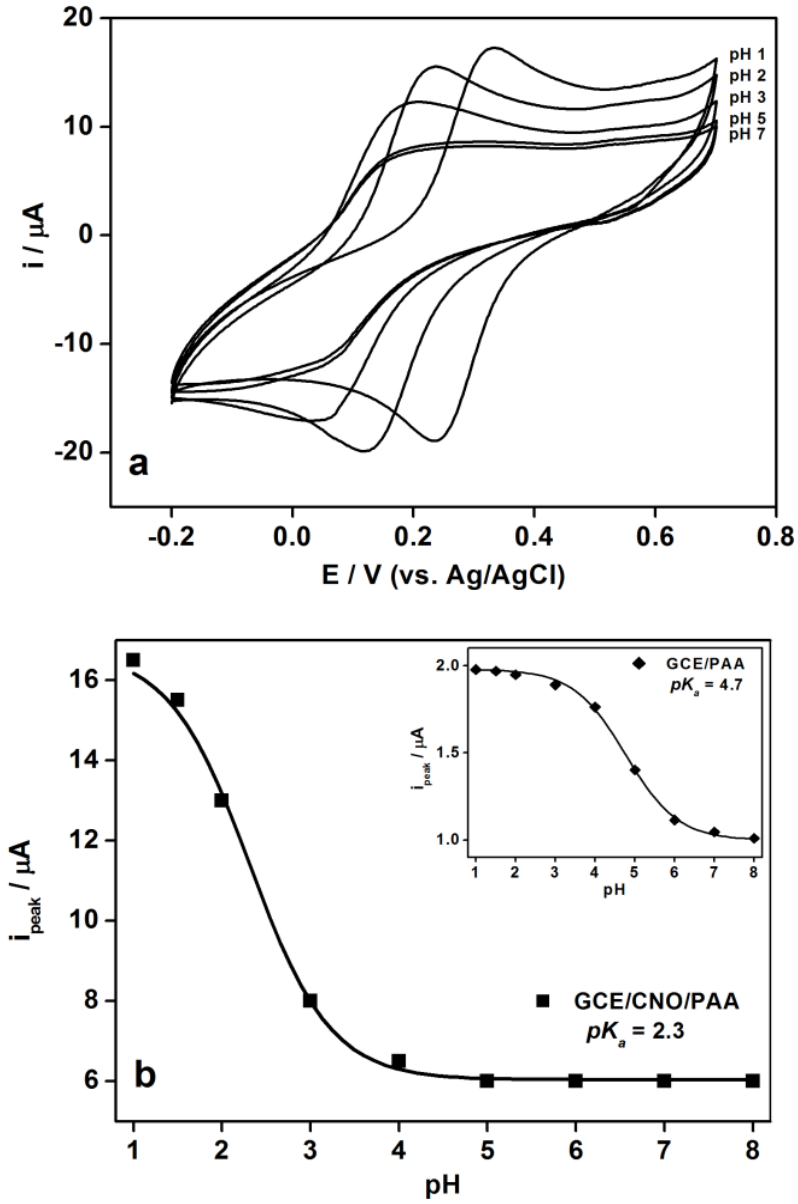

Figure 5.2: a) Cyclic voltammograms (for 1 mM $K_3Fe(CN)_6$ in 0.1 M KCl at 0.1 Vs^{-1}) obtained at different pH values on a GCE/CNO/PAA electrode. b) Titration curve corresponding to the variations of the anodic peak intensity. The solid line was obtained by fitting the experimental points to a sigmoidal curve. Inset: Corresponding titration curve for GCE/PAA.

Phenylmaleimide (PM). The maleimide group has been used as a common crosslinker for the immobilization of thiolated molecules on surfaces [28]. Phenylmaleimide-diazonium was electrografted using cyclic voltammetry on GCE/CNO at different electrodeposition cycles and the resulting GCE/CNO/PM surface was allowed to react with Fc-SH and characterized by CV in 0.1 M tetrabutylammonium tetrafluoroborate in acetonitrile (Scheme 5.3).

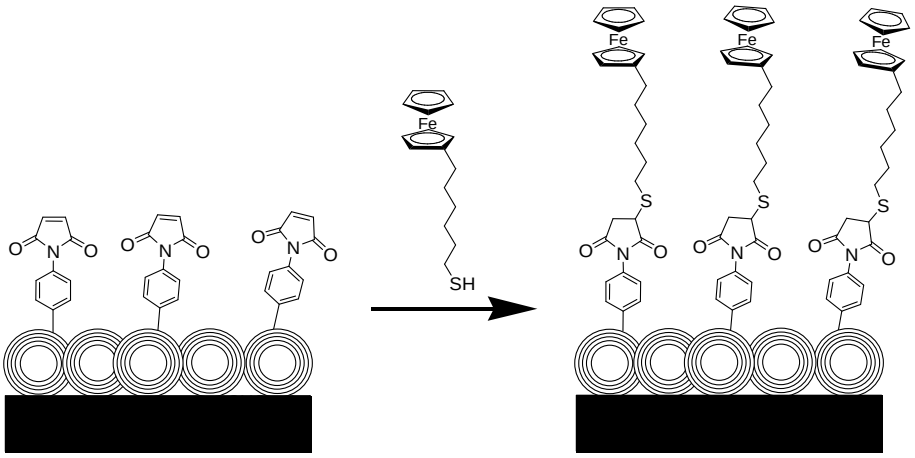

Scheme 5.3: Reaction of GC/CNO/PM with Fc-SH.

Figure 5.3a shows the values of surface coverage of ferrocene (Γ_{FcSH}) at different electrodeposition cycle numbers calculated from the area of the oxidation wave. Γ_{FcSH} values increased steadily with the number of potential cycles until a maximum of 2.4×10^{-9} mol/cm^2 was obtained after 30 cycles. A similar tendency was observed for the GCE/PM surface but in this case the maximum surface coverage obtained was 0.7×10^{-9} mol/cm^2, also after 30 cycles. This marked difference in Γ_{FcSH} values can be explained by considering that the CNOs increase the effective surface active area of the electrodes making more PM molecules available for interaction with FcSH, which results in an enhancement of the current intensity of the electroactive species relative to the GCE-based electrode.

Figure 5.3b shows a comparison of the CV obtained for bare and Fc modified surfaces in the presence and absence of CNOs after 30 electrodeposition cycles in TBA-TFB. The peaks are essentially symmetrical with a peak-to-peak separation ΔE_{ac} = 66 mV for GCE/PM/CNO/Fc. ΔE_{ac} is essentially scan rate independent up to 1 V/s and the peak currents depend linearly with the scan rate indicating that the Fc groups are surface-confined. Interestingly, for the CNO-modified surface, the Fc signal is not only larger than for the GCE/PM/Fc surface but also appears shifted 61 mV to lower potentials.

Figure 5.3c shows the dependence of the peak potential (E_p) with log *v*, where *v* is the scan rate, determined by CV. Using Laviron's formalism [29], the apparent rate constant for electron transfer (*k*) can be calculated from the equation:

$k = \alpha nF\nu_c/RT = (1-\alpha)nF\nu_a/RT$

where α is the transfer coefficient calculated from the quotient $\nu_a/(\nu_c+\nu_a)$, ν_c and ν_a are the limiting cathodic and anodic scan rates obtained from Figure 5.3c and F is Faraday's constant. Under these conditions, $\alpha = 0.51$ and $k = 122\ s^{-1}$ for the GCE/PM/CNO/Fc system, while $k = 19\ s^{-1}$ in the absence of CNO indicating a markedly faster electron transfer rate when the CNOs are present.

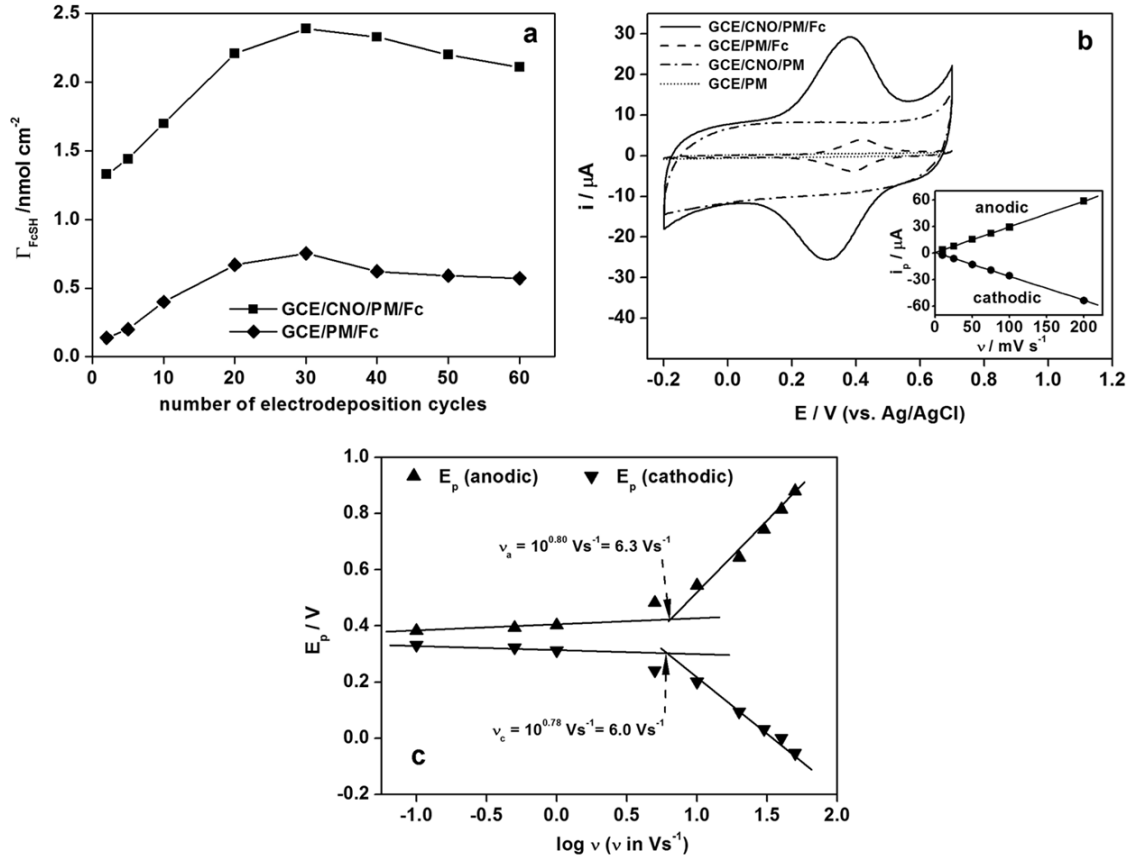

Figure 5.3: a) Dependence of Γ_{FcSH} with the number of electrodeposition cycles. b) Cyclic voltammograms of PM-modified surfaces in 0.1 M TBA-TFB in acetonitrile at 0.1 Vs^{-1} (inset: plot of peak currents vs scan rate for GCE/CNO/PM/Fc. c) Dependence of $\boldsymbol{E}_p$ with log $\boldsymbol{\nu}$ determined from cyclic voltammograms for GCE/CNO/PM/Fc.

Amperometric detection of DNA on CNO-modified electrodes. The possibility to use CNO-modified surfaces in the detection of biomolecules was tested using DNA sequences associated to the human papillomavirus (HPV) as a model system. PAA and PM grafted CNO surfaces were modified with a recognition DNA sequence and a sandwich type assay was used to detect the target sequence using a peroxidase-labeled DNA reporter probe in both cases. The assay conditions used were similar to those previously reported by our group for the detection of HPV sequences on thiol-modified gold electrodes [26, 27]

Scheme 5.4 shows the strategy used for the attachment of the DNA recognition sequence to the GC/CNO/PAA surface. The COOH groups of the surface were activated using carbodiimide chemistry followed by covalent immobilization of streptavidin and incubation of a biotinylated DNA capture probe. Figure 5.4a shows the CV responses for $Fe(CN)_6^{3-/4-}$ as a function of the construction steps of the biosensor. As can be seen, the sequential immobilization of streptavidin, biotinylated DNA and target DNA were accompanied by successive decreases in the signal intensity, as expected for the blocking of the probe upon addition of the different layers. This demonstrates the successful formation of the sensing layer on the CNO-modified GCE.

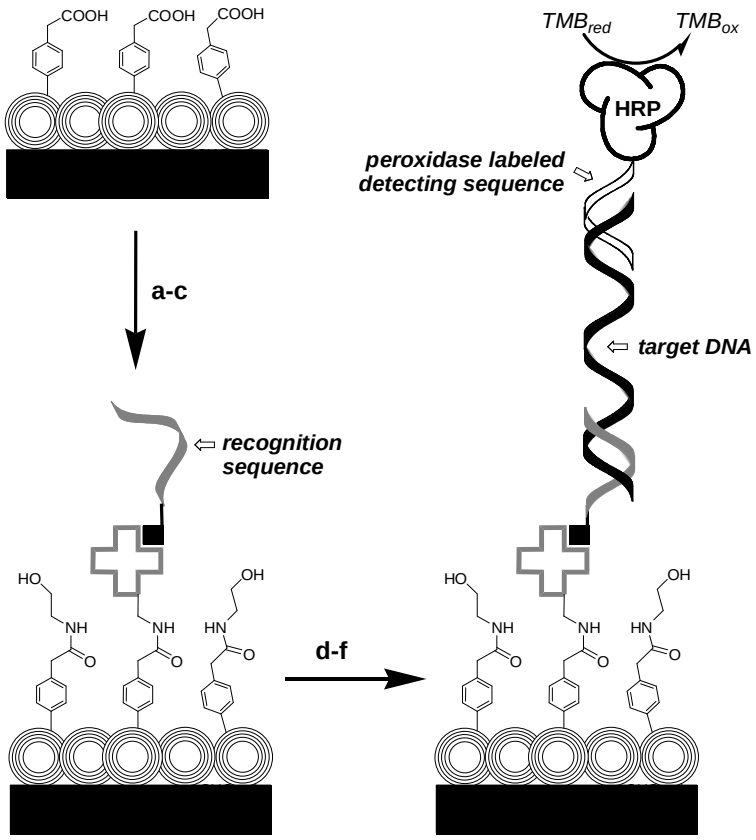

Scheme 5.4: a) EDC/NHS; b) streptavidin; c) ethanolamine; d) biotinylated HPV16 capture probe; e) target sequence; f) HRP-DNA detecting sequence.

Figure 5.4b shows the variation of current intensity with DNA concentration in the presence and in the absence of CNO for PAA-terminated electrodes. For the GCE/CNO/PAA surface, the calibration curve shows a markedly better sensitivity (0.91 $\mu A\ nM^{-1}$) and a lower limit of detection (0.54 nM) as compared with the control surface in the absence of CNO (sensitivity = 0.21 $\mu A\ nM^{-1}$; LOD = 3.9 nM). This is 4.3-fold sensitivity increase and a factor of seven reductions in LOD after the incorporation of CNOs on the surface. Interestingly, no sensitivity increase was observed when the CNO layer was replaced by one prepared with the precursor nanodiamonds (ND), indicating that the CNOs play a key role in the observed improvement of the analytical response (Figure 5.4b).

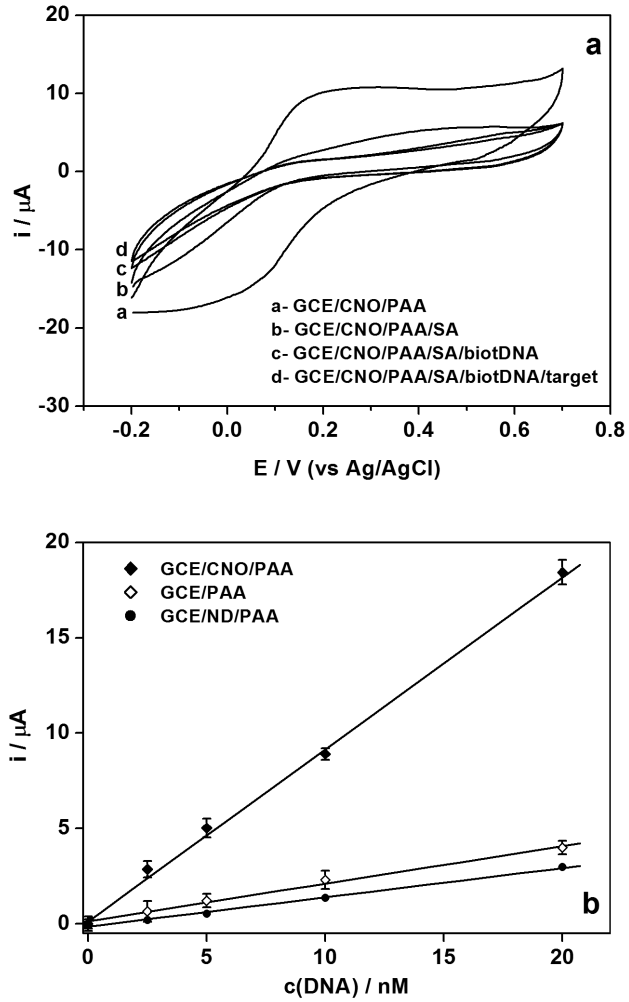

Figure 5.4: a) Cyclic voltammograms in 1 mM $K_3Fe(CN)_6$ in phosphate buffer pH 7.4 at 0.1 Vs^{-1}) corresponding to the sequential immobilization of streptavidin, biotinylated DNA and target DNA (10 nM) on GCE/CNO/PAA electrodes. b) Calibration curves for the detection of target DNA on GCE, GCE/CNO and GCE/ND electrodes modified with PAA.

In the case of the GCE/CNO/PM surface, a thiolated DNA capture probe was reacted with the immobilized maleimide group to form a stable thioether bond (Scheme 5.5). Figure 5.5a shows a comparison of the currents obtained for the detection of 5 and 20 nM target sequence using either a co-immobilization strategy (thiolaled HPV16 capture probe mixed with mercaptohexanol in 1:100 molar ratio) or sequential addition of thiolated probe and mercaptohexanol in the same molar ratio [30]. As can be seen, the co-immobilization strategy gives a 2-fold higher signal as compared to backfilling and is in agreement with previous results reported for the co-immobilization of thiolated

DNA probes with mercaptohexanol on gold surfaces. This result also suggests that the co-immobilization strategy may be generalized to other surfaces and, therefore, was used for the construction of the CNO-based sensor.

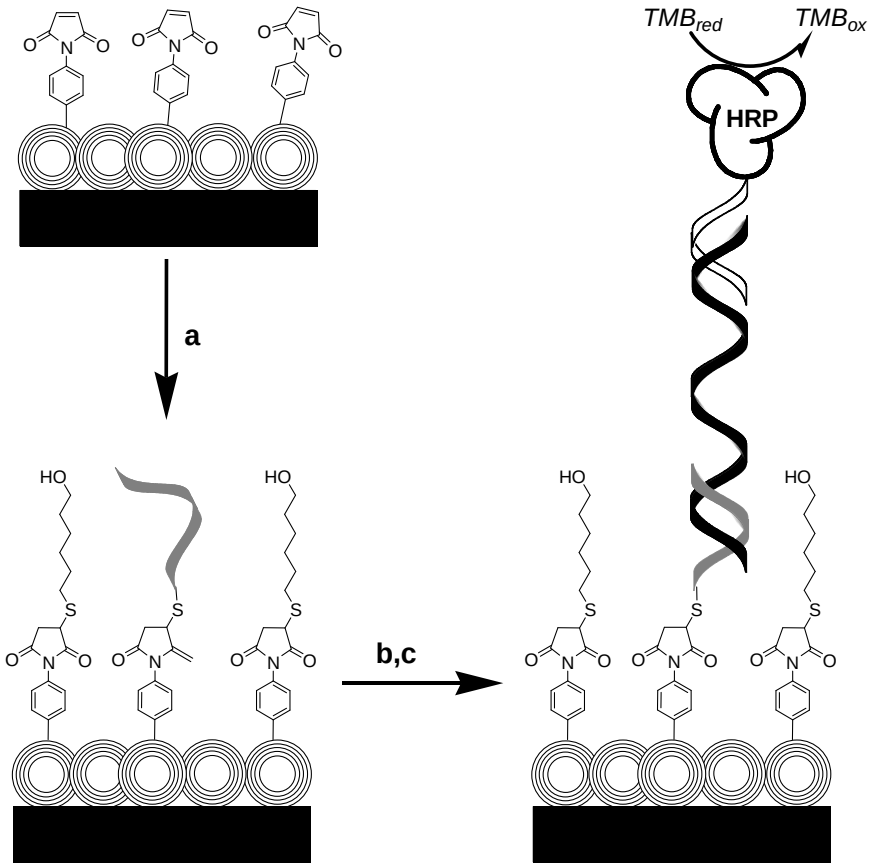

Scheme 5.5: a) Thiolated HPV16 capture probe/mercapto-hexanol, b) target sequence; c) HRP-DNA probe.

Figure 5.5b presents the amperometric detection of different target DNA concentrations for both GCE/CNO/PM and GCE/PM electrodes. The calibration curve for GCE/CNO/PM has a slope of 0.41 μA nM^{-1} with a limit of detection of 0.50 nM as compared with the control surface without CNOs (sensitivity = 0.11 μA nM^{-1}; LOD = 1.4 nM). This represents a 4-fold sensitivity increase and a factor of three reductions in LOD after the incorporation of CNOs on the surface. In addition, the CNO-based sensors showed a markedly larger linear range (0-20 nM) and sensitivity as compared to

the thiol-based immobilization on gold (0-1 nM, 0.15 μA nM^{-1}) [26]. The CNO-based genosensor was evaluated with four clinical samples obtained from cervical scraps previously genotyped to assess the absence or presence of HPV subtypes 16, 18 and 45. As shown in Figure 5.5c, an excellent correlation with the HPV genotyping was obtained as evidenced by the markedly higher signal obtained for the sample containing HPV16, as expected considering that the GCE/CNO/PM genosensor was modified with a thiolated probe selective to HPV16.

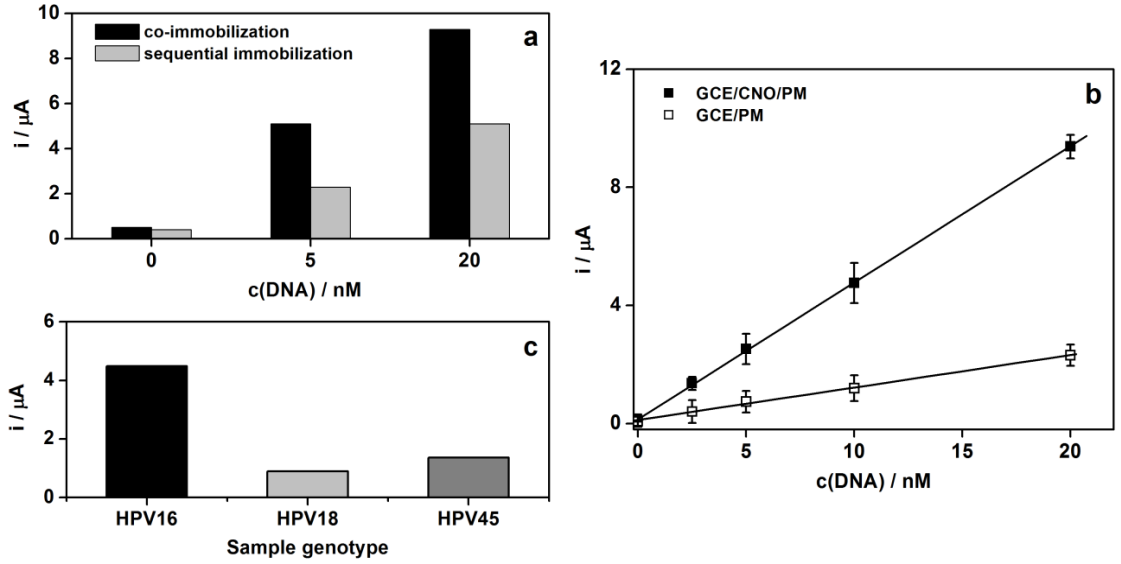

Figure 5.5: a) Comparison of the currents obtained during the detection of 5 and 20 nM target sequence using co-immobilization and sequential addition of thiolated probe and mercapto-hexanol in 1:100 molar ratio. b) Calibration curves for the detection of target DNA on GCE and GCE/CNO electrodes modified with PM using the co-immobilization strategy. c) Current values obtained from undiluted clinical samples on the GC/CNO/PM genosensor modified with an HPV16 capture probe. The HPV subtype of each sample is indicated in the inset.

As can be seen, the presence of CNOs on the surface enhanced the sensitivity and lowered the limits of detection of the amperometric assays with respect to the GC-only electrodes. This result is primarily due to the larger surface area achieved in the presence of CNO, which allows a much higher number of recognition sequences to be immobilized on the surface. Another factor to be considered is the electron transfer rate

of TMB on the CNO-modified surface. It is known that TMB undergoes a quasi-reversible two-proton coupled two-electron redox process in acidic pH. Inspection of the CV of TMB at the GC/CNO surface (Figure 5.6) shows a large current enhancement associated with the increase in surface area. In addition, the CV response shows a marked displacement (-90 mV) towards less positive potentials with respect to the GC-only system, indicating a faster electron transfer, in accord with the results obtained on the GC/CNO/PM/Fc surface. In our case, this favored electron transfer effect is larger than that recently observed for catechol-based neurotransmitters [31], which were ascribed to the semi-metal properties and to the presence of structural defects on the CNOs that enhance electron transfer properties [32]. Thus, the combination of the unique morphological and electronic properties provided by the CNOs to the GC surfaces enhance the sensitivity of the assay and opens the way for further applications of CNO-based surfaces for the detection of other biomolecules. Such studies are currently underway.

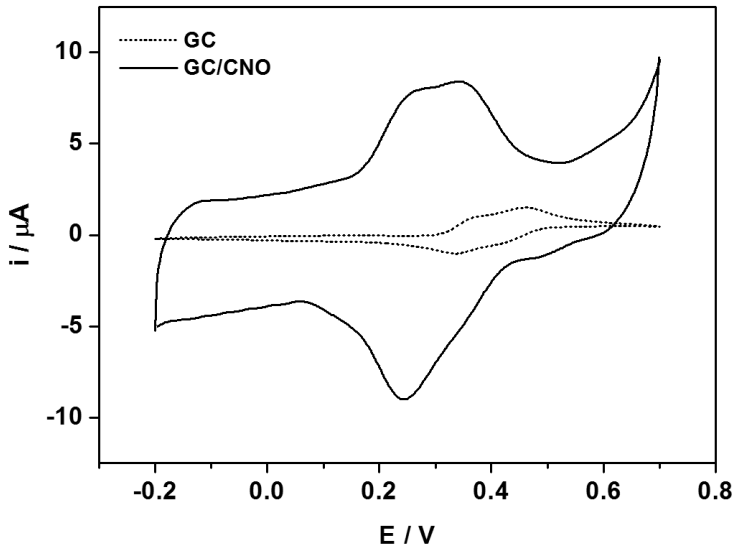

Figure 5.6: Cyclic voltammograms recorded in 0.1 M PBS pH 6 containing 0.1 mM TMB hydrochloride on GC and GC/CNO surfaces. $\nu = 0.1\ Vs^{-1}$.

CONCLUSIONS

Carbon nano-onion dispersions were deposited on the surfaces of glassy carbon electrodes and the modified surfaces were studied by ESEM and AFM revealing a relatively uniform surface. The glassy carbon electrodes modified with CNOs were further modified by electrografting of diazonium salts possessing carboxylic acid or maleimide groups. The attachment of phenyl acetic acid to GCE/CNO generated a COOH-terminated surface to which streptavidin and biotinylated capture DNA sequence was immobilized. On the other hand, the maleimide-terminated surfaces were used for the capture of a thiolated DNA probe and both sensing platforms were investigated for the detection of a DNA sequence associated to the human papillomavirus. In both cases, the incorporation of CNOs on the surface resulted in better sensitivities and lower limits of detection as compared to a GCE electrode without the CNOs. These results were explained on the basis of the large surface area combined with enhanced electron transfer properties of the CNO-modified electrodes. These observations suggest that the developed CNO-modified surfaces are promising and versatile candidates for the development of different and effective analytical sensor systems.

REFERENCES

1. D. Ugarte, *Curling and closure of graphitic networks under electron beam radiation.* Nature, 1992. **359**(6397): p. 707-709.
2. N. Sano, H. Wang, M. Chhowalla, I. Alexandrou, G. A. J. Amaratunga, *Nanotechnology: synthesis of carbon "onions" in water.* Nature, 2001. **414**: p. 506-507.
3. L. Echegoyen, A. Ortiz, M.N. Chaur, A. J. Palkar, *Carbon Nano Onions. In Chemistry of Nanocarbons*, ed. T. Akasaka, F. Wudl, S. Nagase. 2010, Chichester: John Wiley & Sons.
4. J. Bartelmess, S. Giodani *Carbon nano-onions (multi-layer fullerenes): chemistry and applications* Beilstein Journal of Nanotechnology, 2014. **5**: p. 1980-1998.

5. V. Georgakilas, D.M. Guldi, R. Signorini, R. Bozio, M. Prato, *Organic functionalization and optical properties of carbn nano-onions.* Journal of American Chemical Society, 2003. **125**: p. 14268-14269.
6. A.S. Rettenbacher, B. Elliot, J.S. Hudson. A. Amirkhanian, L. Echegoyen, *Preparation and functionalization of multilayer fullerenes (carbon nano-onions).* Chemistry a European Journal, 2006. **12**: p. 376-387.
7. S. Sek, J. Breczko, M.E. Plonska-Brzezinska, A.Z. Wilczewska, L. Echegoyen, *STM-based molecular junction of carbo nano-onion.* CHEMPHYSCHEM Communications, 2013. **14**: p. 96-100.
8. R. Borgohain, J. Li, J.P. Selegue, Y.T. Cheng, *Electrochemical study of functionalized carbon nano-onions for high-performance supercapacitor* Journal of Physical Chemistry, 2012. **116**: p. 15068-15075.
9. K. Flavin, M.N. Chaur, L. Echegoyen, S. Giordani, *Functionalization of multilayer fullerenes (carbon nano-onions) using diazonium compounds and "Click" chemistry.* Organic Letters, 2010. **12**(4): p. 840-843.
10. A. Palkar, A. Kumbhar, A.J. Athans, L. Echegoyen, *Pyridyl-functionalized and water-soluble carbon nano onions: Firts supramolecular complexes of carbon nano onions.* Chemistry of Materials, 2008. **20**: p. 1685-1687.
11. E. Wajs, A. Molina-Ontoria, T.T. Nielsen, L. Echegoyen, A. Fragoso, *Supramolecular Solubilization of cyclodextrin-modified carbon nano-onions by host-guest interactions.* Langmuir, 2015. **31**: p. 535-541.
12. J. Macutkevic, R. Adomavicius, A. Krotkus, D. Seliuta, G. Valusis, S. Maksimenko, P. Kuzhir, K. Batrakov, V. Kuznetsov, S. Moseenkov, O. Shenderova, A. V. Okotrub, R. Langlet, P. Lambin, *Terahertz probing of onion-like carbon PMMA composite films.* Diamond and Related Materials, 2008. **17**: p. 1608-1612.
13. J. Breczko, K. Winkler, M.E. Plonska-Brzezinska, A. Villalta-Cerdas, L. Echegoyen, *Electrochemical properties of composites containing small carbon nano-onions and solid polyelectrolytes.* Journal of Materials Chemistry, 2010. **20**: p. 7761-7768.
14. J. Breczko, M.E. Plonska-Brzezinska, L. Echegoyen, *Electrochemical oxidation and determination of dopamine in the presence of uric and ascorbic acids using a carbon nano-onion and poly(diallyldimethylammonium chloride) composite.* Electrochimica Acta, 2012. **72**: p. 61-67.
15. D. Pech, M. Brunet, H. Durou, P. Huang, V. Mochalin, Y. Gogotsi, P-L. Taberna, P. Simon, *Ultrahigh-power micrometer-sized supercapacitors based on onion-like carbon.* Nature Nanotechnology, 2010. **5**: p. 651-654.
16. L. Joly-Pottuz, E. W. Bulcholz, N. Matsumoto, S.R. Phillpot, S.B. Sinnott, N. Ohmae, J.M. Martin, *Friction properties of carbon nano-onions from experiment and computer simulations.* Tribology Letters, 2010. **37**: p. 75-81.
17. N. Keller, N.I. Maksimova, V.V. Roddatis, M. Schur, G. Mestl, Y.V. Butenko, V.L. Kuznetsov, R. Schlogl, *The catalytic use of onion-like carbon materials for styrene synthesis by oxidative dehydrogenation of ethylbenzene.* Angewandte Chemie Int. Ed., 2002. **41**(11): p. 1885-1888.
18. J. Bartelmess, S. J. Quinn, S. Giordani, *Carbon nanomaterials: multi-functional agents for biomedical fluorescence and Raman imaging.* Chemical Society Review, 2015. **44**: p. 4672-4698.
19. M. Ghosh, S.K. Sonkar, M. Saxena, S. Sarkar, *Carbon nano-onions for imaging the life cycle of drosophila melanogaster.* Small, 2011. **7**(22): p. 3170-3177.

20. J. Bartelmess, E. De Luca, A. Signorelli, M. Baldrighi, M. Becce, R. Brescia, V. Nardone, E. Parisini, L. Echegoyen, P.P. Pompa, S. Giordani, *Boron dipyrromethene (BODIPY) functionalized carbon nano-onions for high resolution cellular imaging.* Nanoscale, 2014. **6**: p. 13761-13769.
21. M. Yang, K. Flavin, I. Kopf, G. Radics, C.H.A. Hearden, G.J. McManus, B. Moran, A. Villalta-Cerdas, L. Echegoyen, S. Giodani, E.C. Lavelle, *Functionalization of Carbon Nanoparticles Modulates Inflammatory Cell Recruitment and NLRP3 Inflammasome Activation.* Small, 2013. **9**(24): p. 4194-4206.
22. J. Luszczyn, M.E. Ploska-Brzezinska, A. Palkar, A.T. Dubis, A. Simionescu, D.T. Simionescu, B. Kalska-Szostko, K. Winkler, L. Echegoyen, *Small noncytotoxic carbon nano-onions: first covalent functionalization with biomolecules.* Chemistry a European Journal, 2010. **16**: p. 4870-4880.
23. P. Yáñez-Sedeño, J. M. Pingarrón, J. Riu, F. X. Rius, *Electrochemical sensing based on carbon nanotubes.* TrAC Trends in Analytical Chemistry, 2010. **29**(9): p. 939-953.
24. W. Yang, K.R. Ratinac, S.P. Ringer, P. Thordarson, J. Justin Gooding, F. Braet, *Carbon nanomaterials in biosensors: Should you use nanotubes or graphene?* Angewandte Chemie Int. Ed., 2010. **49**: p. 2114-2138.
25. J. Thomison, L.K. Thomas, K.R. Shroyer, *Human papillomavirus: molecular and cytologic/histologic aspects related to cervical intraepithelial neoplasia and carcinoma.* Human Pathology, 2008. **16**: p. 154-166.
26. L. Civit, A. Fragoso, C.K. O'Sullivan, *Thermal stability of diazonium derived and thiol-derived layers on gold for application in genosensors.* Electrochemistry Communications, 2010. **12**: p. 1045-1048.
27. L. Civit, A. Fragoso, S. Holster, M. Durst, C.K. O'Sullivan, *Electrochemical genosensor array for the simultaneous detection of multiple high-risk human papillomavirus sequences in clinical samples.* Analytica Chimica Acta, 2012. **715**: p. 93-98.
28. G.T. Hermanson, *Bioconjugate Techniques (Third Edition).* 2013, San Diego: Academic Press.
29. E. J. Laviron, *General expression of the linear potential sweep voltammogram in the case of diffusionless electrochemical systems.* Electroanalytical Chemistry, 1979. **101**: p. 19-28.
30. O. Y. F. Henry, J. Gutierrrez Pérez, J.L. Acero Sánchez, C.K. O'Sullivan, *Electrochemical characterisation and hybridisation efficiency of co-assembled monolayers of PEGylated ssDNA and mercaptohexanol on planar gold electrodes.* Biosensors and Bioelectronics, 2010. **25**: p. 978-983.
31. R. Borgohain, J. Yang, J.P. Selegue, D.Y. Kim, *Controlled synthesis, efficient purification, and electrochemical characterization of arc-discharge carbon nano-onions.* Carbon, 2014. **66**: p. 272-284.
32. D. Kato Ueda. A., R. Kurita, T. Kamata, H. Inokuchi, S. Umemura, S. Hirono, O. Niwa, *Efficient direct electron transfer with enzyme on a nanostructured carbon film fabricated with a maskless top-down UV/Ozone process.* Journal of American Chemical Society, 2011. **133**(13): p. 4840-4846.

Chapter 6

Development of Amperometric Immunosensors for IgG and Carcinoembryonic Antigen based on Carbon Nano-onion Modified Electrodes

ABSTRACT

Immunosensors are affinity biosensors that use antibodies or antigens as the specific sensing element immobilized on the transducer surface. The search for new advanced nanomaterials is an important area in biosensor research and great attention has been paid in recent years to nano-structured materials such as nanoparticles, nanowires or nanotubes as they offer excellent prospects for interfacing biological recognition events with electronic signal transduction. In this chapter, we construct CNO-based immunosensors based on a sandwich assay using electrodeposited diazonium chemistry to immobilize whole antibodies. As model targets we selected immunoglobulin G (IgG) and carcinoembryonic antigen (CEA) and also explore different labels such as HRP and ALP-modified antibodies. The presence of CNOs enhanced the sensitivity of the assay by a factor of 2 and the substitution of HRP for ALP as label of the secondary antibody decreased the LOD by a factor of 6. Therefore, the incorporation of CNO had a positive effect in the biosensor performance and is thus promising materials in immunosensor development.

6.1 INTRODUCTION

According to the International Union of Pure and Applied Chemistry (IUPAC) a biosensor is as a self-contained integrated device capable of providing specific quantitative or semi-quantitative analytical information using a biological recognition element. This biochemical receptor is retained in direct spatial contact with a transduction element capable of detecting the biological reaction and converting it into a signal. The result is an electrical response that is proportional to the concentration of either a single analyte or a group of them [1]. The biological recognition element may be a protein such as an enzyme or antibody, a nucleic acid, a whole cell, or even a plant or animal tissue [2] (Figure 6.1).

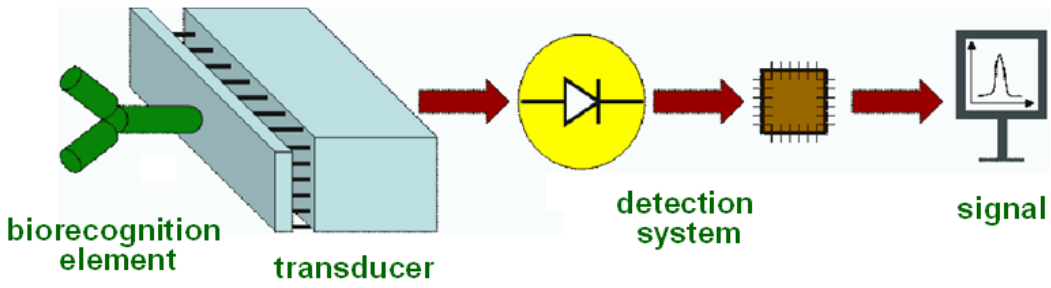

Figure 6.1: Main components of a biosensor.

In particular, an immunosensor is an affinity biosensor that uses antibodies or antigens as the specific sensing element. The fundamental basis of all immunosensors is thus the specificity of the molecular recognition of antigens by antibodies to form a stable complex. There are two main types of immunosensor assays: an indirect immunosensor uses a second labeled species that is detected after binding (sandwich format) and a direct immunosensor detects immunocomplex formation directly by a change in potential, resistance, mass, or optical properties without addition of other species (Figure 6.2). The indirect format, when used in combination with an enzyme

such as peroxidase or alkaline phosphatase, usually gives more sensitive devices but are not capable of real-time monitoring of the antigen-antibody reaction as in the case of the direct immunosensor [3]. These types of assays can also be found in genosensors (biosensors that use DNA probes) as we will see in the next chapter.

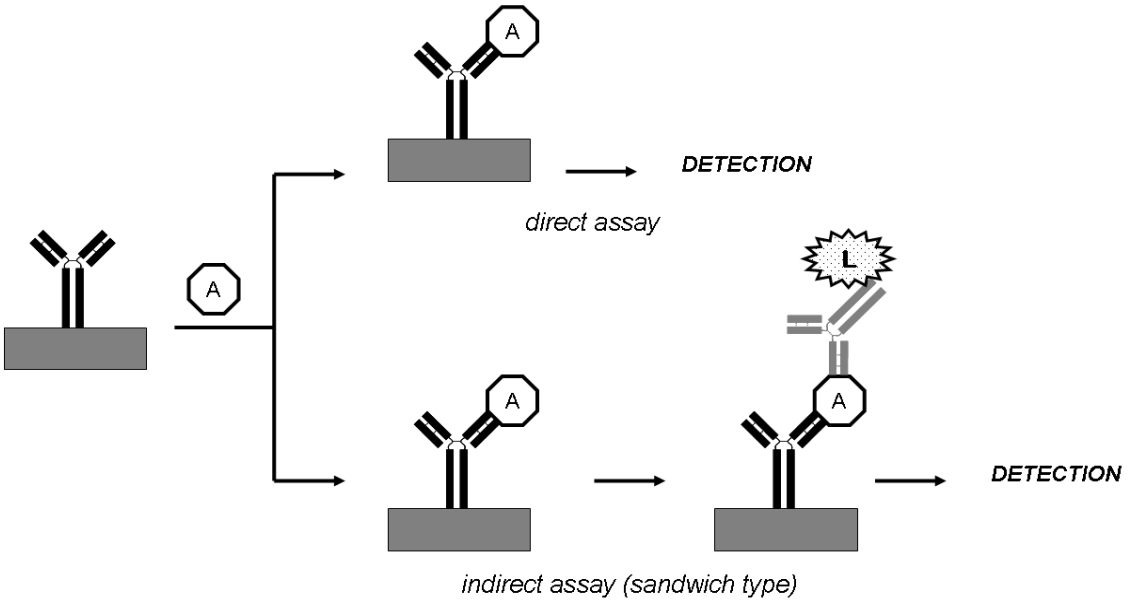

Figure 6.2: Direct vs indirect assay. A: antigen, L: label.

On the other hand, according to the transduction mechanism, immunosensors can be classified into four types: electrochemical (potentiometric, amperometric or conductometric/capacitative), optical (luminescent, fluorescent, reflective, ellipsometric, surface plasmon resonance (SPR)), microgravimetric (piezoelectric or acoustic wave), thermometric (calorimetric) and nanomechanic immunosensors [3, 4]. Electrochemical transducers are the oldest and most common methods used in biosensors and it is the technology used in this work. They combine the high specificity of the bioaffinity methods with low detection limits, high sensitivity, possibility of multiplexing and low cost as compared to other methods and thus exhibit great advantages. They are also not affected by sample turbidity, quenching, or interference from absorbing and fluorescing compounds commonly found in biological samples, as is the case with optical

immunosensors. Electrochemical transducers measure changes of potential, current, conductance, or impedance caused by the immunoreaction [5, 6].

In particular, amperometric biosensors are designed to measure the concentration-dependent current generated by an electrochemical reaction at constant voltage after immuno-complex formation [7, 8]. The resulting current is directly proportional to the antigen concentration. Many proteins are not intrinsically electroactive and cannot be directly detected amperometrically, requiring the use of indirect assays with the incorporation of enzymatic labels that catalyze the formation of electroactive species. Several enzymes have been used for substrate transformation in amperometric systems [9], such as alkaline phosphatise (ALP), which catalyzes the dephosphorylation of phosphates and horseradish peroxidase (HRP), which catalyses the oxidation of H_2O_2 in presence of different redox mediators. The main disadvantages of amperometric immunosensors of having an indirect sensing system is compensated by a high sensitivity and low interferences from matrix components.

The development of an immunosensor requires immobilization of antibodies (or in some cases antigens) on the transducer surface. This can be achieved by physicochemical adsorption or covalent attachment [10]. The former is very commonly used in immunosorbent assays and has the disadvantage that the binding of antibodies to the sensor surfaces is not very strong, it is difficult to reuse and the sensitivity can decrease due to loss of biocomponent from the surface [11]. To improve the uniformity and reproducibility of immobilised antibodies, chemical crosslinking has been used for the covalent immobilisation of proteins onto different solid substrate surfaces using defined linkages such as glutaraldehyde, carbodiimide, and other reagents such as succinimide esters, maleiimides, and periodate [12]. The well established strategy of formation of a self-assembled monolayer for immobilization of biomolecules onto gold

surfaces is based on the strong attachment of thiol (SH) or disulfide (-S-S-) functional groups to a gold surface (Figure 6.3a) and has found many applications in the biosensing field [13-16].

Another alternative strategy is the deposition of diazonium salts already mentioned in the preceding chapter (Figure 6.3b) [17]. In this case, the electrode surface is previously modified with functionalized aryl groups by electrografting of the corresponding diazonium salts followed by biomolecule incorporation with the formation of a covalent bond [18-20]. Alternatively, biomolecule-diazonium salt conjugates are first prepared and isolated, followed by electrografting on the transducer surface [21].

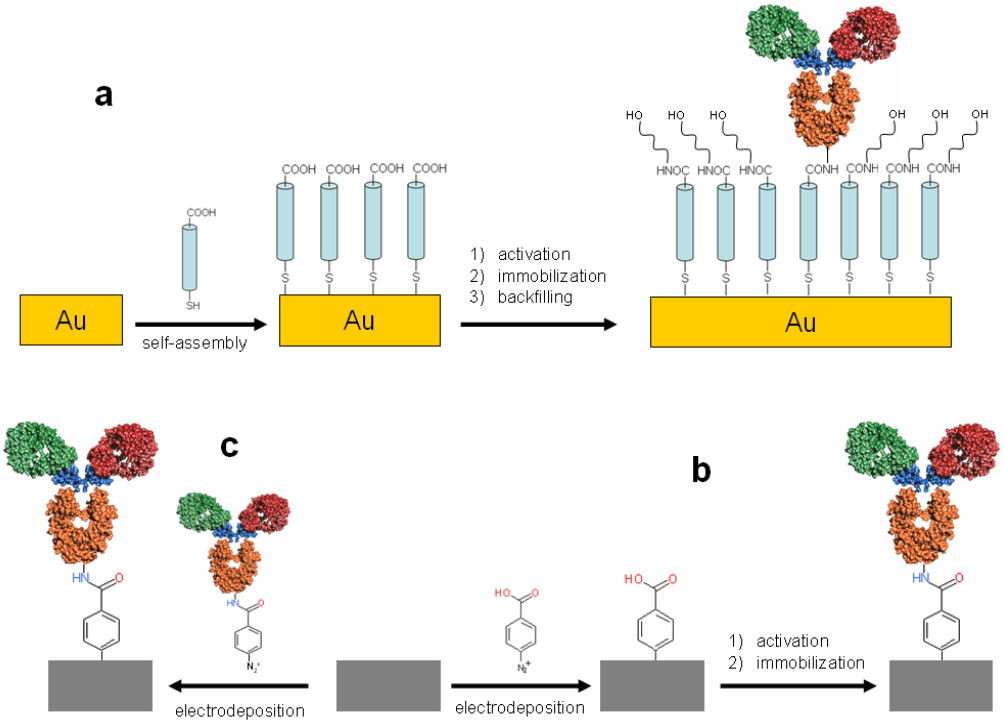

Figure 6.3: Immobilization of antibodies through SAMs on gold (a) or diazonium deposition techniques (b,c).

The advantages of the diazonium reduction approach as compared to alkanethiol self-assembled monolayers include a highly stable surface over time and over a wider potential window, and the ability to synthesize diazonium salts with a wide range of

functional groups [22]. In addition, the ability to create a modified surface by the application of a potential bias allows the selective functionalization of closely spaced microelectrode surfaces. The use of diazonium modification also allows for attachment to a variety of substrates including conducting and semiconducting substrates, carbon nanotubes, etc. [23] but has the disadvantage of multilayer formation, which is often difficult to control [24].

The search for new advanced materials is an important area in biosensor research and great attention has been paid in recent years to nano-structured materials such as nanoparticles, nanowires or nanotubes as they offer excellent prospects for interfacing biological recognition events with electronic signal transduction. Carbon nanotubes (CNT) were among the first carbon nanomaterials exploited in the development of biosensors due to their outstanding mechanical, electrical and electrochemical properties [25-27]. A very elegant application of CNTs to immunoassays involved a “forest” of nanotubes oriented perpendicularly to a pyrolytic graphite surface combined with multi-label secondary antibody-nanotube bioconjugates for highly sensitive detection of a cancer biomarker in serum and tissue lysates (Figure 6.4) [28].

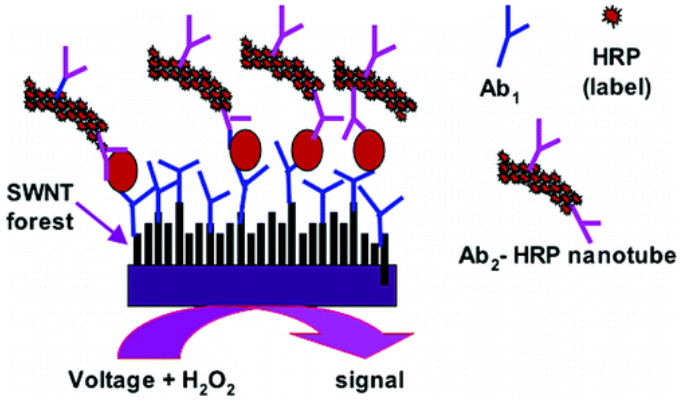

Figure 6.4: CNT-based immunosensor for cancer marker detection [28].

In recent years, research on graphene has seen a revolution that has stimulated the interest in their applications in detection devices [29] and many examples can be found in the literature of pristine, oxidised and reduced graphene based biosensors [30]. Nanodiamonds have also been very recently reported for antibody immobilization using a sonication-assisted nanostructuring method that allowed the impedimetric detection of E. coli [31].

To date, since the discovery of CNOs their potential applications in the area of biosensing and, in particular, in electrochemical biosensors have not yet been explored. CNOs possess higher specific areas and reactivity than carbon nanotubes which combined with newly developed methods of preparation makes them attractive nanomaterials for surface modification. In this chapter, we construct CNO-based immunosensors based on a sandwich assay using electrodeposited diazonium chemistry to immobilize whole antibodies. As model targets we selected immunoglobulin G (IgG) [32] and carcinoembryonic antigen (CEA) [33] and also explore different labels such as HRP and ALP-modified antibodies. The analytical parameters of the different sensing platforms are compared and discussed.

6.2 EXPERIMENTAL SECTION

Reagents and instrumentation. The CNO sample was kindly provided by Dr. Luis Echegoyen (Department of Chemistry, University of Texas at El Paso). Antimouse IgG, IgG from mouse serum, antimouse IgG-HRP antibody, antiCEA, CEA, antiCEA-HRP, antimouse IgG-Alkaline phosphatase produced from goat, alkaline phosphatase from bovine intestinal mucosa and all other chemicals and reagents were purchased from Sigma-Aldrich and used as received. Phosphate buffers (PBS) pH 7.4, TMB solutions, Reaction buffer (RB) consisted of 100mM Tris pH 9 with 10mM $MgCl_2$. Washing

buffer (WB) contained 100mM Tris, pH 8 buffered saline solutions. Hydroquinone diphosphate (HQDP) tetra sodium salt was purchased from DropSens Inc. All solutions used with HQDP were sparged with argon to prevent aerial oxidation. All solutions were prepared with milliQ water.

A tip sonicator (amplitude 60%, cycle 0.5, Ultraschallprocessor UP200S) was used to mechanically disperse CNOs in 10 mL DMF. All electrochemical measurements were carried out using an Autolab model PGSTAT 12 potentiostat/galvanostat controlled with the general purpose electrochemical system (GPES) software (Eco Chemie, The Netherlands), equipped with BASi C-3 Stand (RF-1085) three-electrode cell. This configuration contains a bare or chemically modified glassy carbon electrode (BAS model MF-2012, 3.0 mm diameter) as working electrode, a platinum wire as counter electrode and an Ag/AgCl(sat) as reference electrode. All potentials were recorded with respect to this electrode. Cyclic voltammetry studies were conducted in degassed buffers at a scan rate of 50 mV/s.

Deposition of CNOs on GC electrodes. This step was carried out as described in Chapter 4. Homogeneous dispersions of two-milligrams of CNOs in dimethyl formamide (DMF) were obtained by tip sonication and drop casted unto the surface of cleaned GC electrode and dried using hot air. The process was repeated 10 times until thin layer of CNOs formed in the surface, then thoroughly washed with water and dried again. The electrode was stored in vacuum at 40˚C to create a compact and mechanically stable layer of CNOs into the surface.

Electrochemical grafting of oAP on GCE/CNO. A stirred ice-cold solution of 10 mM 4-aminophenyl acetic acid (PAA) and 0.5 M HCl was mixed with 10 mM $NaNO_2$ for 10 min under argon. After stirring, the GCE/CNO electrode was immersed into the mixed solution and the potential cycle between 0 to -0.6V for 15 cycles at 0.1 V/s. The

obtained modified surface of GCE/CNO with phenylacetic acid (GCE/CNO/PAA) was sonicated to remove the physically adsorbed compounds.

Immobilization of capture antibodies on GCE/CNO/PAA. The carboxyl groups of PAA were activated with an aqueous mixture of 0.2 M EDC and 50 mM NHS for 15 min followed by immobilization of 200 μg/mL antimouse IgG or antiCEA monoclonal antibody in acetate buffer (pH 5) for 2 h at 4˚C. The remaining carboxyl groups were then deactivated with 0.1 M ethanolamine hydrochloride (pH 8.5) for 5 min.

Immunosensor preparation. In the HRP-labeled sytem, the electrodes were washed with PBS pH 7.4 and different concentrations of IgG/CEA in PBS buffer were incubated for 1 h at room temperature. After washing with PBS the HRP-antimouse IgG/CEA-HRP (1:1000 dilution) was introduced and incubated for another hour to complete the IgG/CEA sandwich assay. Amperometric measurements were conducted after washing the developed IgG assay in PBS, placed in 4 mL PBS under stirring conditions and a potential of +150 mV was applied. An aliquot of TMB solution (0.4 mL) was added, and the current response was recorded as a function of time until steady state was reached.

In the ALP system, the electrodes were washed with 100 mM Tris pH 9 buffered saline solutions and the IgG (0, 1.56, 3.125, 6.25, 12.5, 25 μg/mL) was incubated for 1 h at room temperature. After washing with WB the ALP-antimouse IgG (1:1000) was introduced and incubated for another 1 h to complete the IgG sandwich assay. Amperometric measurements were conducted after washing the developed IgG assay in WB, placed in 4 mL degassed 100 mM Tris, pH 9 containing 10 mM $MgCl_2$ under stirring conditions and a potential of +10 mV (+100 mV for GCE assay) was applied.

An aliquot of HQDP was added to a final 1 mM concentration and the current response was recorded as a function of time until steady state was reached.

6.3 RESULTS AND DISCUSSION

Figure 6.5 shows the strategy employed for the immobilization of the antibodies into the surface of GCE/CNO/PAA. A COOH terminated surface was created by electrografting of PAA diazonium salt, which was allowed to react with the amino groups of the capture antibodies by carbodiimide chemistry.

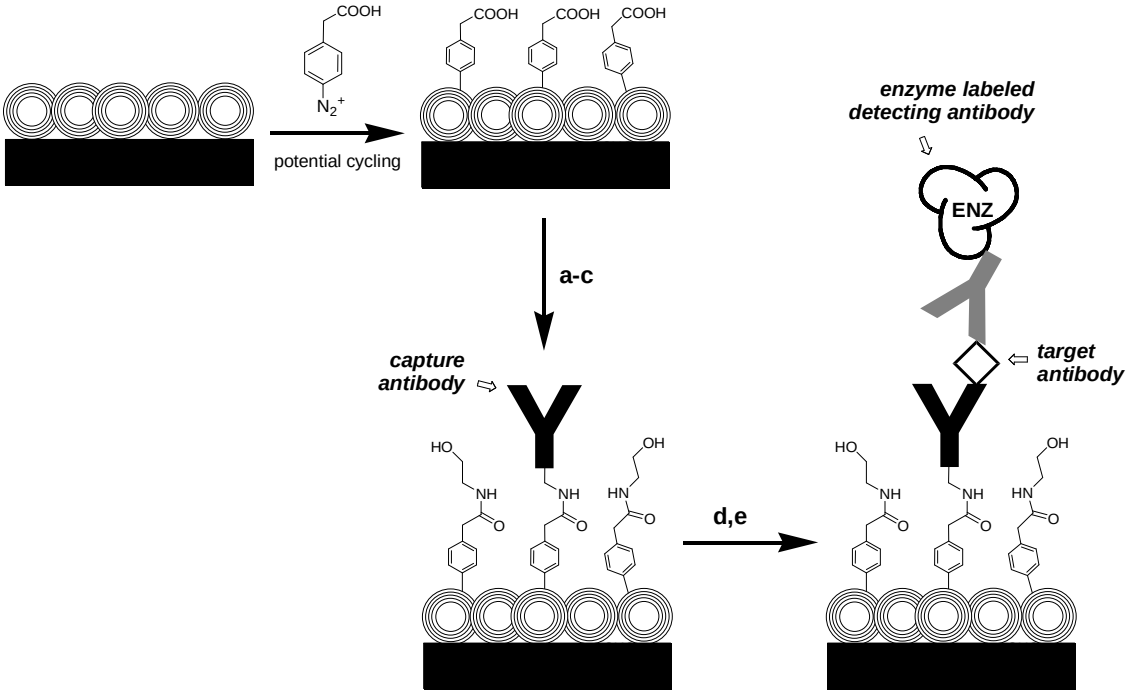

Figure 6.5: Strategy employed for the immunosensor development. a) EDC/NHS; b) antiIgG or antiCEA; c) ethanolamine; d) target antigen (IgG or CEA); e) enzyme-labelled antibodies.

The in-situ chemical functionalization and attachment of the antibodies into the surface of GCE/CNO was followed by cyclic voltammetry as shown in Figure 6.6. Attachment of the different layers on the surface provoked a decrease in the signal of the ferricyanide probe as expected for the blocking of the electroactive signal as the complexity of the immunocomplex increases.

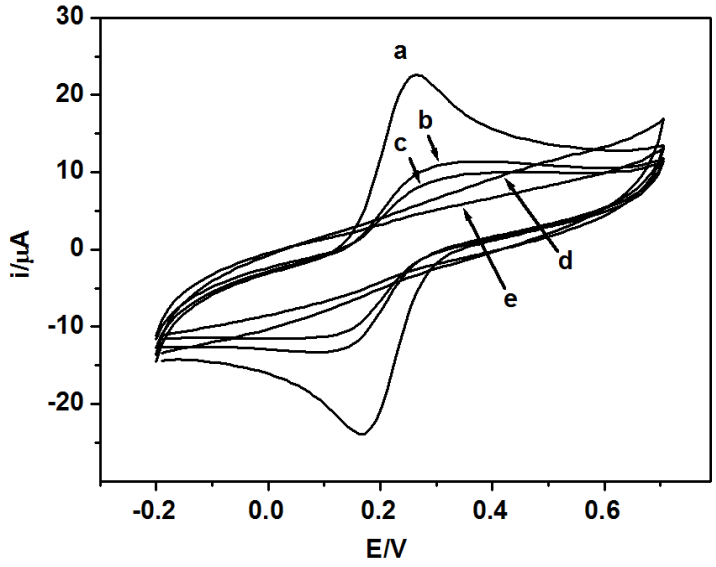

Figure 6.6: Cyclic voltammograms in 1mM $K_3Fe(CN)_6$ corresponding to the GCE/CNO electrode (a) and the sequential immobilization of PAA (b) anti-IgG (c), IgG target (50µg) (d) and anti-IgG-HRP (e).

Figure 6.7 shows the values of current intensity at a fixed concentration of IgG (50 µg/mL) with the number of electrochemical grafting cycles of diazonium salt into the surface of CNO. Interestingly, the maximum number of cycles to obtain high signal was at 15 scan cycles, which is less than the maximum scan cycles required when using DNA sensor (see Chapter 5). This might be due to the larger molecular size of antibodies with respect to DNA probes.

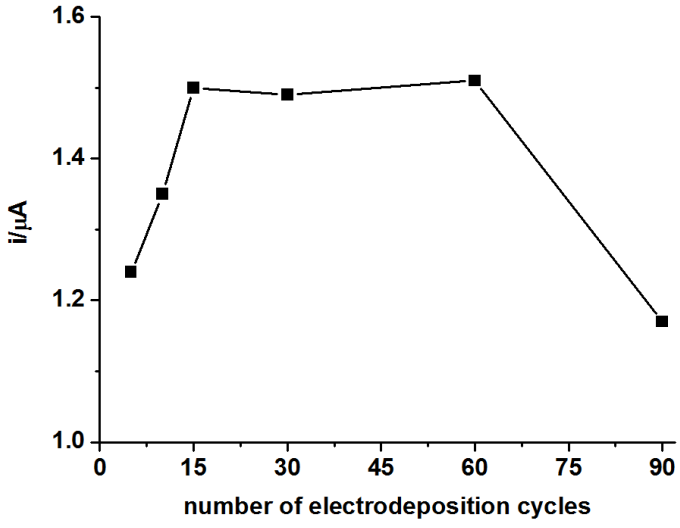

Figure 6.7: Dependence of current intensity (i/µA) with the number of electrodeposition cycles at fixed [IgG] 50 µg/mL.

Using the optimized grafting conditions, the assay was calibrated for the detection of IgG. Figure 6.8 shows the variation of current intensity with increasing IgG or CEA concentrations in the presence and absence of CNO. In Figure 6.8a, the calibration curve of CNO-modified electrode with IgG showed enhanced sensitivity (0.040 μA mL μg^{-1}) and a lower limit of detection (6.8 μg/mL) as compared to the surface without CNOs (sensitivity = 0.024 μA mL μg^{-1}; LOD = 7.2 μg/mL). In the case of CEA, as shown in Figure 6.8b, an increase of sensitivity (4.8 nA mL ng^{-1}) and a lower limit of detection (29 ng/mL) as compared to the surface without CNOs (sensitivity = 2.6 nA mL ng^{-1}; LOD = 32 ng/mL) was also observed. This suggests that the incorporation of CNOs on the surface improves the analytical performance of these biosensors, even in non-optimized assays. However, the achieved sensitivities and LOD values were still far from those reported in other works and, in the case of CEA, the LOD was still above the clinical cut-off value accepted in medical practice (10 ng/mL).

These results prompted us to explore the possibility to use ALP as label in the development of the CNO-based electrochemical immunoassay. ALP catalyzes the hydrolysis of a range of electroinactive phosphate-containing substrates to produce products that can be detected and quantified using electrochemical techniques such as aminophenols, phenol and 1-naphtol [34]. As substrate we selected hydroquinone diphosphatase (HQDP), which is hydrolyzed enzymatically in the presence of ALP to produce hydroquinone (HQ) and has been proposed as a superior substrate for amperometric ALP-based biosensors due to a lower electrode fouling [35]. HQ is an electrochemically active substance that can be detected anodically at low potentials undergoing a two-electron oxidation and deprotonation to produce benzoquinone (Scheme 6.1).

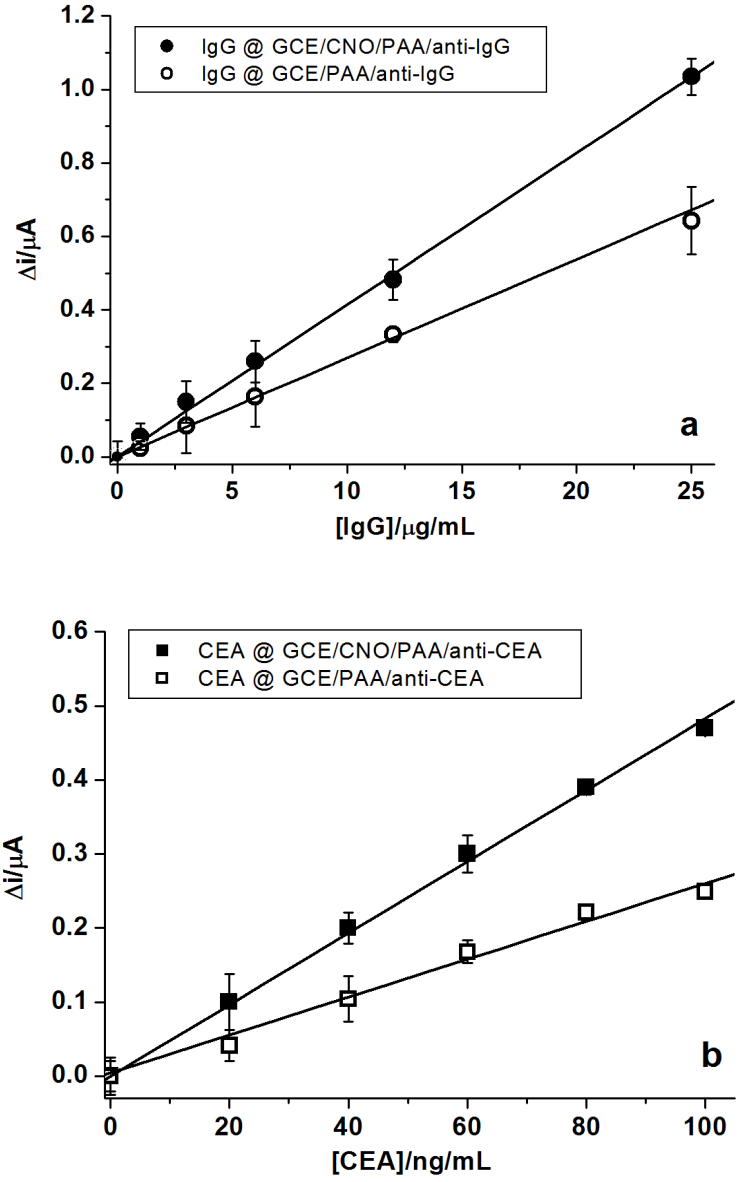

Figure 6.8: Calibration plots for the detection of a) IgG and b) CEA on GCE/CNO/PAA electrodes.

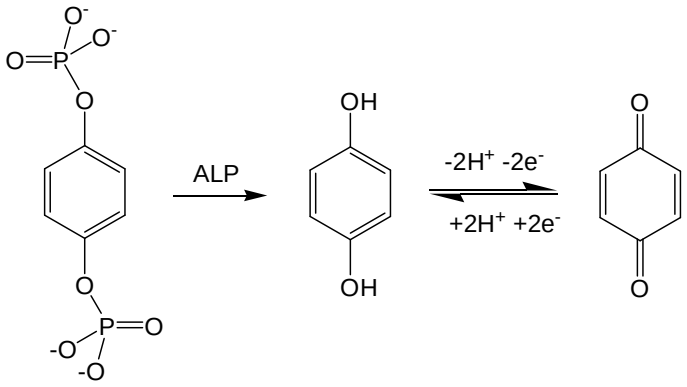

Scheme 6.1: Hydrolysis of HQDP to HQ then deprotonation to produce BQ.

The electrochemical behavior of HQ and HQDP on GCE and GCE/CNO surfaces was first investigated using cyclic voltammetry (Figure 6.9). The cyclic voltammogram of HQ shows well-defined oxidation and reduction peaks in both electrodes GCE and GCE/CNO (Figure 6.9a). The anodic peak potential on GCE/CNO was +20 mV which is lower 44 mV less positive than the oxidation on GCE (+64 mV) denoting an easier oxidation. The peak to peak separation ΔE_{ac} also decreased from 122 mV in GCE to 82 mV in GCE/CNO. These two features indicate that the presence of CNO facilitates the electron transfer of HQ from solution to the electrode. In addition, the current intensity is markedly higher (~2-fold) as a result of an increased electrode area. Therefore, CNO-modified electrodes would be desirable in biosensing applications requiring using low oxidation potentials as this reduces possible interference signals coming from the oxidation of non-target analytes present in biological samples.

HQDP is not electrochemically active and it is important to check the absence of degradation products such as HQ that could appear due to spontaneous hydrolysis of HQDP when not stored properly and not freshly prepared. For this reason, freshly prepared HQDP was checked in degassed solution before and after using in amperometric detection and the absence of signal indicated that HQDP had the required purity (Figure 6.9b). After the addition of ALP the redox peaks corresponding to HQ appear at ~0 mV together with a broad peak at 0.45 V that is presumably due to monophosphorylated HQ.

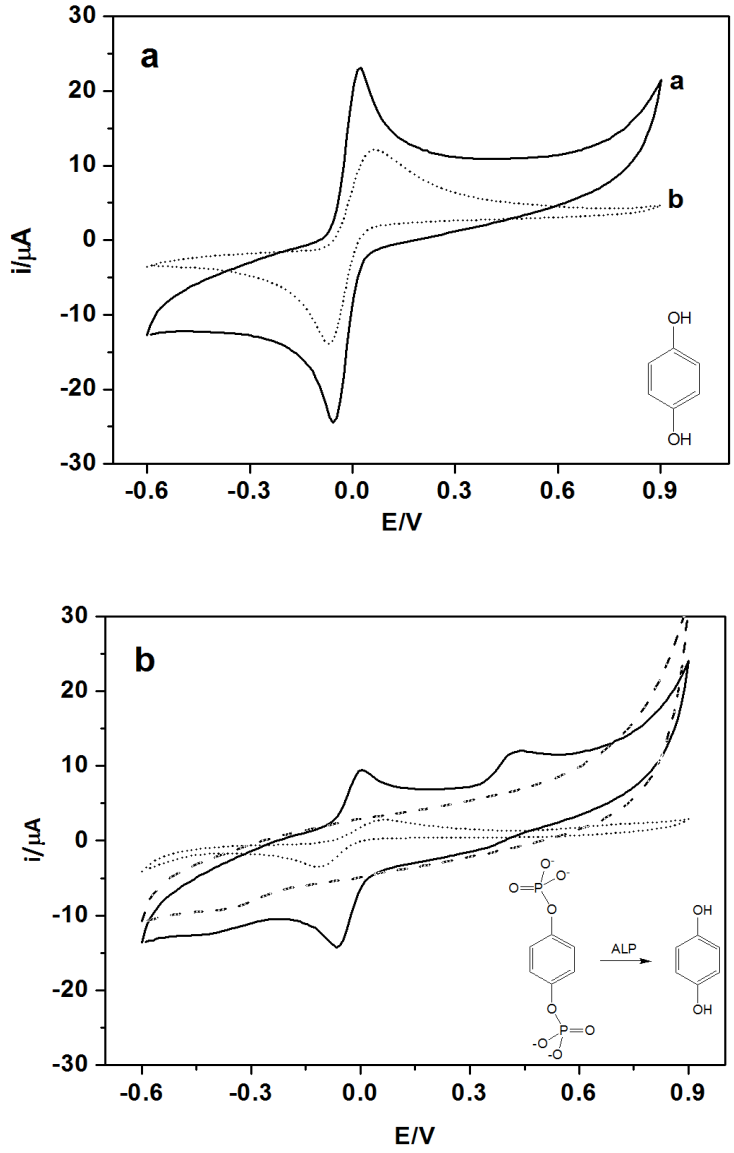

Figure 6.9: Cyclic voltammograms of a) 1 mM HQ in GCE/CNO (—) and GCE (····). b) 1 mM HQDP in Tris buffer pH 9 on GCE/CNO before (----) and after (—) addition of ALP. The dotted line (····) corresponds to 1 mM HQDP after addition of ALP on bare GCE.

Figure 6.10 shows the variation of current intensity with IgG concentration in the presence and absence of CNO using the ALP lapel. The calibration curve of CNO-modified electrode showed a better sensitivity (0.046 μA μg^{-1}) and a lower limit of detection (1.06 μg/mL) as compared to the surface without CNOs (sensitivity = 0.025 μA μg^{-1}; LOD = 1.43 μg/mL). In this case, the sensitivity is 17% higher and more notably the LOD decreased about 7 times as compared with the HRP system.

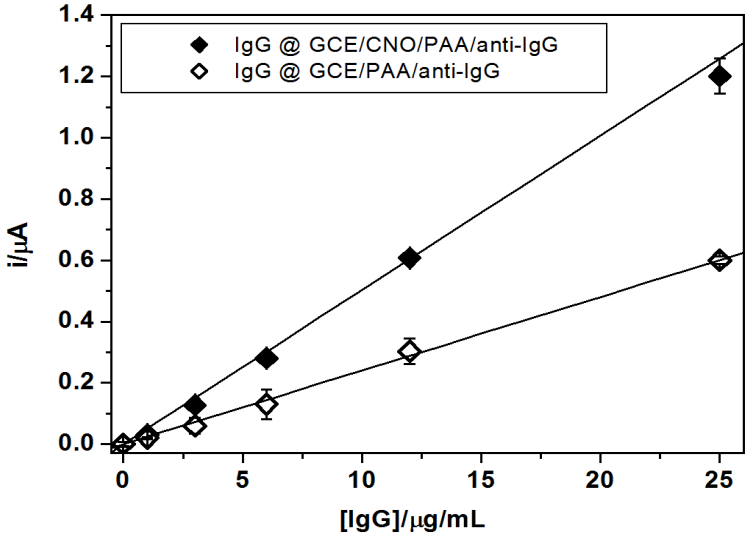

Figure 6.10: Calibration curves for the detection of IgG on GCE and GCE/CNO electrodes using HQDP-ALP system.

After the amperometric detection, cyclic voltammetry has been conducted to check presence of HQ at different concentrations as shown in Figure 6.11. By plotting the peak current of the anodic process, a calibration curve could be constructed that shows similar sensitivity enhancement in the case of the GCE/CNO system with respect to bare GCE as compared to amperometric detection. In this case, the sensitivity was 0.48 μA mL μg^{-1} and the LOD was 1.1 μg/mL, a value slightly better than using carbon nanotubes [36].

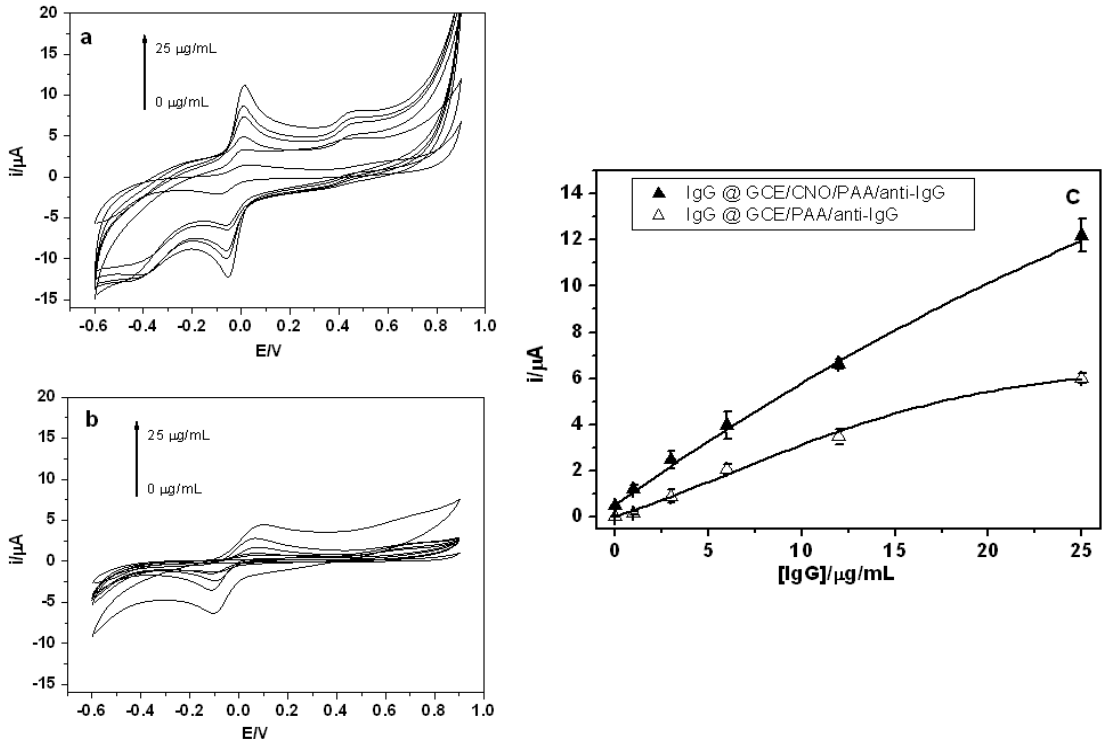

Figure 6.11: Cyclic voltammograms (at 100 mV/s) obtained after enzymatic reaction on GCE/CNO (a) and GCE (b) at different IgG concentrations (0, 1.6, 3.1, 6.3, 12.5, 25 μg/mL). c) Calibration curves obtained from the peak current of the anodic process.

The CNO-based IgG sensor was preliminarily evaluated using a real human serum sample (diluted 1/10 in Tris buffer) to which different known concentrations of IgG were added. As shown in Figure 6.12, the CNO-modified surface showed higher current signal with the presence of serum sample as compared with GCE. The percent of recovery of the obtained current values is presented in Table 6.1. The expected values were interpolated in the calibration curve shown in Figure 6.10 and the obtained recoveries were above 85% for the CNO-modified surface but markedly lower for the non-CNO surface. This suggests that the serum sample contains some interfering substances such as other globulins that could compete in the detection and further optimization needs to be carried out to improve the analytical performance of the developed CNO-based immunosensor.

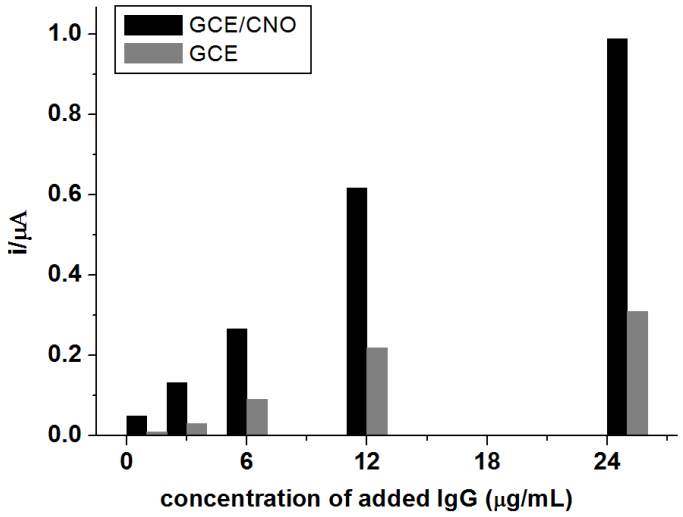

Figure 6.12: Current values obtained from the real serum sample with added IgG concentrations on the GCE/CNO/PAA and GCE/PAA sensors with ALP detection.

Table 6.1. Percent recovery of current values in the calibration curve vs. the values obtained using serum sample.

	Signal recovery (%)	
[IgG] added	**GCE/CNO/PAA**	**GCE/PAA**
1	86	31
3	86	42
6	87	62
12	97	59
25	85	50

CONCLUSIONS

In this chapter we have explored the possibility to use CNO-modified electrodes for the construction of amperometric immunosensors based on a sandwich assay using electrodeposited diazonium chemistry to immobilize whole antibodies. The presence of CNOs enhanced the sensitivity of the assay by a factor of 2 and the substitution of HRP for ALP as label of the secondary antibody decreased the LOD by a factor of 6. Therefore, the incorporation of CNO had a positive effect in the biosensor performance although further work is required to fully optimize the immunoassays in order to

improve the performance of the biosensors, in particular in serum and thus in real samples.

REFERENCES

1. D.R. Thevenot, K. Toth, R.A. Durst, G.S. Wilson, *Electrochemical biosensors: Recommended definitions and classifications.* Pure and Applied Chemistry, 1999. **71**(12): p. 2333 - 2348.
2. A.P. F. Turner, I. Karube, G.S. Wilson, *In Biosensors: Fundamentals and Applications.* 1987, Oxford: Oxford University Press.
3. C.L. Morgan, D.J. Newman, C.P. Price, , *Immunosensors: technology and opportunities in laboratory medicine.* Clinical Chemistry, 1996. **42**(2): p. 193-209.
4. X. Jiang, D. Li, X. Xu, Y. Ying, Y. Li, Z. Ye, J. Wang, *Immunosensors for detection of pesticide residues.* Biosensors and Bioelectronics, 2008. **23**(11): p. 1577-1587.
5. P. Skladal, *Advances in electrochemical immunosensors.* Electroanalysis, 1997. **9**(10): p. 737-745.
6. F. Ricci, G. Adornetto, G. Palleschi, *A review of experimental aspects of electrochemical immunosensors.* Electrochimica Acta, 2012. **84**: p. 74-83.
7. J. Wang, *Amperometric biosensors for clinical and therapeutic drug monitoring: a review.* Journal of Pharmaceutical and Biomedical Analysis, 1999. **19**(1-2): p. 47-53.
8. P.B. Luppa, L. J. Sokoll, D. W. Chan, *Immunosensors—principles and applications to clinical chemistry.* Clinica Chimica Acta, 2001. **314**(1-2): p. 1-26.
9. A.L. Ghindilis, P. Atanasov, M. Wilkins, E. Wilkins, *Immunosensors: electrochemical sensing and other engineering approaches.* Biosensors and Bioelectronics, 1998. **13**(1): p. 113-131.
10. A. Kausaite-Minkstimiene, A. Ramanaviciene, J. Kirlyte, A. Ramanavicius, *Comparative Study of Random and Oriented Antibody Immobilization Techniques on the Binding Capacity of Immunosensor.* Analytical Chemistry, 2010. **82**(15): p. 6401-6408.
11. P. Bianco, *Protein modified-and membrane electrodes: Strategies for the development of biomolecular sensors.* Reviews in Molecular Biotechnology, 2002. **82**: p. 393-409.
12. G.T. Hermanson, *Bioconjugate Techniques (Third Edition).* 2013, San Diego: Academic Press.
13. N.K. Chaki, K. Vijayamohanan, *Self-assembled monolayers as a tunable platform for biosensor applications.* Biosensors and Bioelectronics, 2002. **17**(1-2): p. 1-12.
14. S.K. Arya, P.R. Solanki, M. Datta, B. Malhotra, *Recent advances in self-assembled monolayers based biomolecular electronic devices.* Biosensors and Bioelectronics, 2009. **24**(9): p. 2810-2817.
15. D. Samanta, A. Sarkar, *Immobilization of bio-macromolecules on self-assembled monolayers: methods and sensor applications.* Chemical Society Reviews, 2011. **40**(5): p. 2567-2592.

16. J.J. Gooding, N. Darwish, *The rise of self-assembled monolayers for fabricating electrochemical biosensors—an interfacial perspective.* The Chemical Record, 2012. **12**(1): p. 92-105.
17. M. Delamar, R. Hitmi, J. Pinson, J. M. Saveant, *Covalent Modification of Carbon Surfaces by Grafting of Functionalized Aryl Radicals Produced from Electrochemical Reduction of Diazonium Salts* Journal of American Chemical Society, 1992. **114**: p. 5883-5884.
18. S. Mahouche-Chergui, S. Gam-Derouich, C. Mangeneya, M. M. Chehimi, *Aryl diazonium salts: a new class of coupling agents for bonding polymers, biomacromolecules and nanoparticles to surfaces.* Chemical Society Review, 2011. **40**(7): p. 4143-4166.
19. J.C Harper, R. Polsky , D. R. Wheeler, S. M. Brozik, *Maleimide-Activated Aryl Diazonium Salts for Electrode Surface Functionalization with Biological and Redox-Active Molecules.* Langmuir, 2008. **24**(5): p. 2206-2211.
20. A.J. Haque, K. Kim, *Aldehyde-Functionalized Benzenediazonium Cation for Multiprobe Immobilization on Microelectrode Array Surfaces.* Langmuir, 2011. **27**(3): p. 882-886.
21. B.P. Corgier, C.A. Marquette, L.J. Blum, *Diazonium-protein adducts for graphite electrode microarrays modification: direct and addressed electrochemical immobilization.* Journal of American Chemical Society, 2005. **127**(51): p. 18328-18332.
22. A.J. Downard, *Electrochemically Assisted Covalent Modification of Carbon Electrodes.* Electroanalysis, 2000. **12**(4): p. 1085-1096.
23. R. Polsky, J.C. Harper, D.R. Wheeler, S. M. Dirk, D.C. Arango, S.M. Brozik, *Electrically addressable diazonium-functionalized antibodies for multianalyte electrochemical sensor applications* Biosensors and Bioelectronics, 2008. **23**: p. 757-764.
24. P.A. Brooksby, A.J. Downard, *Multilayer Nitroazobenzene Films Covalently Attached to Carbon. An AFM and Electrochemical Study.* Journal of Physical Chemistry B, 2005. **109**(18): p. 8791-8798.
25. K. Balasubramanian, M. Burghard, *Biosensor based on carbon nanotubes.* Analytical and Bioanalytical Chemistry, 2006. **385**(3): p. 452-468.
26. J. Wang, *Carbon-Nanotube Based Electrochemical Biosensors: A Review.* Electroanalysis, 2005. **17**(1): p. 7-14.
27. M. Trojanowicz, *Analytical applications of carbon nanotubes: a review.* TrAC Trends in Analytical Chemistry, 2006. **25**(5): p. 480-489.
28. X. Yu, B. Munge, V. Patel, G. Jensen, A. Bhirde, J. D. Gong, S. N. Kim, J. Gillespie, J. Silvio Gutkind, F. Papadimitrakopoulos, J. F. Rusling, *Carbon Nanotube Amplification Strategies for Highly Sensitive Immunodetection of Cancer Biomarkers.* Journal of American Chemical Society, 2006. **128**(34): p. 11199-11205.
29. W. Yang, K.R. Ratinac, S.P. Ringer, P. Thordarson, J. Justin Gooding, F. Braet, *Carbon nanomaterials in biosensors: Should you use nanotubes or graphene?* Angewandte Chemie Int. Ed., 2010. **49**: p. 2114-2138.
30. Z. Wang, Z. Dai, *Carbon nanomaterial-based electrochemical biosensors: an overview.* Nanoscale, 2015. **7**(15): p. 6420-6431.
31. W. Zhang, K. Patel, A. Schexnider, S. Banu, A. D. Radadia, *Nanostructuring of Biosensing Electrodes with Nanodiamonds for Antibody Immobilization.* ACS Nano, 2014. **8**(2): p. 1419-1428.

32. V. Carralero, A. González Cortés, P. Yáñez Sedeño, J. M. Pingarrón, *Amperometric IgG Immunosensor using a Tyrosinase‐Colloidal Gold‐Graphite‐Teflon Biosensor as a Transducer.* Analytical Letters, 2008. **41**(2): p. 244-259.
33. N. Laborla, A. Fragoso, W. Kemmner, D. Latta, O. Nllsson, M. L. Botero, K. Drese, C. K. O'Sulllivan, *Amperometric immunosensor for carcinoembryonic antigen in colon cancer samples based on monolayers of dendritic bipodal scaffolds.* Analytical Chemistry, 2010. **82**(5): p. 1712-1719.
34. R.M. Pemberton, J.P. Hart, P. Stoddard, J.A. Foulkes, *A comparison of 1-naphthyl phosphate and 4 aminophenyl phosphate as enzyme substrates for use with a screen-printed amperometric immunosensor for progesterone in cows' milk.* Biosensors and Bioelectronics, 1999. **14**(5): p. 495-403.
35. M.S. Wilson, R. David Rauh, *Hydroquinone diphosphate: an alkaline phosphatase substrate that does not produce electrode fouling in electrochemical immunoassays.* Biosensors and Bioelectronics, 2004. **20**: p. 276-283.
36. Y. Yun, A. Bange, W. R. Heineman, H. B. Halsall, V. N. Shanov, Z. Dong, S. Pixley, M. Behbehani, A. Jazieh, Y. Tu, D.K.Y. Wong, A. Bhattacharya, M. J. Schulz, *A nanotube array immunosensor for direct electrochemical detection of antigen–antibody binding.* Sensors and Actuators B: Chemical, 2007. **123**(1): p. 177-182.

Conclusions and Future Work

The continuously growing demand and search for novel materials in nanoscience and nanotechnology has make researchers explore new horizons in materials chemistry. As described in the present thesis, carbon nano-onions are attractive materials with defined structures and remarkable properties. The focus of the present thesis was to explore strategies for the preparation and modification of novel nanoarchitectures based on CNOs to expand their current applications in the construction of novel detection systems with improved performances.

In the first part of the presented doctoral thesis we illustrated the possibility to prepare carbon nano-onions in gram-amounts by annealing of commercially available nanodiamonds at 1200ºC and apply crown ether/ammonium interactions for the dispersion of CNOs in water. In the presence of biocompatible polymers containing pendant amino groups, such as aminated carboxymethyl cellulose (CMC-NH_2) and poly-L-lysine, the modified CNOs formed stable dispersions in water at acidic pH.

In the second part of the thesis, CNO-modified glassy carbon electrodes were prepared and characterized. Post-functionalization of the surfaces through *in situ* electrochemical grafting of diazonium salts bearing reactive functional groups allowed the construction of detection systems for a variety of analytes. Thus, these electrodes were used for the simultaneous detection of nitrite and ascorbic acid, for the construction of an immunosensor platform to detect immunoglobulin G and carcinoembryonic antigen and, finally, for the detection of a model DNA target sequence associated with the human papillomavirus in both synthetic sequences and clinical samples. In all cases, the incorporation of CNOs resulted in an enhancement in sensitivity and a decrease in detection limits, which was ascribed to a combination of

large surface areas and enhanced electron transfer properties of the CNO-modified electrodes. Although some of the biosensor platforms developed in this work were not fully optimized, it is clear that the use of carbon nano-onions in biosensing has many promising advantages over other nanomaterials. It also seems evident that there is possibility of many other applications such as photovoltaics or molecular electronics in which the interfacial and electronic properties of carbon nano-onions can play an important role in the fabrication and performance of these devices.

Future work

I. Optimization of the RF plasma functionalization method and study of post-functionalization of the prepared CNOs.

II. Optimization of the developed electrochemical assays in terms of electrodeposition cycles, incubation times and buffers, capture probe orientation, etc. to maximize the analytical performance of the developed detection systems.

III. Evaluation of other novel applications on CNOs, for example, in photovoltaic cells and batteries.